INVESTIGATING THE ROLE OF CLASPS IN MICROTUBULE AND ACTIN FILAMENT INTERACTIONS

By

Nicole Christina Rodgers

Dissertation

Submitted to the Faculty of the

Graduate School of Vanderbilt University

in partial fulfillment of the requirements

for the degree of

DOCTOR OF PHILOSOPHY

in

Chemical and Physical Biology

May 12, 2023

Nashville, Tennessee

Approved:

Shane Hutson, Ph.D.

Irina Kaverina, Ph.D.

Adrian Olivares, Ph.D.

Cynthia Reinhart-King, Ph.D.

Marija Zanic, Ph.D.

ACKNOWLEDGMENTS

This dissertation would not have been possible without support, feedback, and encouragement from many people over the years. I would not be writing this thesis without them, and I offer sincere thanks.

First, I would like to acknowledge my dissertation advisor, Dr. Marija Zanic, for her undeniable support and rigorous training. Without her guidance, I would not be the scientist I am today. I am forever grateful for the skills I gained from her mentorship.

I would like to thank my thesis committee members, Dr. M. Shane Hutson, Dr. Irina Kaverina, Dr. Adrian Olivares, and Dr. Cindy Reinhart-King, for their mentorship over the years. Irina deserves a very special "thank you" because she served as a co-sponsor on my F31 fellowship, provided me training opportunities in her laboratory, and strengthened the overall findings of this dissertation through a collaboration on my first-author manuscript. Similarly, I'd like to acknowledge Adrian for introducing me to the actin cytoskeleton during my QCB rotation with him and his help with actin biochemistry, fueling my curiosity for microtubule-actin crosstalk.

I am forever thankful to the Zanic laboratory members who fostered an entertaining work environment and a safe space for discussing science or grieving failed experiments. Previous graduate students, Dr. Claire Strothman and Dr. Veronica Farmer, or jointly, 'Claironica', were additional mentors to me. I can never thank them enough for our discussions about science and life. I will forever look up to them. To the students I had the privilege to mentor while in the Zanic laboratory, especially Tara Hickman, Gabriela Gonzalez-Vasquez, Laura Richardson, and Carson Wright: thank you. These students' work is reflected in my first-author publication and a manuscript in review. I am thankful for their enthusiasm for science and our discussions that aided my thesis work.

Furthermore, I am thankful to the Kaverina laboratory members, especially Dr. Shwetha Narasimhan and Dr. Avishkar Sawant, for their advice and training during our collaboration to conduct cell experiments for my F31 application and manuscript revision. It was always a pleasure to work with them. I would also like to thank my best graduate school friends, Dr. Natalie Wallace, and Nicole Kendrick. In addition to their constant emotional support and our weekly get-togethers, they have provided much guidance in my research endeavors.

I acknowledge the training support from the Quantitative and Chemical Biology (QCB), Chemical and Physical Biology (CPBP), and the Molecular Biophysics Training Program (MBTP). The leadership opportunities provided by the CPB and Dr. Walter Chazin in the MBTP have immensely benefited my graduate training. I thank the Collaborative for STEM Education and Outreach (CSEO) and Dr. Desmond Campbell for teaching me the importance of science accessibility. Through their program, I found opportunities to work with middle and high school students, fulfilling my passion to improve representation of women in STEM in the broader community. In addition, I would like to acknowledge my first scientific advisor, Dr. Anne Murdaugh. Through her considerable support and encouragement, Dr. Murdaugh is largely responsible for my choice to pursue a PhD and to continue encouraging other women to pursue the sciences. Finally, I acknowledge the financial support provided by the F31 fellowship from the National Heart Lung Blood Institute (NHLBI) at the National Institutes of Health (NIH), which supported two years of this work and helped establish our collaboration with the Kaverina lab.

Lastly, I owe many thanks to my family, friends, and newly husband, Adam. My parents, Cindy, and Tom, have been a constant support throughout my PhD journey, guiding me through both successes and challenges. Lots of cheese and chocolate from my mother's travels fueled the completion of this dissertation, I cannot thank her enough for everything. My sibling, Brooke, is one of my biggest supporters and best friends, so I thank them for the hangouts, encouragement, and positivity. I must thank my closest friends, Michelle, Russell, Reshma, Anna, Chrissy, Margaret, Jamie, Mari, and Maggie, for all the video calls and time together who remind me that there is more to life than just science. A special thanks to my 'future in-law family,' the Schoenbachlers, DeLisa, and the McLeroys for their incredible support of my dreams. I thank my cats, Thor, and Loki, for their unwavering companionship. Finally, I will never be able to adequately thank my other half, Adam, for the hours of support, encouragement, and love he has given me since we met in 2019. He encourages me to continue my scientific work, even during the most difficult times. I couldn't have done this work without him. I wish to thank my Grandma Billie, who unexpectedly passed away in 2020. She always said, "I always wanted to have a medical doctor in the family, but never thought a PhD!" During

tough research times, I think of her and my family. I'm proud to be the first in my family to complete a PhD because this dissertation could not have happened without them and a wide community of love and support. I appreciate you all!

TABLE OF CONTENTS

LIST OF FIGURES

LIST OF ABBREVIATIONS

+TIP Microtubule plus-tip interacting protein

Abl Abelson

ABP Actin binding protein

APC Adenomatous polyposis coli

ATP Adenosine triphosphate

Capu Cappucino

CH Calponin homology

ch-TOG Colon and hepatic tumor overexpression gene

CLASP Cytoplasmic linker associated protein

CLIP-170 Cytoplasmic Linker Interacting Protein-170

CMSC Cortical microtubule stabilizing complex

cryo-ET Cryo-electron tomography

DAPI 4',6-diamidino-2-phenylindole

DCX Doublecortin

DMEM Dulbecco's modified Eagle's medium

DNA Deoxyribonucleic acid

DTT Dithiothreitol

EB End binding

ECM Extracellular matrix

ERM Ezrin, radixin, and moesin

F-actin Filamentous actin

FIJI FIJI is just ImageJ

FOV Field of view

FRET Fluorescence resonance energy transfer

G-actin Globular actin

GAPDH Glyceraldehyde-3-phosphate dehydrogenase

GAR Gas2-related

GAS Growth arrest-specific

GDP Guanosine diphosphate

GFP Green fluorescent protein

GMPCPP guanylyl(α,β)-methylene diphosphonate

GSK3β Glycogen synthase kinase 3β

GTP Guanosine-5'-triphosphate

GUI Graphical user interface

IQGAP1 IQ-motif containing GTPase-activating protein 1

IRM Internal reflection microscopy

JACoP Just another co-localization plugin

MACF/ACF Microtubule/Actin crosslinking factor

MAP Microtubule associated protein

MISP Mitotic spindle positioning protein

MTOC Microtubule organizing center

Myo10 Myosin10

MyoVa Myosin Va

NT Non-targeting

PCC Pearson correlation coefficient

PIPES Piperazine-N,N'-bis(2-ethanesulfonic acid)

RNA Ribonucleic acid

SEPT Septin

Ser-Arg Serine-Arginine

Shot Short Stop

TIRF Total internal reflection fluorescence

TOG Tumor overexpressing gene

TRITC Tetramethylrhodamine

CAMSAP Calmodulin regulated spectrin-associated protein

CHAPTER 1

Introduction

1.1 Introduction

The cytoskeleton is composed of several filamentous proteins that are essential in supporting cellular shape and proper function. The components of the cytoskeleton include microtubules, intermediate filaments, and actin filaments (F-actin). Recently, septins—another important group of filamentous proteins—are also considered to be the fourth component of the cytoskeleton (Mostowy and Cossart, 2012; Spiliotis and Nakos, 2021). For the cell to function properly, it must coordinate the cytoskeleton in two ways: 1) chemically through signaling pathways to regulate protein expression and interactions, and 2) physically through direct interactions facilitated by cytoskeletal-associated proteins (Seetharaman and Etienne-Manneville, 2020). For several decades, the cytoskeleton field has thoroughly studied individual components of the cytoskeleton to better understand their specific function in different cellular processes. This work was imperative as it established the fundamental knowledge of our understanding of each cytoskeletal component.

In recent years, the field has shifted from studying individual components to investigating the mechanisms underlying the crosstalk between cytoskeletal components. This shift was made possible due to new developments in high-resolution light microscopy techniques and improvements in biochemical, *in vitro* reconstitution methods. Specifically, the challenge for researchers included, but was not limited to, the ability to visualize these interactions in cells and determine the optimal buffer conditions for reconstituting co-filament systems *in vitro*. To date, the coordination between the microtubule and actin filament networks are of particular interest due to their important roles in cell polarity, cell division, and cell migration ((Dogterom and Koenderink, 2019; Pimm and Henty-Ridilla, 2021; Rodriguez et al., 2003). The dynamic nature of microtubules and actin allow for the cell to actively remodel and reorganize the cytoskeleton for cellular function. This dynamic nature is regulated by microtubule- and actin-associated proteins. Some of these proteins have also been reported to physically crosslink the two polymers together. To better understand cytoskeletal coordination, observations in cells need to be broken down to the components underlying the regulation of microtubule and actin dynamics and interactions.

1.2 Coordination of the microtubule and actin cytoskeleton is essential for several cellular processes important in multiple cell types

For the most part, the microtubule and actin cytoskeleton have been described as independent entities. However, there have been a number of classic studies demonstrating striking overlap of microtubules and actin in neuronal growth cones (Forscher and Smith, 1988; Rochlin et al., 1999; Suter and Forscher, 2000) and examples of growing microtubules within the actin-rich leading edge of cells (Salmon et al., 2002; Waterman-Storer and Salmon, 1997; Wittmann et al., 2003). Previous studies have demonstrated the importance of the microtubule-actin interactions and the proteins for which are involved: 1) establishing cell polarity; 2) coordinating proper cell division; and 3) cell motility (Dogterom and Koenderink, 2019).

1.2.1 Microtubule-actin co-ordination in cell polarity

One such example of the microtubule-actin coordination is in the establishment of cell polarity in differentiated epithelial cells. Epithelial cells tend to form into multi- or mono-layer sheets of cells, which are maintained by cell-cell junctions and a distinct apical-basolateral polar orientation (Rodriguez-Boulan and Macara, 2014). This distinct polarity is organized by the cytoskeleton through crosslinking mechanisms capturing and stabilizing microtubules to the actin cortex (Figure 1.1). Most microtubules are non-centrosomal and highly stable in epithelial cells, as compared to non-polarized cell types (Bré et al., 1987). A microtubule plus-tip interacting protein (+TIP) complex of microtubule associated proteins (MAPs) facilitate microtubule stabilization at the basal plus ends in the vicinity of cortical actin contributing to the height of the epithelial cell (Jaulin and Kreitzer, 2010; Reilein and Nelson, 2005). These aspects contribute to the basally oriented plus end and apical minus end organization of the microtubule network important in polarized cells (Gilbert et al., 1991). This organization of microtubules creates parallel arrays along the apical-basal axis, providing tracks for directional transport.

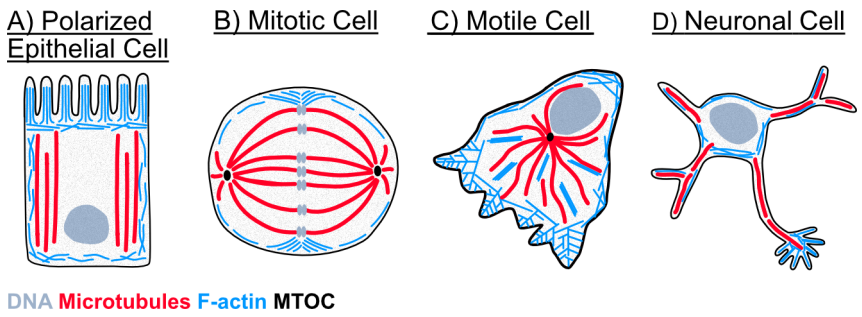

Figure 1.1: Diagrams of the microtubule and actin cytoskeleton in different cell types and processes. A) Example of a polarized epithelial cell type. Microtubule organizing center (MTOC). B) Example of a cell undergoing mitosis at metaphase. C) Example of a migrating cell, moving toward the bottom left. D) Example of a neuronal cell type and an example of a grown cone.

The actin network differs in the apical, lateral, and basal areas of polarized epithelial cells (Rodriguez-Boulan and Macara, 2014) (Figure 1.1A). Actin also forms a contractile belt below the apical membrane, referred to as the zonula adherens (Dogterom and Koenderink, 2019). Some epithelial cells also have actin-based protrusion structures, microvilli, at the apical surface to function in nutrient absorption and are anchored in a rich actin network, termed the terminal web. Otherwise, at the lateral membrane, actin organization is heavily influenced by E-cadherin and associated catenins (Drees et al., 2005).

Actin-microtubule crosstalk is involved in generating and maintaining the columnar shape of epithelial cells (Bazellières et al., 2012). It is unclear whether this columnar shape generates the parallel microtubule arrays by geometrical effects on microtubule dynamics (Gomez et al., 2016) or if the direct interactions between the microtubule plus and minus ends and actin cortex maintain it. Recently, it has been shown that microtubule minus ends are connected to the apical actin cortex by the family of Calmodulin regulated spectrin-associated proteins (CAMSAPs) (Gomez et al., 2016; Noordstra et al., 2016; Toya et al., 2016). Alternatively, Actin crosslinking factor 7 (ACF7) is a spectraplakin that can interact with microtubules as well, thus it remains unclear if ACF7 is directly binding the microtubule or specifically CAMSAP. Since CAMSAP is a microtubule minus-end-capping protein, this interaction directly influences the polarity of the microtubule network, as defined by the actin cortex. This microtubule orientation is essential for directional transport to facilitate formation of actin microvilli at the apical surface (Khanal et al., 2016).

1.2.2 Microtubule-actin co-ordination in cell division

During cell division, the cytoskeleton dramatically changes architecture to create the systems needed for proper chromosome segregation and cytokinesis. Coordination of the reorganization of the microtubule and actin cytoskeletons is necessary. Microtubules form a bipolar mitotic spindle and are placed into three categories: 1) kinetochore microtubules that are attached to chromosomes; 2) antiparallel central spindle microtubules, that are at the spindle midzone and generate pushing forces; and 3) astral microtubules, that extend to the membrane (Figure 1.1B). Actin forms an actomyosin contractile ring around the spindle midzone to round up the cell and create high tension for division. Spindle positioning is dictated by microtubule pushing and pulling forces against the membrane.

Microtubule-actin crosstalk is essential in the proper positioning of the spindle, where microtubule interactions at the actin cortex mediate cell rounding. Cell rounding ensures that there is enough space for microtubules to search and capture kinetochores (Lancaster et al., 2013). The capture and stabilization of

microtubules to the cortex is mediated by Ezrin, Radixin, and Moesin (ERM) , Mitotic spindle positioning (MISP) proteins , end binding (EB) proteins, p150glued, and Myosin 10 (Myo10) described in a future section. These interactions are also involved in cell shape memory due to mechanical sensing by cell-cell junctions (Bosveld et al., 2016). Cytokinesis is also heavily coordinated by microtubule and actin crosslinking. First of all, the position of the cytokinetic ring is determined by two signals, one from the microtubule asters and a second from the spindle midzone supporting microtubule-actin coordination (Bringmann and Hyman, 2005). Anillin, an actin bundling protein that scaffolds the cytokinetic ring, interacts directly with astral microtubules and spatially regulates other cytokinetic proteins (van Oostende Triplet et al., 2014). Further work investigating the cooperativity of the molecular players involved in cytokinetic ring positioning will better our understanding of cell division as regulated by the actin cytoskeleton.

1.2.3 Microtubule-actin co-ordination in cell migration and growth cone guidance

Cell migration is an essential function of cells allowing for proper wound healing and cancer cell invasion. Actin polymerization occurs at the leading edge of motile cells, where branched actin networks generate pushing forces at the membrane. Traction forces are produced by contractile actin stress fibers and linkage to focal adhesions that are anchored to the Extracellular matrix (ECM). Hence, the actin network is branched at the front of the cell, while contractile actomyosin networks are toward the rear (Figure 1.1C). Microtubules are anchored to centrosomes and the Golgi by their minus ends and grow radially out toward the cell cortex. The main role of microtubules is to regulate directional cell migration by providing mechanical stabilization of the leading edge and enabling transport of signaling molecules that coordinate with the actin network (Seetharaman and Etienne-Manneville, 2020).

During cell migration, microtubule and actin network coordination occur in three areas: 1) microtubule interaction at focal adhesions; 2) microtubule anchoring at the cortex; and 3) microtubule interaction at the leading edge, supporting actin nucleation and polymerization. Guidance of microtubules along actin bundles to interact with focal adhesions has been found to be facilitated by spectraplakins and Gas2-like proteins (Girdler et al., 2016; Wu et al., 2008; Yue et al., 2016). The specktraplakins and +TIPs are implicated to be involved in microtubule capture at the cortex, including Cytoplasmic linker associated proteins (CLASPs) , Cytoplasmic Linker Interacting Protein (CLIP-170) , ACF7, Adenomatous polyposis coli (APC) , IQ-motif containing GTPase-activating protein 1 (IQGAP1), and formins (Dogterom and Koenderink, 2019). In addition, the cell cortex can act as a physical barrier to the microtubule network, where actin retrograde flow results in rearward transport of microtubules, microtubule buckling, and breakage (Gupton et al., 2002; Salmon

et al., 2002; Waterman-Storer and Salmon, 1997). This negative feedback loop regulates microtubule turnover in motile cells. Lastly, microtubules have roles in promoting actin nucleation and polymerization at the leading edge of cells due to direct interactions with microtubules and formin or indirectly with EBs and APC. Notably, APC and +TIPs have been observed to travel along microtubules to the actin cortex, where the APC then interacts with formins and the actin network (Mimori-Kiyosue et al., 2000). The specific interactions between each protein are still being investigated.

A lot of the same crosstalk modules discussed so far are also used by neuronal cells to maintain shape and guide axons. Neurons have a polar architecture for proper signal transduction composed of a single axon that extends from the cell body or soma to nearby synaptic junctions of other neurons (Figure 1.1D). In addition, there are shorter dendrite structures that receive signals from other neurons. Dendrites are supported by MAP2-bound microtubule networks of mixed polarity (Conde and Cáceres, 2009). In contrast, axons are composed of plus-end out tau-induced microtubule bundles, surrounded by cortical actin rings (Xu et al., 2013). Along the axon, microtubules are thought to grow along bundled actin filaments in the filopodia to initiate axon elongation and growth cone guidance, like mechanisms described in motile non-neuronal cells. Specifically, it is proposed that actin bundles coated with drebrin guide microtubules via EB3 interaction (Geraldo et al., 2008). Potentially, this interaction can be facilitated by additional proteins present in the growth cone, such as tau, ACF1, or CLASPs, to name a few (Marx et al., 2013). Unraveling the microtubule and actin coordinating factors in axonal elongation and stability will provide important insights into better understanding neurodegeneration.

1.3 Microtubules and actin filaments are dynamic to facilitate remodeling of the cytoskeleton

1.3.1 Microtubule structure and dynamic instability

Microtubules are stiff, hollow cylinders that are comprised of α/β tubulin heterodimers. Microtubules have structural polarity, where tubulin dimers self-assemble longitudinally in a head-to-tail fashion. One end of the microtubule has the β-tubulin subunit exposed, referred to as the plus end, while the other end has the α-tubulin subunit exposed and is referred to as the minus end (Fan et al., 1996; Nogales et al., 1999). Microtubules are typically composed of 13 linearly arranged protofilaments (Tilney et al., 1973). This arrangement and polarity of tubulin dimers lead to significant differences in microtubule dynamics between the plus and minus end.

Interestingly, microtubules are quite dynamic, where they stochastically, switch between phases of growth

and shrinkage. This process is referred to as dynamic instability (Mitchison and Kirschner, 1984; Walker et al., 1988). The transition between growth and shrinkage is termed 'catastrophe' and the inverse is termed 'rescue'. This behavior was first observed using *in vitro* reconstitution methods, with purified protein components (Horio and Hotani, 1986; Walker et al., 1988). During this time, it was also discovered that both microtubule ends are able to undergo dynamic instability (Horio and Hotani, 1986; Walker et al., 1988). Particularly, the microtubule ends have different dynamic instability properties, where the plus end tends to grow faster than the minus end.

1.3.2 Actin filament structure and polymerization

Actin filaments, composed of actin monomers (G-actin), are thinner and less stiff, than microtubules. Like microtubules, actin filaments are polar in structure and polymerize in a head-to-tail fashion into a double helical structure. The fast-growing end is termed the barbed or plus end, and the slow-growing end is referred to as the pointed or minus end (Pollard and Borisy, 2003). This structure was determined based on the arrowhead pattern created by the decoration of myosin on the filament as visualized using electron microscopy (Pollard and Borisy, 2003; Small et al., 1978). Actin filaments can spontaneously self-assemble; however, they do not undergo dynamic instability. Actin filaments tend to be crosslinked in a larger structure, such as in branched or bundled networks in the cell (Blanchoin et al., 2014).

1.3.3 Microtubule and actin co-dynamics

Investigators who have studied the role of the microtubule and actin networks *in vitro* report how these networks alone, without crosslinking proteins, can control cytoskeletal dynamics (Colin et al., 2018; Inoue et al., 2019). Here, the authors investigate how the actin meshwork architecture impacts microtubule dynamics by: 1) looking at microtubules nucleated from the centrosome (Inoue et al., 2019) and 2) looking into branched actin meshworks (Colin et al., 2018). Both reports conclude that actin networks regulate microtubule growth by creating a physical barrier blocking growth. In addition to dynamics, the Blanchoin and Théry groups have also studied the influence of organization (Kučera et al., 2022a,b; Yamamoto et al., 2022). Using microtubule gliding assays, Kučera and colleagues demonstrate how the actin network, either branched or linear, can act as structural memory and therefore, influence microtubule behavior and organization (Kučera et al., 2022a,b). In addition, Yamamoto and colleagues investigated the impact of the actin network in the positioning of microtubule-organizing centers using a cell-free system with purified proteins and cell-sized microwells (Yamamoto et al., 2022). Overall, the authors report how the positioning of the actin network impacts the

distribution of microtubule pushing forces, hence dictating the position of the microtubule organizing center. These reports added to our understanding of the balance of dynamics and forces between microtubules and actin networks involved in greater cytoskeleton organization. However, these systems did not include proteins that are able to physically crosslink microtubules and actin together; this leads to questions regarding the physiological relevance of these studies and the impact of crosslinking proteins on the broader organization of the cytoskeleton.

1.4 Microtubule associated proteins (MAPs) and actin binding proteins (ABPs) physically crosslink the cytoskeleton

It is well understood that MAPs and actin-binding proteins (ABPs) are present in the cell to physically couple the microtubule and actin networks (Dogterom and Koenderink, 2019; Rodriguez et al., 2003). The first evidence that microtubules and actin filaments do not interact alone, but only in the presence of MAPs, was observed by Griffith and Pollard measuring viscosity changes and visualizing close associations of the two filaments using electron microscopy (Griffith and Pollard, 1978). This report was further validated by Sider and colleagues who reported colocalization of microtubules and actin filaments together *in vitro* using Xenopus extracts and fluorescence microscopy (Sider et al., 1999). Decades after, it has been established in the field that crosslinking interactions between microtubules and actin filaments must be facilitated by other proteins. More recent work has organized such proteins into two groups: spectraplakins and microtubule +TIPs (Dogterom and Koenderink, 2019; Rodriguez et al., 2003).

1.4.1 Spectraplakins and Gas2-like family of proteins

Spectraplakins are a family of very large proteins ($>$ 500 kDa) that contain a microtubule-binding, growth arrest-specific (Gas)2-related protein (GAR) domain, and an actin-binding, calponin homology (CH) domain, allowing for these proteins to physically couple the microtubule and actin network (Suozzi et al., 2012). Microtubule-actin crosslinking factor (MACF/ACF) is an example of a spectraplakin that directly binds to microtubules and actin and couples them with important implications in cell motility (Suozzi et al., 2012; Wu et al., 2008). Specifically, ACF7-depleted mouse keratinocytes were reported to have impaired microtubule targeting to focal adhesions (Wu et al., 2008). The interacting domains of the Drosophila spectraplakin, Short stop (Shot), protein were mapped out using Ribonucleic acid (RNA) interference and live cell imaging. Here, it was found that the microtubule end localization of Shot is due to direct interaction with EB and microtubule lattice localization, which is actin-dependent, is due to the Gas2 domain (Applewhite et al., 2010). The au-

thors propose a model where Shot is localized at microtubule ends in the interior of the cell where there is less actin. As microtubules approach the actin-rich cell periphery, Shot localization shifts to the microtubule lattice as Shot binds actin.

Due to the large size of the MACF/ACF protein, it has been difficult for investigators to purify and study their specific protein function. To overcome this challenge, one group engineered a truncated spectraplakin, TipAct-GFP, to study co-organization between microtubules and bundled actin filaments (López et al., 2014). Ultimately, the authors demonstrate that microtubules can be captured and guided along actin filament bundles, validating previous observations in cells. More recently, this group reported that this passive crosslinker can produce forces on the microtubule that result in transport of actin filaments (Alkemade et al., 2022). Advancements are needed in biochemical purification to be able to directly study full length MACF/ACF *in vitro*.

Another protein family containing a single CH domain and a Gas2 domain are the Gas2-like proteins. Stroud and colleagues investigated the localization of the three members of the Gas2-related proteins, Gas2L1, Gas2L2, and Gas2L3, in fibroblasts and reported differential localization (Stroud et al., 2014). The Gas2L1 and Gas2L2 were found to localize to actin stress fibers, where microtubules were coaligned. Yet, Gas2L3 also localizes to actin stress fibers, however there were few instances of coalignment with microtubules. Only endogenous Gas2L1 and Gas2L2 had an impact on microtubule dynamics and guidance along actin stress fibers due to their direct interaction with EB. Similar results were found for the Drosophila Gas2-related protein, Pigs (Girdler et al., 2016). PigsFL comet velocities *in vitro* (S2 cells) and in vivo (Drosophila squamous follicle cells) were similar to EB1 and CLIP170 comets, respectively (Girdler et al., 2016). Finally, purified Gas2L1, has been demonstrated to be autoinhibited, where it is activated when simultaneously bound to actin filaments and microtubules (van de Willige et al., 2019). The authors describe the function of Gas2L1 as an actin regulator that is spatially organized by microtubules.

1.4.2 +TIP protein complexes

There are also +TIP protein complexes that can physically couple the microtubule and actin networks, where EB proteins bind to growing microtubule ends and interact with other proteins that bind actin filaments. For example, a multi-component interaction of MAPs (CLIP-170 and EB) and ABPs (formin (mDia1) and profilin) has been shown to facilitate physical coupling of the cytoskeleton. Specifically, the CLIP-170:mDia1 complex is recruited to microtubule ends and triggers actin filament growth (Henty-Ridilla et al., 2016). Interestingly, it has been reported that EB1, without the acidic tail and full C-terminal domain, can directly

interact with actin filaments, but cannot bind F-actin and microtubules simultaneously (Alberico et al., 2016). In addition, CLIP-170 binding to actin filaments and microtubules is also mutually exclusive, similar to EB (Wu et al., 2021).

Other ABPs, drebrin and APC also interact with EBs to crosslink microtubules and actin filaments. Drebrin directly interacts with EB1/3 and colocalizes with actin filaments and microtubules in filopodia (Geraldo et al., 2008). The authors discovered that the presence of microtubules in filopodia was due to the interaction between drebrin and EB3. Another group proposed the same mechanism for hippocampal neurons, where overexpression of drebrin promotes microtubule entry into dendritic spines (Merriam et al., 2013). In Xenopus epithelial cells, APC signal was first observed to move along microtubules and concentrate at the microtubule end (Mimori-Kiyosue et al., 2000). It was then found that the APC, with EB1, interacts with formin (mDia1) and all are localized at microtubule ends in human adenocarcinoma cells (Wen et al., 2004). The APC has also been implicated in microtubule anchoring at the actin cortex (Juanes et al., 2019). Finally, APC has also been observed to be at the end of microtubules connecting branched actin networks in fibroblasts influencing the organization of the two networks (Juanes et al., 2017).

1.4.3 Other proteins – ABPs

ABPs are proteins that regulate the actin cytoskeleton in cells. Recently, it has been discovered that these proteins have additional functions interacting with microtubules, physically crosslinking the two together. Here, I'll briefly describe these other proteins and their role in the crosstalk of the actin and microtubule cytoskeletons.

1.4.3.1 Nucleators

The formin family of actin nucleators have been implicated to interact with microtubules (Chesarone et al., 2010; Gaillard et al., 2011). It was first reported using *in vitro* reconstitution that the human formin, mDia2, stabilizes microtubules and protects from depolymerization induced by tubulin dilution (Bartolini et al., 2008). Also, the Drosophila formin, Cappucino (Capu), was found to interact with microtubules via the FH2 domain and tail, however, there was no evidence of simultaneous binding of microtubules and actin filaments *in vitro* in the tested conditions (Roth-Johnson et al., 2014). Despite the inability of formin to simultaneously bind actin filaments and microtubules, mDia2 has been shown to be involved in protein complexes involved in coordinated actin and microtubule dynamics as described above (Henty-Ridilla et al., 2016; Wen et al.,

2004). Furthermore, profilins, ABPs that bind actin to regulate actin nucleation, have also been reported to interact with microtubules and impact their dynamics, *in vitro* and in mouse melanoma cells (Henty-Ridilla et al., 2017; Nejedla et al., 2016). Profilin increases the growth rate of microtubules *in vitro* and in mouse neuroblastoma cells (Henty-Ridilla et al., 2017). Interestingly, Nejedla and colleagues suggest that profilin is functionally linked to microtubules by formins, adding to the dynamic interplay between actin nucleators and microtubules (Nejedla et al., 2016).

1.4.3.2 Crosslinkers

Another ABP, coronin and Pod-1 in Drosophila, is a well-known actin-microtubule crosslinker and has been shown to crosslink microtubules and actin *in vitro* (Goode et al., 1999; Rothenberg et al., 2003). Intriguingly, the yeast coronin (coronin1p) has a strong sequence homology with the worm, mold, cow, and human coronins, but uniquely, it contains two additional sequences homologous to the microtubule-binding domain of MAP1B (Goode et al., 1999; Noble et al., 1989). The fly coronin (Dpod1) has one sequence weakly homologous with the microtubule-binding domain of MAP1B and can also crosslink microtubules and actin filaments (Rothenberg et al., 2003). The MAP1B-homologous region of coronin1p is needed to crosslink microtubules and actin (Goode et al., 1999). Thus, the microtubule-binding and actin-binding regions are necessary for coronin's function as a crosslinker in yeast and flies.

MISP is a poorly understood ABP that is involved in spindle orientation (Maier et al., 2013; Zhu et al., 2013). Depletion of MISP slows down the transition from metaphase to anaphase and cytokinesis took over 5 times longer to complete in Hela cells (Zhu et al., 2013). MISP is also required for centrosome clustering and colocalizes with actin and focal adhesions (Maier et al., 2013). These reports also found that MISP interacts with EB1 and p150glued, a subunit of the dynein-dynactin complex, proposing a model where these interactions stabilize cortical and astral microtubule attachments. A new study reported the role of MISP in epithelial microvilli, where the authors observe localization at the rootlets of microvilli and determined that MISP can bundle actin filaments *in vitro* (Morales et al., 2022). Future studies should investigate whether the crosslinking ability of MISP is involved in stabilizing actin bundle formation with connections to the microtubule network at the root of the microvillus. To date, MISP has not been reported to simultaneously crosslink microtubules and actin filaments *in vitro*.

The ERM ABP family are responsible for crosslinking actin filaments to the plasma membrane when active (Fehon et al., 2010). Moesin was also shown to directly bind microtubules and stabilize microtubules

at the cell cortex (Solinet et al., 2013). This report also found ezrin to be able to bind microtubules. Another interesting role of ezrin is to stabilize microvilli by linking the plasma membrane to the actin network (Morales et al., 2022). Ezrin, and MISP, a binding partner of ezrin, were found to be mutually exclusive for localization at the rootlets of microvilli (Morales et al., 2022). This leaves questions regarding the interplay between ERM proteins and MISP in the crosstalk of the cytoskeleton in microvilli and other systems.

1.4.3.3 Motors

There are a few myosins, motor proteins that bind and exert forces on actin filaments, that have been reported to interact with microtubules. Myo10, an unconventional myosin, was reported to associate with microtubules and is involved in proper spindle orientation in mitotic cells (Kwon et al., 2015; Toyoshima and Nishida, 2007; Weber et al., 2004). The Myo10-depleted cell spindle orientation are misoriented as represented by greater spindle angle, the angle between the metaphase spindle axis and the subsrate surface (Toyoshima and Nishida, 2007). In plants, myosin VIII has been found to be involved in coupling the dynamics of the spindle and actin filaments facilitating persistent polarized growth of plant cells (Wu and Bezanilla, 2014, 2018). Finally, Myosin Va (MyoVa), in dilute (myosin Va-) melanocytes, is involved in microtubule-dependent melanosome transport (Wu et al., 1998). Melanosome transport no longer persists in nocodozole treated and dilute melanocytes, indicating that microtubules and MyoVa, respectively, are involved (Wu et al., 1998). Further investigation has determined that MyoVa binds to melanophilin to interact with Rab27a, a melanosome-bound small GTPase, for transport of melanosomes, and dephosphorylated melanophilin can interact with microtubules (Oberhofer et al., 2017, 2020). Hence, MyoVa has been reported to switch its motility along actin filaments to microtubules.

1.4.4 Other proteins – MAPs

MAPs are proteins that regulate the microtubule cytoskeleton in cells. In recent years, it has been discovered that these proteins have additional functions interacting with actin filaments: physically crosslinking the two together. Here, I'll briefly describe these other proteins and their role in the crosstalk of the microtubule and actin cytoskeletons.

1.4.4.1 Stabilizers

Microtubule stabilizing proteins are MAPs that regulate microtubule dynamics by sustaining microtubule growth, either by promoting growth or by preventing shrinkage. Doublecortin (DCX) is a neuronal MAP that is important in neuronal migration and is the most common cause for X-linked lissencephaly (Moon and Wynshaw-Boris, 2013). The first indication that DCX was involved in microtubule-actin crosstalk was when ABP, neurabin II, was discovered to be an interacting protein of DCX (Tsukada et al., 2003). Then it was revealed that DCX can directly interact with actin filaments, crosslink microtubules and actin filaments, and when co-transfected with neurabin II, DCX colocalized with actin filament structures as well as microtubules (Tsukada et al., 2005). A pollen-specific MAP, SB401, was found to bind and bundle microtubules, while also enhancing tubulin polymerization—acting as a stabilizer (Huang et al., 2007). In the same study, it was also reported that SB401 could bind and bundle actin filaments, as well as crosslink microtubules to actin filaments. More work needs to be done to further investigate the specific interactions that occur for this form of crosstalk.

Tau, a well-studied neuronal MAP, that promotes microtubule polymerization and bundling, is implicated in Alzheimer's disease and related neurodegenerative disorders (Ballatore et al., 2007). Specifically, the tau-induced abnormal bundling of actin filaments has been reported to cause neurodegeneration in vivo (Fulga et al., 2007). Tau has also been shown to interact with actin, bundle actin filaments, and promote coalignment and co-organization of the microtubule-actin networks (Cabrales Fontela et al., 2017; Elie et al., 2015). Finally, tau has been shown to be involved in the proper navigation of pioneer microtubules into the actin-rich region of cortical growth cones (Biswas and Kalil, 2018). Two similar proteins, also from the classical MAP family, MAP2c and MAP4, have been shown to bind and bundle both microtubules and actin filaments (Doki et al., 2020; Roger et al., 2004). MAP2c binds and bundles F-actin, where the microtubule-binding domain is necessary and sufficient for this activity (Roger et al., 2004). MAP4 crosslinks and colocalizes to F-actin and microtubules *in vitro* and in neuronal processes, respectively (Doki et al., 2020). These proteins demonstrate the importance of physical crosslinking of microtubules and actin networks in neuronal contexts.

1.4.4.2 Tumor Overexpressing Gene (TOG) domain proteins

The Tumor Overexpressing Gene (TOG)-domain protein family was named after the human microtubule polymerase, the Colon and hepatic tumor overexpression gene (ch-TOG). The well-studied TOG protein, *Xenopus* microtubule polymerase XMAP215, is involved in proper microtubule localization into the growth cone during axonal guidance. Direct interactions between XMAP215 and the actin network in the growth

cone are thought to potentially be involved (Lowery et al., 2013). Soon after that report, XMAP215 was shown to directly bind actin filaments (Slater et al., 2019). XMAP215 contains five TOG domains that are understood to interact with the microtubule lattice and soluble tubulin. Slater and colleagues demonstrated that all five TOG domains were required for XMAP215 localization to actin in the growth cone.

Another TOG domain protein family, CLASPs are +TIPs that contain 2-3 canonical TOG domains (Figure 1.2). The TOG1 domain is homologous to the XMAP215 TOGs (Akhmanova et al., 2001). CLASPs are also implicated to interact with microtubules and actin filaments. Specifically, it has been reported that CLASP1 and CLASP2 colocalize with stress fibers in fibroblasts and interact with actin in coimmunoprecipitation experiments (Tsvetkov et al., 2007). Here, the authors suggest that the TOG1 domain and serine-arginine-rich region of CLASPs facilitate the interaction (Tsvetkov et al., 2007) (Figure 1.1). Another report demonstrates a direct interaction between monomeric actin and microtubules in the presence of CLASP2α using a co-sedimentation experiment with purified proteins (Engel et al., 2014). If CLASPs can interact with microtubules and actin filaments, then can it simultaneously bind the two? These two reports provide the only evidence for CLASP-mediated microtubule-actin interaction.

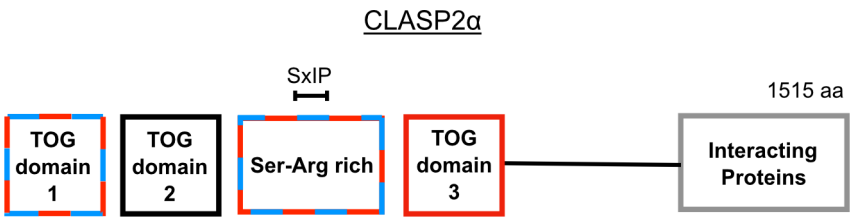

Figure 1.2: Schematic of CLASP2α domain structure.
CLASP2α contains three TOG domains, responsible for microtubule interaction (blue) and proposed actin filament interaction (red) for TOG1. CLASP2α also contains a Serine-Arginine rich region, which include the SxIP motif, facilitating direct interaction with EB proteins. The Serine-Arginine rich region is implicated in CLASP-mediated actin interaction and binding to the microtubule lattice. Finally, the CLIP-ID or interacting protein region mediates interactions with other MAPs, including CLIP-170.

1.4.4.3 Motors

The plant Kinesin-14 protein family include a unique class of minus-end motors that have a CH domain, referred to as KCHs, that are only in land plant cells and serve as microtubule-actin crosslinkers. Notably higher order plants lack cytoplasmic dynein and instead contain a large number of KCHs, where it's been speculated to compensate for the loss of dynein (Lawrence et al., 2001; Tseng et al., 2018). For example, the rice Kinesin-14 OsKCH1 has been characterized as a protein that can bind both microtubules and actin filaments, where actin regulates the motors ATPase activity (Umezu et al., 2011). Newly, it was shown *in*

vitro, that OsKCH1 can transport actin filaments along microtubule tracks and the transport velocities are dependent on the motor orientation (Tseng et al., 2018; Walter et al., 2015). This is a great example of how actin filament networks can regulate microtubule-dependent transport.

1.4.5 Other proteins – septins

The fourth component of the cytoskeleton, septins (SEPTs), have been an interest of study in the past few years. Septins are a family of Guanosine-5'-triphosphate (GTP)-binding proteins that assemble into complexes and have slower turnover rates after photobleaching than cortical actin, tending to be more stable filaments (Hagiwara et al., 2011; Spiliotis and Nakos, 2021). The hetero-hexamer SEPT2, SEPT6, and SEPT7 (SEPT 2/6/7) have been reported to regulate microtubule dynamics by tuning EB1 interaction with microtubule plus ends (Nakos et al., 2019). A new report demonstrates how SEPT2/6/7 can also crosslink dynamic actin filaments to the microtubule lattice and are involved with the maintenance of the peripheral actin network in growth cones (Nakos et al., 2022). The mechanical implications with this three-polymer, bundle structure is of great interest in the mechanisms underlying growth cone guidance.

1.5 Summary

The cytoskeleton remodels and provides mechanical reinforcement for the cell to function properly. This remodeling requires synchronized changes in the architecture of all four components of the cytoskeleton. Of particular interest are the specific mechanisms underlying microtubule and actin filament crosstalk, due to its broad functions in several cell types and implications in disease. This coordination is facilitated by many crosslinking proteins that have recently been implicated in either directly interacting with multiple cytoskeletal filaments or by forming complexes with other proteins linking the two polymers together. Researchers are still identifying novel proteins that can simultaneously crosslink microtubules and actin filaments, along with characterizing specific interactions observed *in vitro* and in cells. The cytoskeletal crosstalk field is relatively new, and an abundance of questions remain to be explored. With advancements in imaging techniques, biochemical reconstitution, and computational methods, the future of this field looks bright for furthering our understanding of the cytoskeleton.

A question that remains in the microtubule-actin crosstalk field regard the role of CLASPs and if it can physically crosslink microtubules and actin filaments together. There are several instances in the coordination of microtubules and actin filaments where CLASPs are implicated, markedly in cell motility. This disserta-

tion investigates the role of CLASPs in microtubule and actin coordination *in vitro* and provides insight into its role in cells. In Chapter 2, I discuss the powerful use of *in vitro* reconstitution and image analysis methods to investigate CLASP-mediated microtubule and actin filament interactions. Then in Chapter 3, I confirm that CLASP2α weakly interacts with actin filaments and preferentially localizes to bundled actin filaments, supporting the hypothesis that CLASPs can directly crosslink microtubules and actin filaments. In Chapter 4, I demonstrate that CLASP2α can simultaneously crosslink microtubules and actin filaments, where CLASP can support multiple actin filaments binding along the microtubule lattice. In Chapter 5, I explore the dynamic organization of microtubules and actin where I report that CLASP2 can mediate dynamic actin organization as templated by microtubules. In collaboration with the Kaverina laboratory, we provide exciting insights into the physiological relevance of the microtubule-CLASP-actin interaction. In Chapter 6, I discuss the overall implications of these results in the broader context of our understanding of microtubule and actin coordination and implications in the mechanical stability of cytoskeletal networks.

CHAPTER 2

in vitro reconstitution of microtubule and actin filament interactions

2.1 Introduction

The eukaryotic cell is a complex system with many different components. This complexity creates challenges in investigating the underlying mechanisms of cytoskeletal function in the cellular context. Over several decades, researchers have developed techniques to isolate components of the cytoskeleton from the cell to study in a minimal system. This concept, "bottom-up reconstitution," has led to major advances in the cytoskeletal field (Vale, 2014). Notably, the first successful use of *in vitro* reconstitution to study the contraction of actomyosin threads was done in the 1940's, where researchers demonstrated that muscle could be extracted from the animal and still contract with addition of nucleotide and salt (Szent-Gyorgyi, 1942). In the same journal publication, actin was first identified as a protein in the muscle stroma involved in muscle contraction (Szent-Gyorgyi, 1942). These findings encouraged others to use *in vitro* reconstitution to investigate the dynamic properties of cytoskeletal filaments.

The dynamic nature of microtubule and actin filaments was first observed *in vitro* in the late 20th century. First, the polymerization of purified actin was reconstituted *in vitro*, where researchers developed an understanding for the mechanisms underlying actin polymerization (Kasai et al., 1962; Woodrum et al., 1975). Shortly after, microtubules were reconstituted *in vitro* with the use of purified tubulin (Weisenberg, 1972) and further characterized by Mitchison and Kirschner, who discovered that microtubules undergo stochastic transitions between growth and shrinkage, termed dynamic instability (Mitchison and Kirschner, 1984). With established actin and microtubule *in vitro* reconstitution methods, scientists continued to advance these techniques exemplified by the introduction of purified actin binding proteins (ABPs) and microtubule associated proteins (MAPs) to study their role in the regulation of actin and microtubule dynamics.

In recent years, scientists in the cytoskeleton field have furthered the complexity of the *in vitro* reconstitution system to include a protein of interest and several types of cytoskeletal filaments, such as microtubules and actin filaments (Preciado López et al., 2014; Prezel et al., 2017). Preciado-López and colleagues published an *in vitro* reconstitution system that includes bundled actin filaments and dynamic microtubules to investigate the ability of an engineered protein, TipAct-GFP, to co-align dynamic microtubule extensions with bundled actin filaments (López et al., 2014; Preciado López et al., 2014). Shortly after, Prezel and colleagues

published a similar *in vitro* reconstitution system with both dynamic microtubules and actin filaments (Elie et al., 2015; Prezel et al., 2017). This system allowed researchers to investigate the role of tau in actin filament bundling and in crosslinking microtubules and actin filaments together. The minimal systems used in these studies were essential for characterizing the direct interactions between these proteins, which would be difficult to characterize in cells.

These recent methodological reports were the inspiration and basis for the study of the microtubule-CLASP-actin system presented in this work. This investigation takes advantage of the *in vitro* reconstitution technique, specifically to study the interactions between microtubules, actin filaments, and CLASP2. Using *in vitro* reconstitution provided a controlled system to study these interactions. We were able to control the concentrations of purified protein and visualize experiments with high-resolution Total internal reflection fluorescence (TIRF) microscopy. Subsequent data was suitable for image analysis using ImageJ (Schindelin et al., 2012) and MATLAB to investigate colocalization and detailed interactions of the three proteins. In this chapter, the major components and themes of the primary approach are included, with more specific detailed methods at the end of each results chapter.

2.2 Experimental Approach

2.2.1 Protein Purification

Multiple methods were used to prepare purified proteins for this study. Tubulin and actin are the essential building blocks for studying the cytoskeleton and were purified in a similar fashion. First, tubulin was extracted from bovine brains and was purified through rounds of temperature-dependent microtubule polymerization and depolymerization (Castoldi and Popov, 2003). Briefly, the brain was pre-clarified and then was homogenized in ice-cold depolymerization buffer. Then, the brain homogenate was centrifuged at 4C to collect the supernatant and discard the pellet containing any remaining brain tissue or debris. Next, nucleotides, glycerol, and high-molarity Piperazine-N,N'-bis(2-ethanesulfonic acid)(PIPES) buffer were added to the collected supernatant and incubated at 37C to allow for microtubule polymerization. Then, the supernatant was ultracentrifuged to pellet the polymerized microtubules; the supernatant containing incompetent tubulin was discarded. Microtubules were then depolymerized in ice-cold depolymerization buffer and ultracentrifuged, where the supernatant was collected and the pellet, containing incompetent microtubules, was discarded. Next, the polymerization step was repeated, where the pellet of microtubules was collected. Finally, the microtubule pellet was depolymerized again at 4C and then subjected to a final cold spin. The supernatant was collected and immediately flash-frozen for long term storage and use in experiments. The use of the high-molarity buffer assists in excluding contaminating MAPs, by interrupting MAP interaction

with microtubules. This improvement removed an ion-exchange chromatography step in the purification of tubulin (Castoldi and Popov, 2003).

As stated above, actin was purified in a similar fashion as tubulin, with a round of polymerization and depolymerization. Here, actin was purified in two steps, 1) preparing muscle acetone powder and 2) muscle actin isolation (Pardee and Spudich, 1982). First, muscle acetone powder was prepared by first mincing 500 grams of flash frozen chicken breast and then subjecting to 10 extraction steps. The muscle residue is extracted with subsequent stirring in potassium chloride, baking soda, an aminopolycarboylic acid, water, and acetone. The remaining residue is air-dried overnight and stored at -20C for use. For actin isolation, 5 grams of acetone powder was further extracted in Buffer A, a Tris buffer made for depolymerizing conditions containing Adenosine triphosphate (ATP), a reducing agent (βME), calcium chloride, and azide. Then, the extraction was filtered through cheesecloth and subjected to centrifugation to remove bulk solids. The supernatant was collected, and salts and nucleotide were added to induce actin polymerization at 4C. To remove tropomyosin, solid potassium chloride is added to the supernatant for a high salt wash. After this wash, the sample is ultracentrifuged to remove incompetent actin in the supernatant and keep the actin filaments in the pellet. Over three days, the actin filaments were put under dialysis at 4C with 2-3 Buffer A changes to allow for complete depolymerization. Finally, the sample was then centrifuged to remove any remaining filaments or oligomers of actin and the supernatant was flash-frozen for storage.

Isolated tubulin and actin were labeled with fluorescent dyes for imaging and tubulin was biotinylated to allow for surface binding to the coverslip. Purified tubulin was polymerized and covalently labeled with biotin, tetramethyl rhodamine, or Alexa 647, and then depolymerized, followed by another round of polymerization and depolymerization to obtain labeled, functional tubulin (Hyman et al., 1991). Purified G-actin was labeled with AlexaFluor 647 in a similar fashion for actin polymerization experiments (Shekhar, 2017). It is important to note here that tubulin and actin are polymerized into filament form before covalently labeling, to ensure the fluorescent dye binds to residues not involved in the polymerization activity of tubulin or actin.

Microtubule associated proteins were purified using standard biochemical approaches. Full-length CLASP2α with histine, eGFP, and strep tags, was expressed using a *S.frugiperda* (Sf9) insect cell system. CLASP2*a* was purified from cell lysates through a HisTrapHP column and then further purified through size exclusion chromatography. The minimal CLASP construct, L-TOG2-S, with His and eGFP tags, was expressed using an *E.coli* bacterial system. L-TOG2-S was purified from cell lysates through a HisTrapHP column and then was desalted in a PD-10 desalting column. Proteins were flash frozen into small, single use aliquots for ex-

periments.

2.2.2 in vitro reconstitution of microtubules and actin filaments

To study the ability of CLASP to crosslink microtubules and actin filaments simultaneously, an *in vitro* reconstitution approach was used with purified protein components and TIRF microscopy. In brief, this assay consists of stabilized microtubules, immobilized on the surface with a protein of interest and stabilized actin filaments floating in solution. In other experiments, the actin form was adjusted, where monomeric G-actin was in solution. The experiment is imaged over time using TIRF microscopy, resulting in a time-lapse movie. Fluorescently tagged proteins are used to visualize their location. Movies are analyzed using methods described below, to measure co-localization and characterize actin filament landing events. Any modifications to this experimental design in the results will be specified in the corresponding chapters.

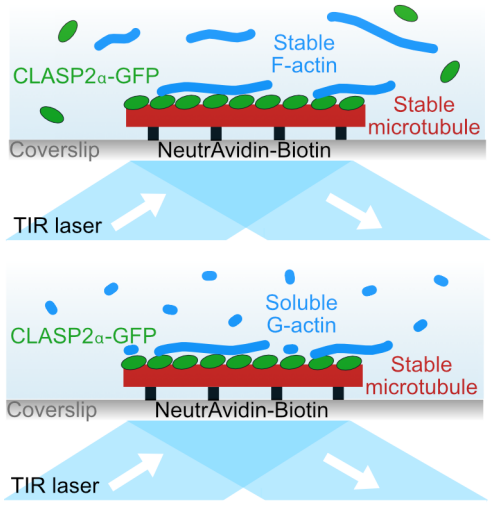

Figure 2.1: Schematic diagrams for experimental setup for investigating microtubule-actin interactions as mediated by CLASP2α using TIRF microscopy
The primary experimental setup for the F-actin landing assay. Taxol stabilized biotinylated microtubules are bound to the coverslip via NeutrAvidin-biotin linkage, then CLASP2α-GFP and phalloidin stabilized F-actin (Chapter 3 and 4) or soluble G-actin (Chapter 5) are added together to measure crosslinking interactions. For all experiments, dynamics and interactions are limited to the coverslip surface, ideal for TIRF microscopy described in further sections.

Much of the work presented here used *in vitro* reconstitution of microtubules and actin filaments, specifically the actin filament landing assay, a novel method in the field that will be described briefly here (Figure 2.1). To increase the amount of positive signal to background noise in our imaging, high-precision coverslips are cleaned with piranha solution (30/70% (v/v) hydrogen peroxide and sulfuric acid) to remove all organic material (Gell et al., 2010). Then coverslips were treated with silane to make the glass surface hydrophobic.

The hydrophobic surface assists with passivation of the glass surface for experiments. Also, the silane treatment further protects the surface from future debris. Coverslips of 18 x 18 and 22 x 22 nm size were cleaned in this manner. Two coverslips are used to create flow channels for experiments. Assembled on a custom brass holder, one 22 x 22 mm coverslip is placed in the holder. Then, three narrow strips of parafilm, of about 3 mm in width, are placed horizontally, 2-3 mm apart, on the coverslip in an arrangement making two lanes, termed flow channels. Next, one 18 x 18 mm coverslip is placed on top creating a sandwich, with the parafilm in between the coverslips. A hot, 18 x 18 mm heat block is placed gently on top to melt the parafilm and bind the coverslips together. Due to the size difference in the coverslips, a platform is created for easy addition of new solutions and flow through the channel.

Once assembled, solutions are flown through the channel to passivate the surface. For most experiments, NeutrAvidin (25 µg/ml) was used to passivate the surface for binding to biotinylated microtubules. Then, the surface was blocked with Pluronic F127 to decrease non-specific binding of proteins to the surface. The channels are washed in between these steps with a microtubule-actin buffer (MRB80; 80 mM PIPES, 4 mM MgCl2, 1 mM EDTA, pH 6.8). Channels were prepared immediately before experiments and were stored in humid conditions to avoid channels drying out.

Taxol is a antimitotic agent and is a commonly used drug to treat specific cancers (Rowinsky et al., 1990). Taxol functions by changing the structure of the microtubule and stabilizing it (Arnal and Wade, 1995). Here, Taxol was used to stabilize microtubule templates for investigating F-actin co-alignment. Long, Taxol stabilized microtubules, composed of 16% biotinylated and 5% Cy5 tubulin, were prepared for experiments. Briefly, 35 µM tubulin was polymerized with GTP and MgCl2 at 35C for 1 hour. Then, microtubules were ultracentrifuged at 126,000 x g for 5 minutes to remove any remaining tubulin dimers from solution. The microtubule pellet was resuspended in 50 - 100 µl of MRB80 supplemented with Taxol. Taxol stabilized microtubules stock was used for up to 5 days. For experiments, microtubules were perfused through the flow cell to bind to the surface. Channel was then washed with MRB80, once an optimal density of microtubules was observed. An imaging buffer (40 µg/ml glucose oxidase, 40 mM di-glucose, 18 µg/ml catalase, 0.08 mg/ml casein, 10 mM Dithiothreitol (DTT), and 0.2 mM ATP) was then added to the flow cell in preparation for imaging. The reagents in the imaging buffer consist of oxygen scavengers to promote a protein-friendly reducing environment.

Finally, a reaction mix is perfused through the channel. For most experiments, 100 nM CLASP2α-GFP and 6.5 µM phalloidin stabilized F-actin was perfused through the channel with simultaneous imaging. In

brief, F-actin was prepared by first pre-clarifying G-actin and then was polymerized with the addition of KCl, MgCl2, and ATP for 1 hour. Then, equimolar amount of Tetramethylrhodamine (TRITC)-Phalloidin was added to the F-actin mix and incubated for 15 minutes at room temperature. Finally, F-actin was ultra-centrifuged at 150,000 x g for 10 minutes and resuspended with MRB80, DTT, and ATP. F-actin stock was used for up to a week. This method can easily be modified with different proteins in solution or different cytoskeletal polymers immobilized on the surface (Figure 2.1). Such modifications were used in this study, depending on the experimental question, and are specified in the corresponding chapters.

2.2.3 TIRF microscopy

In combination with *in vitro* reconstitution, we use TIRF microscopy to visualize the interactions and dynamics of our system. TIRF microscopy is a light microscopy technique that provides the excitation of fluorophores in a very thin region (Fish, 2022; Gell et al., 2010). TIRF relies on the laser beam hitting the coverslip at a specific critical angle, where the light is completely reflected from the glass/solution interface (Figure 2.2). This reflection generates a thin electromagnetic field, termed the evanescent wave, within the sample. The depth of the evanescent wave is dependent on the angle of the incident light, wavelength, and its refractive index difference (Figure 2.2). Typically, the evanescent wave is 100 – 200 nm in depth. The very thin slice of the imaging plane greatly reduces the number of fluorescent proteins excited within the sample decreasing background signal, hence improving the signal to noise ratio. For our purposes, we immobilize microtubules to the surface to then measure dynamics occurring within the microtubule plane, excited within the evanescent wave.

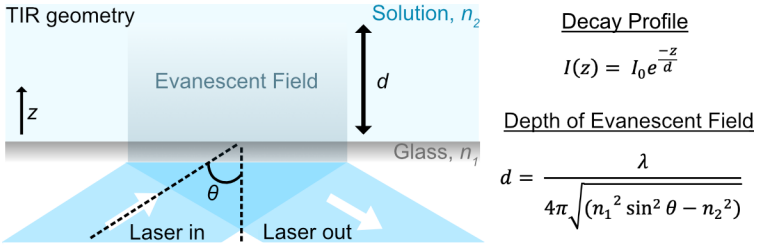

Figure 2.2: Simplified optical geometry of the total internal reflection (TIR) generation of the evanescent wave used in TIRF microscopy.

The intensity of the evanescent field (I) decays exponentially in the z plane, perpendicular to the glass surface into the solution. This decay has a characteristic depth (d), which is the distance at which the intensity has decreased e-fold. The laser wavelength (λ), the incidence angle of the laser light (θ), which is the critical angle for complete internal reflection, the refractive index of the glass (n_1), and refractive index of the solution (n_2) determine the depth of the evanescent field generated. To facilitate TIR, the refractive index of the glass should be greater than that of the solution. Fluorophores within the evanescent field depth will be excited and visualized using TIRF microscopy.

For most of this work, the imaging was performed on a Nikon Eclipse Ti microscope with a 100x/1.49 n.a. TIRF objective, equipped with Andor iXon Ultra EM-CCD camera, 488-nm, 561-nm, and 640-nm solid state lasers (Nikon Lu-NA), Finger Lakes Instruments HS-625 high-speed emission filter wheel, and standard filter sets. Laser exposure time was 100 ms for all experiments. Experiments were performed at 35C using a Tokai Hit objective heater. Images were acquired using NIS-Elements (Nikon). Time-lapse lengths of movies varied between 10 – 60 minutes and frame rates varied between 0.3 – 5 frames per second depending on the experimental question.

2.3 Image Analysis

Colocalization is a very common analysis method when using fluorescence microscopy to compare two fluorescence distributions to infer whether those particles are associated (Dunn et al., 2011). There are several statistical measurements to quantify colocalization of images and for this work we used the Pearson correlation coefficient (PCC) value. To measure colocalization of an image, the intensity of one color (Red, R) is plotted against the intensity of the second color (Green, G). The slope of the distribution reflects how colocalized the fluorescent probes are. The PCC value is a statistical measure of correlation for two colors and is represented as,

$$PCC = \frac{\sum_i (R_i - R) x (G_i - G)}{\sqrt{\sum_i (R_i - R)^2 x \sum_i (G_i - G)^2)}}, \tag{2.1}$$

where R_i and G_i refer to the color intensity values of pixel i, and R and G are the mean intensities from the entire image. PCC values range between -1 and 1, where 1 represents a perfect correlation, a value of 0 represents no relation, and -1 represents an inverse relationship between the two. We used an ImageJ plugin, JACoP (Just Another Co-localization Plugin) to measure colocalization of microtubules and F-actin (Bolte and Cordelières, 2006; Dunn et al., 2011). Colocalization was also measured using the MATLAB correlation coefficient function. This quantification allowed for us to quantify the relationship between microtubules-CLASP, F-actin-CLASP, and microtubules-F-actin when CLASP2 is localized along the microtubule lattice (Chapters 3-4).

2.4 Summary

The use of both biochemical *in vitro* reconstitutions, TIRF microscopy, and quantitative image analysis allows for the robust study of the direct interactions of microtubules and actin filaments together in the presence of MAPs. Future work will continue to increase the complexity of this minimal system to build up the cell to elucidate the mechanisms underlying cellular function.

CHAPTER 3

CLASP2 weakly interacts with actin filaments in vitro

Adapted from: Rodgers, N.C., E.J. Lawrence, A.V. Sawant, N. Efimova, G. Gonzalez-Vasquez, T.T. Hickman, I. Kaverina, and M. Zanic. 2023. CLASP2 facilitates dynamic actin filament organization along the microtubule lattice. Molec. Biol. Cell. 34(3). doi: 10.1091/mbc.E22-05-0149

3.1 Introduction

3.1.1 CLASPs are a family of MAPs that regulate the microtubule cytoskeleton

Cytoplasmic linker associated proteins (CLASPs) are a well-studied family of microtubule-associated proteins (MAPs), that have been implicated in interacting with both microtubules and actin filaments (Dogterom and Koenderink, 2019; Engel et al., 2014; Tsvetkov et al., 2007). CLASPs are known as microtubule stabilizers with essential roles in cell division, cell migration, and neuronal development (Lawrence et al., 2020). There are two paralogs of CLASP, CLASP1 and CLASP2, that are alternatively spliced resulting in multiple isoforms, which are differentially expressed and may have some isoform-specific functions (Akhmanova et al., 2001; Lawrence et al., 2020). *in vitro* studies with purified proteins established that CLASPs promote sustained microtubule growth by suppressing microtubule catastrophe and promoting microtubule rescue (Aher et al., 2018; Akhmanova et al., 2001; Al-Bassam et al., 2010; Lawrence et al., 2018; Leano et al., 2013; Maki et al., 2015; Patel et al., 2012). In cells, CLASPs are targeted to growing microtubule plus ends via a direct interaction with microtubule end-binding EB proteins and can specifically regulate microtubule dynamics at the actin-rich cell cortex (Mimori-Kiyosue et al., 2005). Furthermore, CLASPs are involved in the process of microtubule plus-end capture at the cell cortex through interactions with LL5β, a component of the cortical microtubule stabilization complex (Hotta et al., 2010; Lansbergen et al., 2006; Stehbens et al., 2014). CLASPs' stabilization and anchoring of microtubules is also important for the regulation and dynamics of podosomes, polymerizing actin-based structures, in vascular smooth muscle cells (Efimova et al., 2014; Zhu et al., 2016). All these studies suggest CLASPs' roles in the interplay between the microtubule and actin networks. However, it remains unclear if CLASPs directly interact with the actin network in these contexts.

3.1.2 CLASPs are implicated to interact with the actin cytoskeleton

A previous study investigating CLASP-actin interaction reported that the two CLASP paralogs, CLASP1 and CLASP2, colocalize with actin stress fibers in primary fibroblasts and spinal cord neurons (Tsvetkov

et al., 2007). The authors found that both CLASP paralogs coimmunoprecipitated with actin from fibroblast cells and suggested that the TOG1 domain and serine-arginine rich region of CLASP2α facilitate the F-actin interaction. Another study, using co-sedimentation experiments with purified proteins reported a direct interaction between F-actin and CLASP2α, as well as co-sedimentation of G-actin with microtubules in the presence of CLASP2α (Engel et al., 2014). To our knowledge, these two reports provide the only evidence of CLASP-actin interaction, leaving open the question of whether CLASP alone is sufficient for crosslinking of microtubules and actin filaments, which may play a role in the organization of stress fibers in cells.

3.2 Results

3.2.1 CLASP2α does not co-localize with single actin filaments in vitro

To investigate CLASP2α interaction with F-actin, we first used TIRF microscopy to directly observe colocalization of CLASP2α and F-actin in an *in vitro* reconstitution assay with purified proteins (Figure 3.1). Here, we used stabilized microtubules, as a positive control, to measure colocalization. Microtubules were stabilized using a slowly hydrolysable GTP analog, guanylyl(α,β)-methylene diphosphonate (GMPCPP) (Hyman et al., 1991). As expected, CLASP2α localized along the entire microtubule lattice (Figure 3.1A). CLASP2α-GFP colocalized with microtubules with a mean PCC value of 0.831 ± 0.006 (mean, SEM, N = 24 field of views) (Figure 3.1B). Phalloidin-stabilized F-actin was then used to probe CLASP2α interaction. Surprisingly, under the same conditions, no colocalization of CLASP2α with single F-actin was observed with a mean PCC value of 0.026 ± 0.004 (mean, SEM, N = 25 field of views) (Figure 3.1A-B). In these conditions, CLASP2α does not colocalize with single actin filaments.

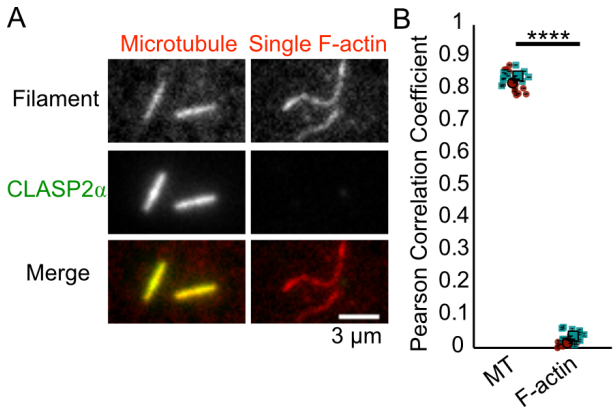

Figure 3.1: CLASP2 does not co-localize with single actin filaments *in vitro*
A) TIRFM images of CLASP2 (green) co-localization with microtubules (red) and single F-actin (red). The microtubules and single F-actin intensities are scaled differently for better visualization. CLASP2α intensity is scaled the same. B) The Pearson correlation coefficient (PCC) values for co-localization of CLASP2 on microtubules (N = 24 field of views) and single F-actin (N = 25 field of views) over 2 experimental days noted by color. Error bars are the SEM. Mann-Whitney t-test: **** $p < 0.0001$.

3.2.2 The minimal CLASP construct, L-TOG2-S, weakly binds F-actin

Previous reports using co-immunoprecipitation from fibroblast cells implicated a Serine-Arginine rich region of CLASP2α in its interaction with actin (Tsvetkov et al., 2007). Recently, a minimal CLASP2 construct, L-TOG2-S, containing a single TOG2 domain and the Serine-Arginine rich region, was reported to recapitulate CLASP's effect on microtubule dynamics (Aher et al., 2018)(Figure 3.2A). Based on our difficulty measuring colocalization of CLASP2α with F-actin using TIRF microscopy, we alternatively measured the direct interaction of the L-TOG2-S minimal construct of CLASP2 with F-actin using co-sedimentation experiments (Figure 3.2B). We measured the fraction of GFP-L-TOG2-S protein pelleting with F-actin over a range of F-actin concentrations and determined the binding affinity of the L-TOG2-S – F-actin interaction to be 1.1 ± 0.6 µM (95% CI) (Figure 3.2C). This result supports that the CLASP2α TOG2 domain with serine-arginine rich region can bind weakly to phalloidin-stabilized F-actin.

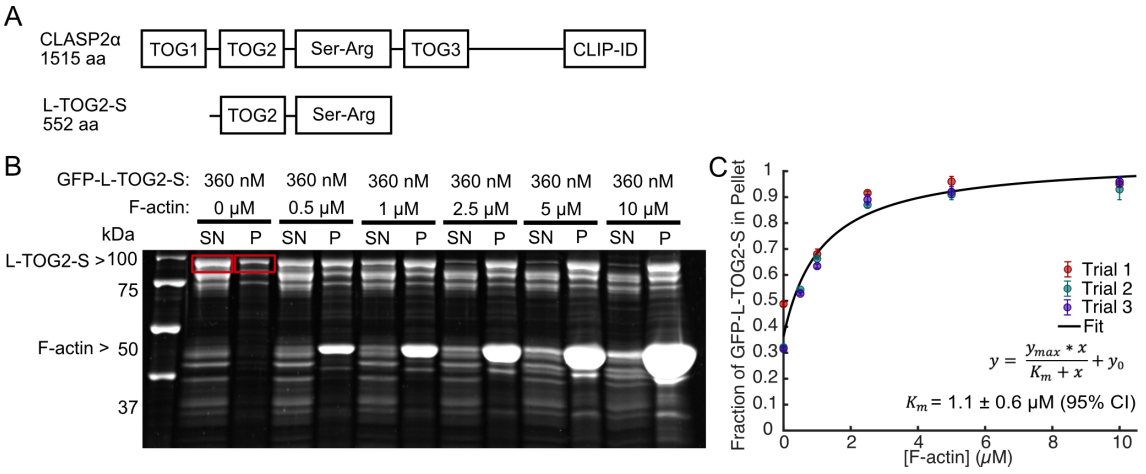

Figure 3.2: Minimal CLASP construct, L-TOG2-S, weakly binds F-actin
A) Schematic of the domain structure of human CLASP2α and minimal construct, L-TOG2-S. B) Example SDS-PAGE gel from high-speed co-sedimentation experiments. Red boxes represent L-TOG2-S bands quantified for supernatant and pellet. C) The quantification of the fraction of GFP-L-TOG2-S in the pellet as a function of F-actin concentration Data points of different colors represent measurements from one experiment. Errors bars are the error propagation (see Methods). Results are fit to the equation in panel and represented by the black line. Experiments performed in triplicate.

3.2.3 CLASP2α preferentially localizes to bundled actin filaments *in vitro*

In cells, CLASP2α was observed to colocalize with actin stress fibers (Tsvetkov et al., 2007). Therefore, we hypothesized that CLASP2 may colocalize with bundled actin structures *in vitro* using TIRF microscopy. To investigate whether CLASP2α interacts with bundled F-actin, we generated bundles using crowding agents, similar to previously published reports (Figure 3.3) (Preciado López et al., 2014). Here, we observed some colocalization of CLASP2α with bundled actin structures (Figure 3.3A). Interestingly, CLASP2α localiza-

tion appeared to be stronger for brighter bundles of actin filaments (Figure 3.3B). Drawing an intensity line scan across a dimmer actin structure and brighter actin structure within the same area, we find the CLASP2α signal to correlate with the actin signal, only for the brighter actin structure. Therefore, we measured the PCC for CLASP2α localization on varying intensities of F-actin (Figure 3.3C-D, see Methods). Comparing the PCC values for low intensity F-actin and bright intensity F-actin in the same field of view, we observed a significant increase in colocalization for bundled F-actin (Figure 3.3D, mean PCC = 0.025 ± 0.003 versus PCC = 0.61 ± 0.03, SEM, N = 39 field of views). CLASP2α colocalization with microtubules was measured in parallel, where we found no significant difference between localization of CLASP2α to microtubules as compared to higher intensity F-actin (Figure 3.3D). Together, these results support that CLASP2α weakly interacts with F-actin and may preferentially interact with bundled F-actin.

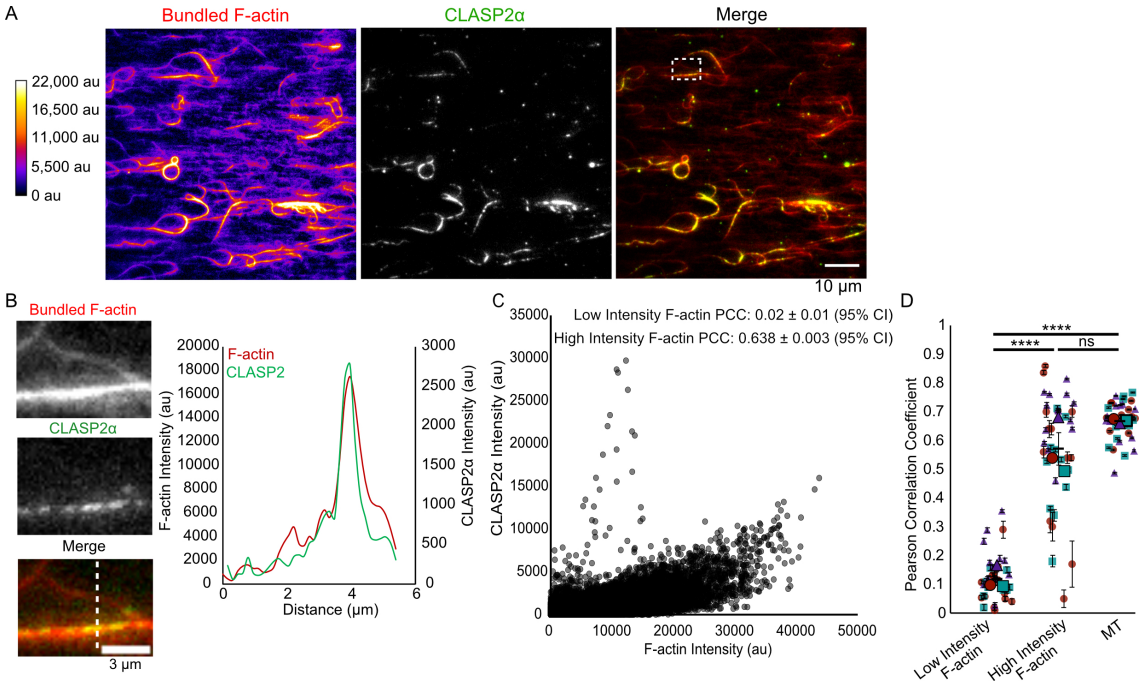

Figure 3.3: CLASP2 preferentially localizes to bundled actin filaments *in vitro*
A) Example images of CLASP2α (green) localization to phalloidin-stabilized methylcellulose bundled F-actin (red). Bundled F-actin alone image is colored based on intensity. White dashed-box indicates the zoomed in images in Panel B. B) Example images of CLASP2 (green) localization on methylcellulose bundled F-actin (red). Dashed white line denotes intensity line scan below images. Plot of F-actin and CLASP2 intensity along the line. C) CLASP2 intensity versus F-actin intensity for image in Panel A to demonstrate PCC calculation. D) Quantification of the PCC values for CLASP2 localization on methylcellulose-bundled F-actin (N = 39 fields of view over 3 experimental days) and microtubules as a positive control (N = 37 fields of view over 3 experimental days). Different colored data points represent different experimental days. The PCC is reported for methylcellulose bundled F-actin intensities divided into low intensity F-actin and bundled intensities (see Methods). Error bars are the SEM. Kruskal-Wallis test, with multiple comparisons, ns $p > 0.05$, **** $p < 0.0001$.

3.3 Discussion

CLASP2α has been reported to interact with actin filaments previously, even though CLASP2α does not contain a recognized actin binding domain (Engel et al., 2014; Tsvetkov et al., 2007). Due to this discrepancy, we first investigated the ability of CLASP2α to directly interact with F-actin. In our experiments, we were able to determine a relative affinity for the interaction between the minimal CLASP2 construct and F-actin. The minimal CLASP2 construct (L-TOG2-S) contains the TOG2 domain and portion of the Serine-Arginine rich region of CLASP2 (Aher et al., 2018). Tsvetkov and colleagues reported that the Serine-Arginine rich region colocalized with actin stress fibers and coimmunoprecipitated with actin (Tsvetkov et al., 2007). Our result that the minimal CLASP2 construct can bind actin is thus consistent with previously published results.

We determined that the relative affinity for the L-TOG2-S construct with F-actin to be in the micromolar range, which is relatively weak compared to the nanomolar range affinity of CLASP for microtubules (Patel et al., 2012). The Serine-Arginine rich region of CLASP2 is highly electrostatic (Al-Bassam et al., 2010; Patel et al., 2012). This low affinity and electrostatic region may explain the differential localization of CLASP2 to single actin filaments versus larger actin structures. Other MAPs and binding partners of CLASPs, EB and CLIP-170, were reported to weakly interact with F-actin and these interactions were found to be electrostatic in nature (Alberico et al., 2016; Wu et al., 2021). However weak, these interactions can still occur in the cell in regions of high actin density, such as the lamella in migrating cells, which has been shown to have actin concentrations in the hundreds of micromolar (Abraham et al., 1999; Koestler et al., 2009). Thus, proteins that have weaker interactions with F-actin, such as CLASP, EB, and CLIP-170, could be important when located near large actin networks or actin bundles. Future work investigating the CLASP domains and the role of ionic interactions with F-actin will better our understanding of CLASP as an actin binding protein.

3.4 Methods

3.4.1 Protein Purification

His-CLASP2α-EGFP-Strep was expressed in baculovirus-infected Sf9 insect cells and His-EGFP-L-TOG2-S was expressed in BL21(DE3) E. coli cells, purified and stored in CLASP storage buffer (25 mM PIPES [piperazine-N,N'-bis(2-ethanesulfonic acid)] (pH 6.8), 150 mM KCl, 5% (v/v) glycerol, 0.1% (v/v) Tween-20, 50 mM L-glutamate, 50 mM L-arginine, and 1 mM DTT). Tubulin and G-actin purification and labeling are described in Chapter 2. G-actin was stored in general actin buffer (2 mM Tris-HCl pH 8.0, 0.2 mM ATP, 0.5 mM DTT, 0.1 mM CaCl2, and 1 mM NaN3) (Pardee and Spudich, 1982). Protein concentration was determined using absorbance at λ = 280 nM and 290 nM for G-actin. For colocalization experiments, unlabeled and rhodamine labeled G-actin was purchased from Cytoskeleton, Inc and stored in general actin

buffer.

3.4.2 Colocalization Experiments

GMPCPP microtubules were prepared by incubating 1 mM GMPCPP with 1 mM MgCl2, 5 μM tubulin, and MRB80 for about an hour. GMPCPP microtubules were labeled with 20-24% tetramethyl rhodamine. GMPCPP microtubules were then spun down and resuspended in 100 μL MRB80. Phalloidin-stabilized F-actin, labeled with 30% tetramethyl rhodamine (Cytoskeleton, Inc), were prepared as described by Preciado-López and colleagues (Preciado López et al., 2014). F-actin (2-3 μM) was bundled with 0.5% methylcellulose for 5 minutes at room temperature. Either GMPCPP microtubules, single F-actin, or bundled F-actin were added to an anti-rhodamine functionalized chamber and allowed to bind to the surface. Chamber was then washed with imaging buffer (MRB80, 0.1% methylcellulose, 0.2 mM ATP, 40 μg/mL glucose oxidase, 40 mM glucose, 16 μg/mL catalase, 0.08 mg/mL casein, and 10 mM DTT). Then, 100 nM CLASP2α-GFP in imaging buffer was added. Experiments were done 2-3 times. 10-15 fields of view were randomly imaged along the channel for colocalization. 488- and 561-nm lasers were used for colocalization experiments.

3.4.3 Colocalization Image Analysis

ImageJ was used to measure the intensity values of the microtubule or F-actin and CLASP channels. First, images were cropped to remove out of focus pixels. Then, the background intensity was subtracted using the 50-pixel rolling ball background subtraction plugin. The intensity values were saved, and Pearson correlation coefficient was calculated using the corrcoef MATLAB function. Single and bundled F-actin were differentiated using intensity. For each image, single filaments were cropped out of the field of view and the mean filament intensity was measured, along with the standard deviation. Single filaments were then defined as a range between one standard deviation below the mean and two standard deviations above the mean. Bundled F-actin were defined as intensities two standard deviations above the single F-actin mean. Then, the PCC values were measured for those ranges of F-actin pixel intensities. Plots produced in GraphPad Prism.

3.4.4 High speed co-sedimentation experiments

F-actin was prepared as described in Chapter 2, however with unlabeled phalloidin stabilization. GFP-L-TOG2-S protein was pre-clarified by spinning down at 400,000 x g for 10 minutes at 4C. A titration of F-actin concentrations (0, 0.5, 1, 2.5, 5, and 10 μM) were incubated with 360 nM GFP-L-TOG2-S at 37C for 15-30 minutes in general actin buffer. Then, samples were ultracentrifuged at 184,000 x g for 20 minutes at 26C. 50 μL of the top supernatant was collected and 13 μL of 5X SDS Loading Dye was added. The remaining supernatant was collected and stored as waste. The pellet was resuspended in 63 μL of 1X SDS

Loading Dye and subsequently stored at -20C. Samples were then prepared for electrophoresis. The pellet sample was thawed and 15 µl of sample was added to 15 µl of 1X SDS Loading Dye. 30 µl of top supernatant sample was thawed and then samples were boiled at 95C for 5 minutes, and then loaded onto a 12% SDS-PAGE gel. Gels were stained with SYPRO Ruby Protein Gel Stain and imaged with a Gel Doc EZ system. Experiments were performed in triplicate.

3.4.5 Protein Gel Densitometry

Gels were quantified using the Gel Analyzer ImageJ plugin. In brief, lane profile plots were produced using the rectangular selection tool, lines were drawn to enclose the peaks of interest, and the peak areas were measured in triplicate. The top band of the GFP-L-TOG2-S protein was measured. The peak area measurements for the GFP-L-TOG2-S protein were averaged. Then, each supernatant and pellet peak areas were summed and the peak area of the GFP-L-TOG2-S in the pellet sample was divided by the total amount of protein in the sample. Then, the fraction of GFP-L-TOG2-S in the pellet was plotted as a function of F-actin concentration and fit to the equation,

$$y = \frac{y_{max} * [x]}{K_m + [x]} + y_0, \tag{3.1}$$

using the MATLAB Curve Fitting Tool (MathWorks, Inc.). The ymax, yo, and Km values were calculated with the 95% confidence interval. The resulting fit was plotted with the individual data points in MATLAB. Error bars on the individual data points are the error propagation.

CHAPTER 4

CLASP2 directly crosslinks multiple actin filaments to the microtubule lattice

Adapted from: Rodgers, N.C., E.J. Lawrence, A.V. Sawant, N. Efimova, G. Gonzalez-Vasquez, T.T. Hickman, I. Kaverina, and M. Zanic. 2023. CLASP2 facilitates dynamic actin filament organization along the microtubule lattice. Molec. Biol. Cell. 34(3). doi: 10.1091/mbc.E22-05-0149

4.1 Introduction

Our previous findings demonstrate that CLASP2α can directly interact with actin filaments and microtubules, thus we were interested in determining if CLASP2α could simultaneously bind both. Since we suspected that the CLASP2α interaction with F-actin is relatively weak, we were interested in investigating crosslinking when CLASP2 is concentrated along the entire microtubule lattice. A form of microtubule and actin filament crosslinking in the cell includes interactions that occur along the microtubule lattice, such as what has been reported for neuronal MAP tau (Elie et al., 2015). Tau has been shown to be involved with supporting microtubule growth into the filopodia of cortical growth cones (Biswas and Kalil, 2018). Intriguingly, CLASPs are also implicated in the crosstalk of the microtubule and actin network in neurons (Dogterom and Koenderink, 2019). Specifically, *Xenopus* CLASP1 depletion in spinal cord neurons resulted in similar defects in microtubule outgrowth into actin-rich growth cones, as was found for tau (Marx et al., 2013). Here, we explored the crosstalk interactions between microtubules and actin filaments that occur when CLASP2 is localized along the microtubule lattice.

4.2 Results

4.2.1 Human CLASP2α directly crosslinks actin filaments to microtubules

To investigate CLASP2α's ability to directly crosslink microtubules and actin, we bound Alexa-647-labeled, Taxol-stabilized microtubules to the surface of a coverslip. Next, we added 6.5 μM TRITC-phalloidin-stabilized F-actin in the absence (Figure 4.1A, top) or presence (Figure 4.1A, middle) of 100 nM purified CLASP2α-GFP to the flow-cell. As expected, we observed specific CLASP2α-GFP localization along the microtubule lattice (Figure 4.1A, middle). We quantified the correlation between the CLASP2α-GFP and microtubule signals after 10 minutes of incubation using the PCC and measured a high degree of correlation (PCC = 0.88 ± 0.06, SD, N = 9 fields of view (FOV) over 3 independent experimental days) (Figure 4.1B). The investigation of TRITC-phalloidin-F-actin showed that F-actin robustly co-localized with microtubules in the presence of CLASP2α-GFP (PCC = 0.86 ± 0.05, SD, N = 9 FOVs over 3 independent experimental

days) (Figure 4.1A,C). No significant colocalization between microtubules and F-actin was observed in the absence of CLASP2α (PCC = 0.022 ± 0.001, SD, N = 9 FOVs over 3 independent experimental days) (Figure 4.1A,C). Furthermore, we confirmed that the co-localization of F-actin with microtubules did not depend on stabilization of F-actin using phalloidin, as F-actin also localized to CLASP2-coated microtubules in the absence of phalloidin (Figure 4.2). Taken together, we conclude that CLASP2α directly crosslinks F-actin to microtubules.

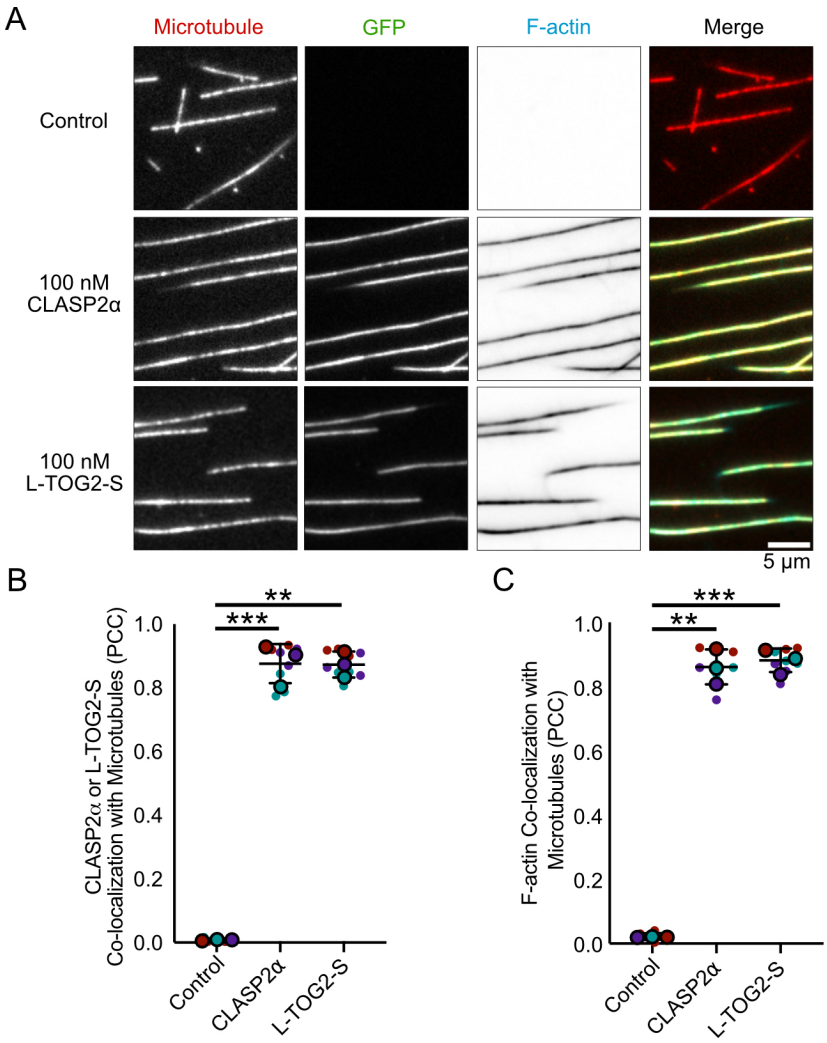

Figure 4.1: Human CLASP2α directly crosslinks actin filaments to microtubules.
A) Representative images of Taxol-stabilized microtubules incubated for 10 minutes with storage buffer, 100 nM CLASP2α-GFP, or 100 nM GFP-L-TOG2-S and 6.5 µM TRITC-Phalloidin F-actin. B) Quantification of co-localization between either CLASP2α or L-TOG2-S with microtubules using the Pearson correlation coefficient (PCC). C) Quantification of co-localization between actin filaments and microtubules, using the PCC. Small data points are individual PCC measurements and large data points are the mean PCC for three independent experimental days, represented by color. Error bars are the standard deviation. Kruskal-Wallis test multiple comparisons, ** $p < 0.01$ and *** $p < 0.001$. Comparisons between CLASP2α and L-TOG2-S are ns, $p > 0.05$.

Since we were able to determine the relative binding affinity of the minimal CLASP2 construct and F-actin, we wondered whether this CLASP2 construct is also sufficient to crosslink microtubules and F-actin. We used the same TIRF-based approach to investigate TRITC-phalloidin-F-actin localization on microtubules in the presence of purified 100 nM GFP-L-TOG2-S. As expected, GFP-L-TOG2-S showed strong localization to microtubules (PCC = 0.87 ± 0.04, SD, N = 9 FOVs over 3 independent experimental days) (Figure 4.1A,B). Furthermore, we found that F-actin also robustly colocalized with microtubules in the presence of GFP-L-TOG2-S (PCC = 0.88 ± 0.04, SD, N = 9 FOVs over 3 independent experimental days) (Figure 4.1A,C). Taken together, these results demonstrate that, despite the relatively weak direct interaction with F-actin, the minimal CLASP2α construct containing a single TOG2 domain and the Serine-Arginine rich region is sufficient to crosslink F-actin to microtubules.

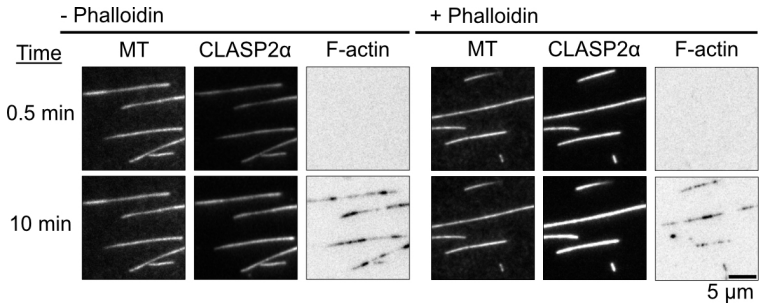

Figure 4.2: Accumulation of multiple actin filaments on microtubules is not dependent on TRITC-phalloidin stabilization.

Example TIRF time-lapse images of 1 μM phalloidin-stabilized F-actin and 1 μM F-actin (20% Alexa647-labeled) localizing along CLASP2α-coated microtubules.

4.2.2 CLASP2α mediates sequential binding of actin filaments along the microtubule lattice

To further investigate how actin filaments interact with microtubules in the presence of CLASP2α, we imaged TRITC-phalloidin-F-actin on microtubules over time for up to 40 minutes. We observed the initial landing of actin filaments within two minutes (Figure 4.3A). Notably, the F-actin signal continued to increase over time, reaching saturation within the duration of the experiment (Figure 4.3B). A closer inspection of the increasing TRITC-phalloidin-F-actin intensity on individual microtubules revealed step-like increases in fluorescence intensity on a region of microtubule lattice (Figure 4.3C), suggesting sequential binding of actin filaments. Using a stepping analysis (Bronson et al., 2009), we measured the accumulation of F-actin within a 3-pixel-wide (480 nm) microtubule segment over a period of 40 minutes. The mean number of landing events was 18 ± 0.6 (SD, N = 91, 99, and 54 microtubule lattice segments analyzed on three experimental days), with up to 11 sequential F-actin landing events occurring on a single microtubule segment (Figure 4.3D).

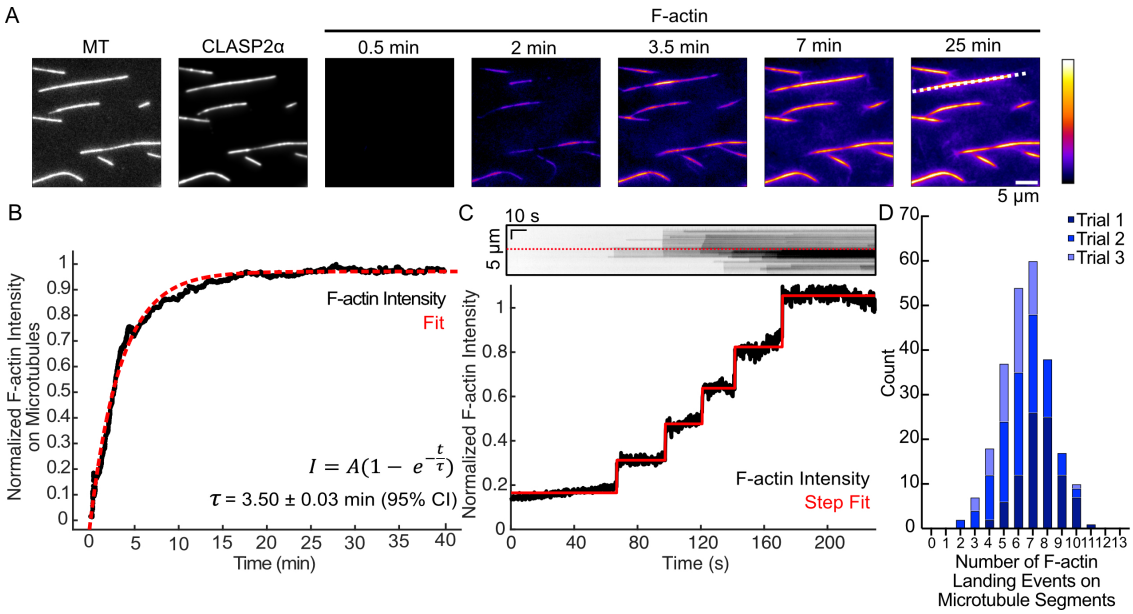

Figure 4.3: CLASP2 mediates sequential binding of actin filaments along the microtubule lattice. A) Example time-lapse TIRFM images of Taxol-stabilized microtubules, in the presence of 100 nM CLASP2α-GFP and addition of 6.5 µM TRITC-phalloidin-stabilized F-actin. White dotted line corresponds to the kymograph in Panel C. B) Example normalized actin filament intensity in microtubule areas over time for the images in panel A. Red dotted line represents the fit to the intensity over time equation. C) Top: kymograph of the F-actin channel for an example microtubule (denoted by a dotted orange line in Panel A) for the first 5 minutes. Red dotted line corresponds to the intensity line scan. Bottom: 3-pixel intensity line scan for the F-actin channel in the kymograph. Red line represents the vbFRET stepping algorithm fit to count steps of F-actin landing events (see Methods). D) Stacked histogram of the total number of F-actin landing events on microtubule segments. Experiments done in triplicate (N = 91 (Trial 1), 99 (Trial 2), and 54 (Trial 3) microtubule regions analyzed).

4.2.3 Purified human CLASP2α does not bundle actin filaments

We wondered if the sequential accumulation of F-actin on microtubules could be supported by potential F-actin bundling activity of CLASP2α. To test whether CLASP2α on its own can bundle F-actin, we incubated 200 nM CLASP2α-GFP with 1 µM TRITC-phalloidin-F-actin for 10 minutes at room temperature, and then imaged using our *in vitro* reconstitution approach (see Methods). Our results showed that CLASP2α on its own does not induce F-actin bundling in these conditions (Figure 4.4A). We only measured 3% of the field of views to contain at least one bundle structure (Figure 4.4B). In contrast, robust F-actin bundles were observed in the presence of 200 nM fascin, a well-known actin bundler (Figure 4.4). Additionally, as expected, CLASP2α alone was sufficient to induce bundling of microtubules in these conditions (Figure 4.4). These results suggest that the CLASP2α-mediated F-actin accumulation on microtubules does not occur through bundling of actin filaments by CLASP2α.

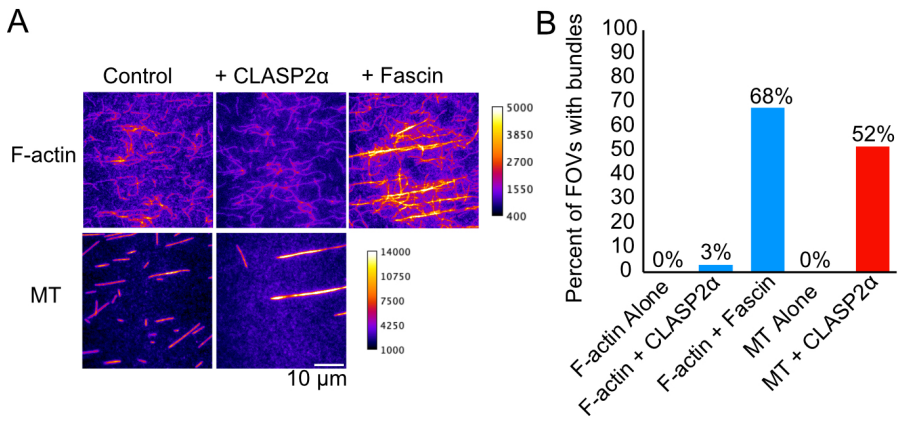

Figure 4.4: Purified human CLASP2α does not bundle actin filaments
A) Example TIRF images of F-actin or microtubule (MT) structures in control (alone), with 200 nM CLASP2α-GFP, or with 200 nM fascin. Scale is for heat map coloring. B) Quantification of the percent of field of views (FOVs) with at least one bundle as defined by intensity thresholding (see Methods). Experiments done in triplicate. F-actin alone, N = 29; microtubules alone, N = 24; F-actin + CLASP2α, N = 29; microtubules + CLASP2α, N = 27; and F-actin + fascin, N = 31 FOVs.

4.3 Discussion

Interestingly, the serine-arginine rich region contained within the minimal L-TOG2-S was previously implicated in microtubule binding (Aher et al., 2018). Furthermore, the same serine-arginine region contains a SxIP motif, which encodes CLASP's direct interaction with EB proteins, facilitating targeting of CLASP to growing microtubule ends (Maki et al., 2015; Patel et al., 2012). How interactions of the serine-arginine region with microtubules, actin and EBs are regulated in different cellular contexts is not known. Furthermore, a previous report using co-immunoprecipitation and colocalization experiments in fibroblasts suggested that the TOG1 domain of CLASP2α also interacts with F-actin (Tsvetkov et al., 2007). Our results show that the TOG1 domain is not necessary for the CLASP-mediated crosslinking of microtubules with F-actin; to what extent TOG1 domain may contribute to the direct CLASP-actin interaction warrants further investigation. Notably, a recent report suggested that another TOG-domain protein, XMAP215, directly interacts with F-actin to promote microtubule-actin coalignment in the neuronal growth cone (Slater et al., 2019). There, the authors found that all five TOG domains of XMAP215 were required for XMAP215's localization to F-actin. Future work will be needed to determine the affinities of individual TOG domains for F-actin and their direct effects on the microtubule-actin crosstalk.

Our finding that microtubule-associated CLASP2α supports the binding of up to 11 actin filaments to a single microtubule region raises the question of F-actin organization on the microtubule lattice. Our results don't show any evidence of actin bundling along microtubules. The number of F-actin landing events

saturated within the duration of our experiment, and we never observed more than 11 sequential landing events, suggesting a limit to the number of F-actin that can be linked to the microtubule lattice. Furthermore, we found no evidence of CLASP2α being able to directly bundle F-actin. This is different from the effects of another well-studied MAP, tau, which directly bundles F-actin and facilitates actin elongation and bundling along growing microtubules (Elie et al., 2015). Given that Taxol-stabilized bovine microtubules typically contain 13 individual protofilaments (Amos and Klug, 1974; Arnal and Wade, 1995), and that the full microtubule surface may not be accessible to F-actin binding in our experiments (due to the tethering of microtubules to the coverslip), the number of landing events we observed is consistent with the model in which individual actin filaments bind around the microtubule perimeter along microtubule protofilaments. High resolution structural approaches, such as cryo-electron microscopy, will be needed to determine the exact organization of F-actin on CLASP2α-coated microtubules. Overall, we conclude that CLASP2α can simultaneously bind actin filaments to the microtubule lattice, a new function for CLASPs.

4.4 Methods

4.4.1 Protein Purification

His-CLASP2α-EGFP-Strep was expressed in baculovirus-infected Sf9 insect cells and His-EGFP-L-TOG2-S was expressed in BL21(DE3) *E.coli* cells, purified and stored in CLASP storage buffer (25 mM PIPES [piperazine-N,N'-bis(2-ethanesulfonic acid)] (pH 6.8), 150 mM KCl, 5% (v/v) glycerol, 0.1% (v/v) Tween-20, 50 mM L-glutamate, 50 mM L-arginine, and 1 mM DTT). Tubulin and G-actin purification and labeling are described in Chapter 2. Protein concentration was determined using absorbance at λ = 280 nM and 290 nM for G-actin.

4.4.2 F-actin binding along CLASP2-coated microtubule experiments

Taxol microtubules and phalloidin-stabilized F-actin were prepared as described in Chapter 2. Flow channels and sample preparation were done as described in Chapter 2. For the actin filament and microtubule co-localization experiments, reaction mixes with imaging buffer, and either 100 nM CLASP2α-GFP or 100 nM L-TOG2-S, and 6.5 µM TRITC-phalloidin-stabilized F-actin were added to the imaging channel. Control experiments were performed with CLASP storage buffer. Several images were taken throughout the channel after the 10-minute incubation.

For F-actin accumulation experiments, a three-color image to visualize the CLASP2α-GFP (488-nm), TRITC-phalloidin F-actin (561-nm), and microtubules (640-nm) was taken before adding the F-actin-CLASP reaction mix as a control for fluorescence bleed through. Then, fast imaging at 5 fps for the 561-nm channel

was started while flowing in the reaction mix to capture the initial F-actin landing events. After 5 minutes, another three-color image to visualize the CLASP (488-nm), F-actin (561-nm), and microtubule (640-nm) channels was taken and then 488-nm and 561-nm channels were imaged every 3 seconds for 35 minutes. Once done, a final three-color image was taken. Experiments were performed in triplicate. Control experiments with and without phalloidin were done in duplicate. Control experiments with and without phalloidin stabilization were performed with 1 μM F-actin. All solutions were supplemented with 20 μM Taxol.

4.4.3 F-actin/Microtubule bundling experiments

TRITC-Phalloidin F-actin (2.8 μM) and Taxol-stabilized microtubules (2.5 μM, 24% TAMRA labeled) were prepared as described in Chapter 2, however coverslips were passivated with a TRITC antibody. Reaction mixes with imaging buffer, 1 μM F-actin, and 200 nM Fascin (Cytoskeleton, Inc) or 200 nM CLASP2α-GFP or CLASP2α-GFP storage buffer were incubated at room temperature (17 C) for 10 minutes. As a positive control, 200 nM CLASP2α-GFP or storage buffer was incubated with 1 μM Taxol microtubules, imaging buffer, and 10 μM Taxol at room temperature (17 C) for 10 minutes. Then, reaction mixes were added to an imaging channel and then immediately washed with imaging buffer. Ten to twelve TIRF images were taken every 750 μm along the channel. 488-nm was used to visualize CLASP2α-GFP and 561-nm was used to visualize F-actin or microtubules. Experiments were done in triplicate.

4.4.4 Colocalization using PCC

Three, three-color images of 488-nm (Control, CLASP2α-GFP, or GFP-L-TOG2-S), 561-nm (TRITC-phalloidin F-actin), and 640-nm (5% A647-labeled microtubules) channels were cropped to 335 x 170 pixel size (54 μm x 27 μm). Then, the PCC was measured as described in Chapter 2. Individual PCC values with the standard deviation were plotted in GraphPad Prism. Kruskal-Wallis one-way ANOVA with multiple comparisons test was used to test for significance in GraphPad Prism. Experiments were done in triplicate.

4.4.5 Average actin intensity on CLASP2-coated microtubules

All microscopy movies were first drift-corrected using the Image Stabilizer plugin for ImageJ. To avoid heterogeneous illumination occurring in the TIRF field, all the microscope images were cropped (300 x 512-pixel size) to eliminate out of focus or dimmer microtubules. For F-actin landing experiments, the microtubule channel image taken between the first 5-minute movie and the second 35-minute movie was used to determine the microtubule region. This microtubule image was thresholded, using the Auto MaxEntropy method, and recorded. Then a selection was created around the thresholded microtubule region and overlayed on the F-actin channel. A ROI was created, and the average F-actin intensity along microtubules over time

was measured using the Time Series Analyzer V3 ImageJ plugin. F-actin intensity was normalized to the maximum intensity and fit to the following intensity equation,

$$I = A(1 - e^{\frac{-t}{\tau}}), \tag{4.1}$$

where I is the F-actin intensity, A is the maximum F-actin intensity, t is time, and τ is the half time in the MATLAB Curve Fitting Tool. Results were plotted in MATLAB.

4.4.6 Kymograph and F-actin landing analysis

A method to quantify changes in fluorescent intensity as a function of space and time is to create a kymograph, a distance versus time image of the mean intensity for each pixel. Before producing kymographs, movies were drift corrected using the Image Stabilizer plugin in FIJI is just ImageJ (FIJI). For kymograph production, straight or segmented lines were drawn along microtubules and then overlaid on the F-actin channel. Straight line kymographs were produced using a custom ImageJ plugin, and segmented line kymographs (used occasionally for curvy microtubules), were produced using the KymographBuilder ImageJ plugin. Line traces were analyzed separately for 5-minute and 35-minute movies and reported results are the summation of the two movies to ensure all F-actin landing events are measured.

Since F-actin landing events appear as steps, we used the open-source, vbFRET Graphical user interface (gui) to measure the number of "steps" (Bronson et al., 2009). This software was created to analyze single-molecule Fluorescence resonance energy transfer (FRET) data using hidden Markov modeling and finds the most probable fit using the variational Bayesian expectation maximization algorithm (Bronson et al., 2009). For analysis, kymographs were loaded into a custom MATLAB function that extracts vertical line scans of a designated width (3-pixels) and intensity values were normalized to 90% of the maximum intensity. This normalization is recommended when analyzing non-single molecule FRET data using the vbFRET software (Bronson et al., 2009). To use this software, the FRET efficiency, which is defined as

$$FRETEfficiency = \frac{I_A}{I_A + I_D}, \tag{4.2}$$

was set equal to the F-actin intensity or donor intensity (I_D), by defining the acceptor intensity (I_A) as,

$$I_A = \frac{I_D^2}{1 - I_D}. \tag{4.3}$$

Line scans were selected based on the center-most line scan and then additional line scans were selected

in intervals of 15 pixels or 2.5 microns along the microtubule lattice, as permitted by individual microtubule lengths. Selected line scans were then loaded into the vbFRET gui for stepping analysis (Bronson et al., 2009). The number of possible states was set to a minimum of 1 and maximum of 20, and the number of fitting attempts per trace was set to 25. The vbFRET session and idealized traces were saved, and steps were extracted using custom MATLAB codes. Steps were measured after F-actin was visible in solution (after 30-40 seconds). Due to overfitting of noise, step fits were filtered, with steps of sizes smaller than the 3 standard deviations below the mean step size removed. F-actin landing events followed by F-actin unbinding (negative steps) were additionally removed to consider the maximum number of F-actin accumulating on a microtubule segment. This unbiased, automated analysis was beneficial in the ability to account for local background noise and variability in fluorescence over time to give a more accurate estimation of the number of F-actin accumulating on microtubules (Figure 4.5).

Previous literature used fluorescence intensity measurements to estimate the number of actin filaments in an actin bundle (Breitsprecher et al., 2011; Park et al., 2021). In our experiments, we found that simply measuring the fluorescence intensity of the actin filaments in microtubule regions was not a reliable approach. We found a significant variability in the illumination across our field of view, which is not uncommon for the TIRF imaging approach. Using microtubules as our intensity calibration because of their distinguished morphology and brightness, we determined that the microtubule intensity can range between 3300 – 7500 au, depending on their location in the TIRF field (Figure 4.5A). The individual standard deviations are also large (700 – 1000 au), meaning that there is additional significant variability along the microtubule lattice. Such large variability can cause uncertainty in determining the absolute intensity of a single filament even for microtubules, let alone for single F-actin filaments.

Also, we found that the background noise in our images increases greatly over time (Figure 4.5B). This is not surprising, given that more and more actin particles are being retained at the surface in our experiments over time. Notably, there are few publications specifically addressing how the background noise is accounted for or how it may impact the determination and validity of a single-filament brightness 'standard' over time. Lastly, using kymograph analysis and an established automated stepping algorithm (Bronson et al., 2009) in lieu of a manual intensity analysis allowed us to be completely agnostic with respect to the size of the particles that land (i.e. whether we are observing landing of single actin filaments versus bundles). We strictly reported the number of landing events, rather than the absolute number of actin filaments on microtubule regions due to these reasons.

Finally, we directly compared a manual analysis approach of estimating F-actin bundle size against our kymograph-stepping analysis (Figure 4.5C,D). We took a closer look at our representative example from Figure 4.3 for this comparison. We first manually determined the single F-actin intensity by producing an intensity line scan for the first F-actin landing event (Figure 4.5C). Then, we estimated the background intensity by averaging the intensity along the microtubule lattice. For the same line scan, we then measured the F-actin signal intensity in the last frame. Dividing the last frame intensity by the single F-actin intensity, we determined a total number of six F-actin on the microtubule. In contrast, our stepping analysis counted a total of five F-actin landing events (Figure 4.5D). This was due to some variability in the intensity of the F-actin landing events (Figure 4.5D). Overall, we think that our analysis more adequately represents the properties of F-actin accumulation on CLASP2-coated microtubule lattice regions than a simpler intensity calibration approach. Example F-actin intensity trace in Figure 4.3, with vbFRET generated fit, was produced in MATLAB and F-actin landing event numbers were plotted in GraphPad Prism.

4.4.7 F-actin/Microtubule bundle quantification

Images were cropped (273 x 285 square pixels or 43.7 x 45.6 square microns) and the 561-nm (F-actin or microtubule) channel was analyzed. First, the single filament intensity was determined from the F-actin alone and microtubule alone images. This was determined by using the Adjust Threshold plugin in ImageJ, where the 'Auto' 'Default' method was used to mask single filaments. The mean intensity in this area was measured and averaged with other images from the same day. From this measurement, we determined a minimum bundle intensity as defined by two times the intensity of the single filament. This value was determined for each experimental day. Using the 'Default' threshold method, we thresholded intensities greater than the minimum bundle intensity for all images. Then, the Analyze Particles plugin in ImageJ was used to identify F-actin and microtubule bundles. The minimum particle size was set to 60 square pixels and the particle size, mean intensity, and standard deviation were recorded for all conditions. Results are represented as the number of field of views that contained at least one F-actin or microtubule bundle particle.

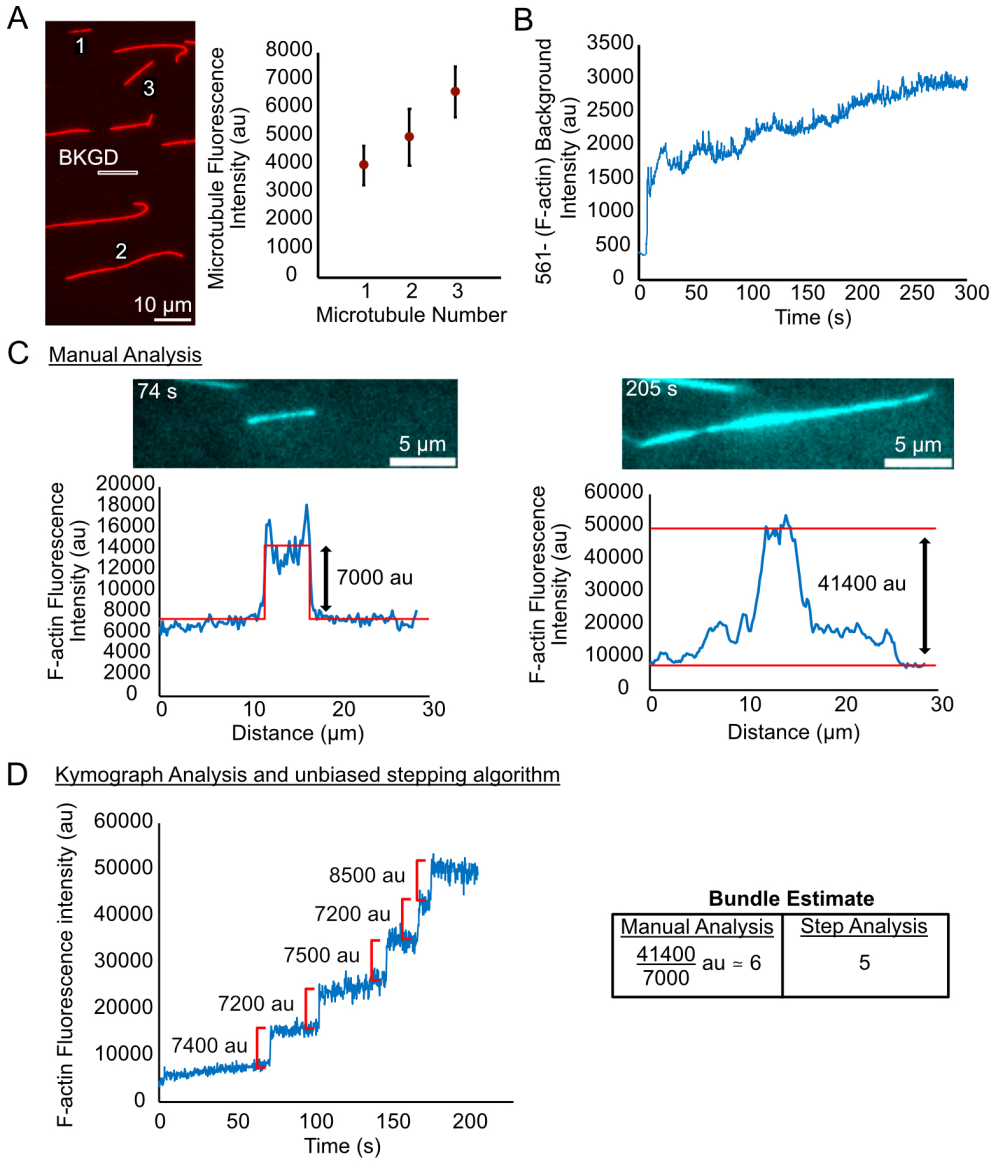

Figure 4.5: Kymograph and stepping analysis improve the estimation of the number of F-actin landing events onto CLASP2α-coated microtubules

A) Left: a TIRF image of microtubules corresponding to experiments done in Figure 10. Right: the mean fluorescence intensities of the microtubules denoted by corresponding numbers on the left, with standard deviation. B) The background intensity, as measured in the white box in panel A, for the 561-nm (F-actin) channel over time. The initial jump in intensity corresponds to introduction of F-actin into the channel. C) Example of a manual analysis used to estimate the number of F-actin based on an intensity calibration. Left, the first F-actin landing event at 74 seconds. Right, the last frame of the analysis at 205 seconds. The two images are scaled the same in intensity. Plots of the F-actin fluorescence intensity versus distance along the line scans. Blue line is the raw intensity, and the red line is a representation of the background intensity and average intensity measurements. D) Plot of the F-actin fluorescence intensity over time for a 3-pixel line scan from the kymograph in Figure 4.3. Blue line is the raw intensity. Red brackets represent stepping analysis estimation for F-actin step size. Step fit is shown in Figure 4.3.

CHAPTER 5

CLASP mediates dynamic co-organization of actin filaments and microtubules

Adapted from: Rodgers, N.C., E.J. Lawrence, A.V. Sawant, N. Efimova, G. Gonzalez-Vasquez, T.T. Hickman, I. Kaverina, and M. Zanic. 2023. CLASP2 facilitates dynamic actin filament organization along the microtubule lattice. Molec. Biol. Cell. 34(3). doi: 10.1091/mbc.E22-05-0149

Results section 5.2.2 was done in collaboration with the Kaverina group at Vanderbilt University with AV Sawant, N Efimova, and I Kaverina. Experiments presented in Figure 5.2 were done by AV Sawant and N Efimova and Figure 5.3 by AV Sawant.

5.1 Introduction

In the cell, microtubules and actin filaments are dynamic to remodel the cytoskeleton. Many crosslinking proteins are involved in the dynamic coordination of microtubule and actin organization, observed *in vitro* and in cells (Dogterom and Koenderink, 2019). Several *in vitro* reports have exemplified co-organization by microtubule end guidance (López et al., 2014), hybrid bundle formation (Elie et al., 2015), and guided actin polymerization (Nakos et al., 2022). One group demonstrated how an engineered spectraplakin, TipAct-GFP, can pull and transport stabilized actin filaments to create co-organized networks (López et al., 2014). Soon after, tau, a neuronal MAP was shown to be able to co-organize dynamic actin filaments and dynamic microtubules, creating hybrid bundle networks (Elie et al., 2015). More recently, septins 2/6/7 were revealed to be able to mediate actin polymerization along stabilized microtubules (Nakos et al., 2022). Podosomes are actin-based adhesion structures that contains a core of polymerizing actin that are regulated by microtubules (Biosse Duplan et al., 2014; Gil-Henn et al., 2007; Kopp et al., 2006). Interestingly, CLASPs are implicated to provide stable microtubule tracks for proper podosome organization (Efimova et al., 2014; Zhu et al., 2016). Thus, we wanted to better understand the CLASP-microtubule role in organization of dynamic actin *in vitro* and in cells.

5.2 Results

5.2.1 CLASP2α facilitates dynamic actin filament organization templated by the microtubule arrangement

We wondered if CLASP2α could facilitate dynamic actin polymerization along the microtubule lattice. To probe this, we introduced 250 nM soluble, Alexa-647-labeled, G-actin into a flow-cell containing Taxol-stabilized, coverslip-bound microtubules (Figure 5.1). In the presence of CLASP2α, we observed the binding

and growth of dynamic actin filaments along the microtubule lattice, which continued to grow off the ends of the microtubule polymer (Figure 5.1A,B). Although individual microtubules were sparsely distributed on the coverslip surface, we often observed growing F-actin forming connections between microtubule polymers (Figure 5.1A). We measured the length of the individual F-actin connections between microtubules to be 7 ± 3 μm (SD, N = 26 F-actin bridges over 3 independent experimental days, Figure 5.1C). Thus, under these conditions, CLASP2α can promote linking of microtubules by actin filaments. Without CLASP2α, microtubules were not covered by F-actin and no connections were observed (Figure 5.1A). These results demonstrate that CLASP2α can support dynamic F-actin organization templated by microtubules, and that F-actin can bridge microtubules forming an interconnected network.

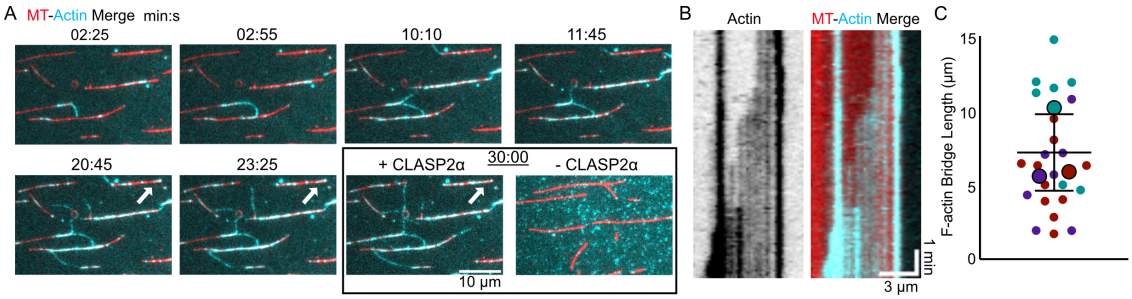

Figure 5.1: CLASP2 facilitates dynamic actin filament organization templated by the microtubule network A) Example time-lapse images demonstrating dynamic F-actin (cyan) connecting multiple microtubules (red). White arrow highlights an example of growing F-actin shown by a kymograph in Panel B. Th last image in the sequence represents CLASP2 storage buffer control after 30 minutes. B) Example kymograph demonstrating growing F-actin along a microtubule lattice (left: actin channel alone, right: merged image). C) Quantification of the individual lengths of F-actin connections between microtubules. Smaller data points are the individual measurements and larger data points are the mean lengths for each repeat (N = 12, 7, and 7). The error bar is the standard deviation of the mean lengths.

5.2.2 CLASP depletion results in disruption of ventral stress fiber organization in rat vascular smooth muscle cells

Lastly, we were interested in furthering our understanding of CLASPs' role in the organization of the actin cytoskeleton in cells. We collaborated with the Kaverina laboratory at Vanderbilt University to explore this. To probe CLASPs' role in actin organization in cells, we depleted CLASPs in a rat vascular smooth muscle cell line A7r5, chosen due to its notable actin stress fiber structure (Figure 5.2). For prominent phenotypes, both CLASP paralogs (CLASP1 and CLASP2) were depleted by siRNA oligo combinations, achieving reliable reduction of CLASP protein levels and carefully validated in previous work (Figure 5.3) (Efimova et al., 2014; Zhu et al., 2016). Our results revealed that actin fiber organization was severely disturbed in CLASP-depleted cells (Figure 5.2B-C). Actin organization was efficiently rescued by ectopic overexpression of non-silenceable mutant of CLASP2 in depleted cells (Figure 5.2D), indicating that the CLASP2 paralog is

likely sufficient for proper actin organization in this context. Interestingly, co-alignment of actin fibers with microtubules in CLASP-depleted cells (Figure 5.2F-G) was reduced as compared to the control (Figure 5.2E), suggesting a diminished coordination of these filaments. These findings suggest that CLASPs contribute to co-organization of higher-order actin structures with microtubules in cells.

5.3 Discussion

Our results demonstrate that CLASP2α-coated microtubules can template dynamic F-actin organization, specifically by F-actin linking multiple microtubules and forming an interconnected cytoskeletal network. Other crosslinking proteins have been shown to organize F-actin in a microtubule-centric fashion, with notable examples belonging to the spectraplakin protein family (Dogterom and Koenderink, 2019; Pimm and Henty-Ridilla, 2021; Rodriguez et al., 2003; Suozzi et al., 2012). Some of the +TIPs may not be able to directly crosslink F-actin and microtubules, thus interactions among +TIPs in combination with other actin binding proteins result in the collective regulation of microtubule-actin crosstalk. For example, the combination of CLIP-170 and EB1 with actin-regulators formin, mDia1, and profilin mediates F-actin polymerization from growing microtubule ends *in vitro* (Henty-Ridilla et al., 2016). In another example, the +TIP protein APC was reported to promote actin assembly, activity that is negatively regulated by interaction of APC with EB1 (Juanes et al., 2020). Future work investigating how CLASP's interactions with its binding partners may impact the crosstalk between the microtubule and actin networks is needed. It remains unclear if CLASP can interact with F-actin when targeted to growing microtubule ends via EBs, and whether such interaction could also promote actin polymerization from the dynamic microtubule ends, as shown for the complex with CLIP-170 (Henty-Ridilla et al., 2016).

The result that CLASP2 mediates actin polymerization along microtubule templates is very similar to the interactions reported between microtubules, septins, and dynamic actin filaments. Here, SEPT2/6/7, the minimum septin complex to bind either actin or microtubules, was shown to crosslink actin filaments when microtubules were coated with septin (Nakos et al., 2022). Furthermore, they demonstrated that dynamic actin filaments are recruited to microtubule lattices and can grow along the microtubule, like the microtubule-CLASP-actin interaction found here. There is still much to learn about the role of actin polymerization templated by microtubules and its relevance in cells.

Microtubule-dependent actin filament coalescence demonstrated in our minimal component system could be important for building higher-order actin structures in cells. In our study, we find that both actin-microtubule association and the architecture of contractile actin fibers are severely disrupted when CLASPs are depleted

in vascular smooth muscle cells. Actin defects observed in actin stress fiber structures are consistent with previous findings that CLASP depletions cause defects in actin-based invasive protrusions in vascular smooth muscle cells (Efimova et al., 2014; Zhu et al., 2016). Overall, our results identify a potential role for CLASP-mediated organization of actin filaments along microtubules in the process of actin fiber assembly in contractile cells.

5.4 Methods

5.4.1 Actin dynamics on CLASP2-coated microtubule experiments

Taxol microtubules and channels were prepared as described in Chapter 2; however microtubules were labeled with 16% biotin and 5% Alexa555 tubulin and stored in BRB80T (BRB80; 80 mM PIPES, 1 mM MgCl2, 1 mM EGTA, pH 6.8; and 10 µM Taxol). Before adding the reaction mix, the chamber was washed with imaging buffer (BRB80, 0.1% methylcellulose, 40 µg/ml glucose oxidase, 40 mM D-glucose, 18 µg/ml catalase, 0.8 mg/ml casein, 10 mM DTT, and 0.2 mM ATP). Then, either 100 nM CLASP2α-GFP or CLASP2α-GFP storage buffer in imaging buffer was added to the chamber and incubated for 5 minutes to allow for full coating of Taxol microtubules. Then a reaction mix with 250 nM, 20% Alexa647 labeled G-actin and either 100 nM CLASP2α-GFP or CLASP2α-GFP storage buffer were added. Three-color imaging every 5 seconds for 30 minutes immediately followed. All solutions were supplemented with 20 µM Taxol. Experiments were done in triplicate.

5.4.2 F-actin Bridge Length

After 30 minutes, F-actin bridge lengths were measured by drawing segmented lines along F-actin in ImageJ. Error bars are the standard deviation of the mean F-actin bridge lengths for each repeat. Analysis and plots were done in Microsoft Excel and GraphPad Prism.

5.4.3 Cell culture

A7r5 rat smooth muscle cells (ATCC # CRL-1444) were grown in low-glucose (1000 mg/l) Dulbecco's modified Eagle's medium (DMEM) without Phenol Red, supplemented with 10% fetal bovine serum at 37°C and 5% CO2. Cells were plated on glass coverslips coated with 10 μg/ml fibronectin 24 hours prior to experiments.

5.4.4 siRNA sequences, CLASP2 expression rescue, and transfection

Two different combinations of mixed siRNA oligonucleotides against CLASP1 and CLASP2 were used. Combination 1 (custom design, Sigma) included the CLASP1-targeted siRNA sequence 5'-CGGGAUUGCAUCUUUGAAA-3' and the CLASP2-targeted siRNA sequence 5'-

CUGAUAGUGUCUGUUGGUU-3'. Combination 2 (Mimori-Kiyosue et al., 2005) included the CLASP1-targeted siRNA sequence 5'-CCUACUAAAUGUUCUGACC-3' and the CLASP2-targeted siRNA sequence 5'-CUGUAUGUACCCAGAAUCU-3'. Non-targeting siRNA was used for controls. For siRNA oligonucleotide transfection, HiPerFect was used according to the manufacturer's protocol. Experiments were conducted 72 hours after siRNA transfection, as at this time minimal protein levels were detected. For CLASP2 expression rescues, a GFP-labeled CLASP2 mutant using alternative codons and therefore non-silenceable by anti-CLASP2 siRNA from combination 2 (Mimori-Kiyosue et al., 2005) was transfected into depleted cells at 48 hours after siRNA transfection. For Deoxyribonucleic acid (DNA) transfection, Fugene6 was used according to the manufacturer's protocol. Cells were processed for imaging after additional 24 hours to meet the 48-hour depletion optimum.

5.4.5 Cell labeling, imaging, and image processing

For actin imaging, cells on coverslips were fixed in 4% paraformaldehyde plus 0.3% Triton X-100 in cytoskeleton buffer (10 mM MES, 150 mM NaCl, 5 mM EGTA, 5 mM glucose and 5 mM MgCl2, pH 16) for 10 minutes. For co-staining with tubulin, 0.1% glutaraldehyde was added into the fixative solution. The actin cytoskeleton was visualized by phalloidin conjugated to Alexa Fluor 488. Tubulin was immunostained using anti-alpha-tubulin monoclonal antibodies, DM1a and Alexa 568-conjugated goat anti-mouse IgG antibodies as secondary antibodies. CLASPs were immunostained by non-paralog-specific rabbit polyclonal antibodies VU-83 (pan-CLASP antibodies) (Efimov et al., 2007). Nuclei were visualized by DAPI. Staining was performed at room temperature. After washing, samples were mounted into ProLong® Gold Antifade Reagent on glass slides and stored at -20°C.

Wide-field fluorescence imaging (Figure 5.2A-D and Figure 5.3) was performed using a Nikon 80I microscope with a CFI APO 60× oil lens, NA 1.4 and CoolSnap ES CCD camera. Laser-scanning confocal imaging was performed using Nikon A1r based on a Ti-E inverted microscope with SR Apo TIRF 100× NA1.49 oil lens run by NIS Elements C software. Laser scanning confocal imaging (Figure 5.2E-G) was performed using a Nikon A1r with a 100x lens NA 4.5. Maximum intensity projection over the whole cell is shown in overview images. Single confocal slices processed through the emboss filter are shown in insets. In all cell images, each fluorescent channel was contrasted by whole-image histogram stretching. In overview images in Figure 5.2E-G, the tubulin channel was gamma-adjusted to highlight microtubules at the cell periphery.

5.4.6 Phenotype verification

Actin channel images (as in Figure 5.2A-C) were separated and coded for double-blind phenotype verification. Three researchers independently sorted images to detect actin fiber disturbance. These blinded analyses resulted in $>84\%$ of correct image designation into NT control and CLASP-depleted phenotypes.

5.4.7 CLASP Western Blotting

Western blotting was performed using the Protein Electrophoresis and Blotting System (Bio-Rad). Briefly, A7r5 cells were transfected with two different combinations of mixed siRNA oligonucleotides against CLASP1 and CLASP2 using TransIT-X2 (Mirus). After 72 h, the cells were collected, lysed, and resuspended in Laemmli Sample Buffer. 20 µg total protein for each condition was resolved on 12% SDS-PAGE gels and transferred to nitrocellulose membranes at 350 mA for 3 h for blotting. The membranes were then blocked with 5% nonfat dried milk for 1 h and incubated overnight with primary antibodies: anti-rat CLASP1 (KT 67, Absea), anti-rat CLASP2 (KT69, Absea) and anti-mouse GAPDH (Santa Cruz). IRDye 700 or 800 (LI-COR Biosciences) were used as secondary antibodies. The membranes were imaged on an Odyssey Infrared Imaging system.

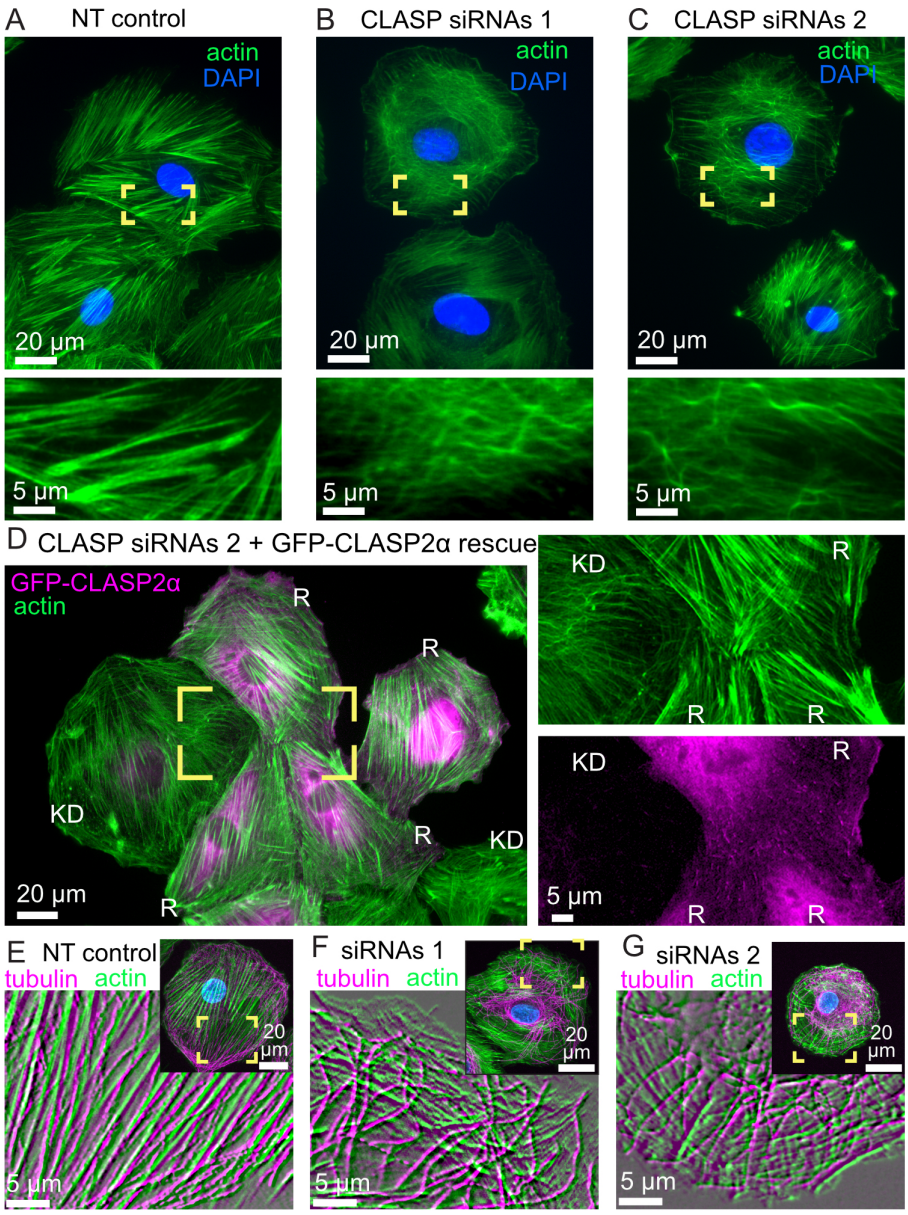

Figure 5.2: CLASPs are essential for correct stress fiber organization in vascular smooth muscle cells A) Prominent actin stress fibers in cells treated with a control (non-targeting, NT) siRNA. B-C) Disorganized actin mesh in cells treated with two alternative combinations of siRNA oligos. Phalloidin-stained actin, green. 4',6-diamidino-2-phenylindole (DAPI), blue. Yellow boxes are enlarged below to highlight details. The phenotypes have been vetted by a double-blinded evaluation (see Methods). D) Cells treated with siRNA combination 2 and transfected with GFP-CLASP2 (pseudo-colored magenta) resistant to this siRNA. Separate channels from the yellow box are enlarged at the right. Actin organization in GFP-CLASP2-rescued cells (R) is like control (as in Panel A), while in a non-expressing cell (KD) it is like knockdown phenotype (as in Panel C). Phalloidin-stained actin, green. GFP-CLASP2, magenta. E-F) Actin and microtubules in cells treated with a control (non-targeting, NT) siRNA (E) or with siRNA combinations 1 (F) or 2 (G). Phalloidin-stained actin, green. Tubulin, magenta. DAPI, blue. Yellow boxes in overview images are enlarged in insets. Inset images are processed through the emboss filter for exclusive visualization of fibers and illustration of their alignment with microtubules, which is diminished in (F, G) as compared to (E). Scale bars, 20 μm in overviews and 5 μm in insets. All panels show representative images out of more than 45 cells per condition over 3 or more repeated experiments.

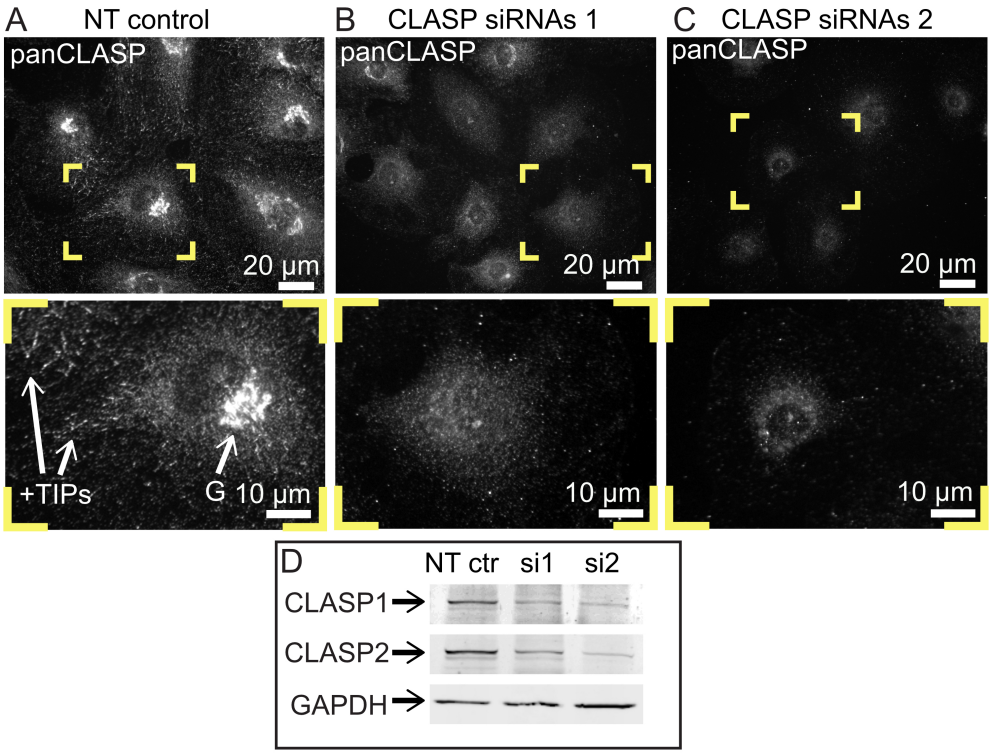

Figure 5.3: CLASPs are efficiently knocked down by siRNA in A7r5 cells
A-C) immunostaining with pan-CLASP antibody (grayscale). A) Non-targeting (NT) control, B) siRNA combination 1, and C) siRNA combination 2. Yellow boxes are enlarged below to highlight details. +TIPs label highlights CLASP signal at microtubule ends and G label highlights CLASP signal at the Golgi. D) Western blotting indicating CLASP1 and CLASP2 protein level reduction in cell population treated with siRNA combinations 1 and 2 as compared to control. Loading control, Glyceraldehyde-3-phosphate dehydrogenase (GAPDH).

CHAPTER 6

Conclusions and Discussion

Microtubule and actin filament coordination is essential for proper cellular function. Many proteins have been identified to be involved in this crosstalk, however numerous questions remain regarding the underlying molecular mechanisms and interactions that occur. Here, we investigated the role of CLASPs in the interactions between microtubules and actin filaments. Our results demonstrate that CLASP2α can directly crosslink multiple actin filaments to microtubules. We find that a minimal CLASP construct, containing the TOG2 domain and the Serine-Arginine (Ser-Arg) rich region of CLASP2, is sufficient for this crosslinking activity. The F-actin – microtubule crosslinking is achieved despite the relatively weak direct interaction between L-TOG2-S and F-actin. We propose that the strong interaction with microtubules concentrates L-TOG2-S (as well as full length CLASP2α) along the microtubule lattice, thus providing a local abundance of weak F-actin binding sites, and ultimately facilitating robust microtubule–CLASP–F-actin crosslinking. Here, I will discuss how these findings add to the broader microtubule-actin crosstalk field and its implications in providing mechanical stability to the cell.

6.1 Domains of CLASP2 that facilitate crosslinking of microtubules and actin filaments

The spectraplakin family of proteins that crosslink actin and microtubules, contain well-studied calponin homology (CH) and Gas2-related (GAR) domains (Suozzi et al., 2012). The CH domain is responsible for actin filament binding and the GAR domain interacts with microtubules. However, in recent years, crosslinkers have been identified that do not contain the typical binding domains for both filaments. One such protein family identified were CLASPs. CLASPs are primarily MAPs that contain TOG domains that directly interact with tubulin and the microtubule lattice (Lawrence et al., 2020). Yet, CLASPs do not contain any established actin binding domain. The first report revealing that CLASPs can interact with actin filaments suggested that the TOG1 domain or the Ser-Arg rich region of the protein was responsible for actin filament interaction (Tsvetkov et al., 2007). Later, an additional study confirmed this result, reporting that purified, full length CLASP2α can co-sediment with actin filaments (Engel et al., 2014). We then discovered that the TOG2 and the Serine-Arginine rich region can bind actin filaments with a relatively low affinity and is sufficient for microtubule and actin crosslinking (Figure 6.1).

Interestingly, the TOG2 domain of CLASP2α has been reported to have a weak affinity for microtubules, while the Ser-Arg rich region interacts electrostatically with the microtubule lattice (Aher et al., 2018; Al-

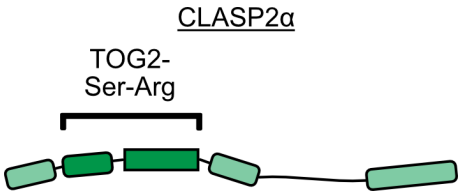

Figure 6.1: CLASP2α cartoon highlighting a region sufficient to directly crosslink microtubules and actin filaments.
Dark green regions correspond to the TOG2 and Serine-Arginine rich regions of the protein. Light green shapes represent other domains within CLASP2α, such as the TOG1, TOG3, and CLIP-ID domains. Refer to Figure 1.2 for CLASP2α domain structure.

Bassam et al., 2010). This leaves the question if TOG2 can directly interact with actin filaments? Tsvetkov and colleagues reported no evidence for actin binding by a CLASP2 deletion mutant only containing the TOG2 domain (CLASP2-N3) (Mimori-Kiyosue et al., 2005) as determined by coimmunoprecipitation and colocalization studies in fibroblasts (Tsvetkov et al., 2007). The TOG2 domain was only found to colocalize and co-immunoprecipitate with actin when portions of the Ser-Arg rich region, CLASP2-N2 (36-443 aa) and CLASP2-N1 (36-580 aa), were included in the protein (Mimori-Kiyosue et al., 2005; Tsvetkov et al., 2007). The CLASP2 deletion mutant containing a portion of the Ser-Arg rich region (CLASP2-M, 444-580 aa) was found to interact with actin. This work suggests that the Ser-Arg rich region is likely interacting with F-actin, rather than the TOG2 domain. However, these results are concluded from indirect biochemical assays, where it is still unknown how and if these CLASP2 constructs can directly interact with F-actin. Alternatively, these CLASP2 constructs could be binding to other ABPs present in the cell lysate, thus indirectly interacting with F-actin. Altogether, our finding that the minimal CLASP2 construct, containing the TOG2 and Ser-Arg rich region, can directly bind F-actin is consistent with these previous results and is the strongest evidence to date of CLASP direct interaction with F-actin.

Other TOG domain proteins have been implicated to directly interact with F-actin, such as the MAP, XMAP215. XMAP215 is a microtubule polymerase and its array of five TOG domains is necessary for its polymerase function (Widlund et al., 2011). The five TOG domains have recently been shown to be necessary to facilitate XMAP215 colocalization with actin in the growth cone periphery (Slater et al., 2019). Furthermore, the authors reported full length XMAP215 to bind F-actin with a relative affinity of 32 nM (Slater et al., 2019). CLASP2α has one TOG domain that is homologous to XMAP215 TOG domains, the TOG1 domain (Akhmanova et al., 2001)). The TOG1 domain from CLASP2 is also implicated to interact with F-actin (Tsvetkov et al., 2007). Interestingly, the TOG2 domains in CLASPs have been found to have some sequence divergence from polymerase TOG domains (Lawrence et al., 2020; Leano et al., 2013; Maki et al.,

2015). To date, there is little evidence supporting CLASP TOG2 domain interaction with F-actin (Tsvetkov et al., 2007). Notably, we measured a lower affinity for F-actin binding than XMAP215 for the minimal CLASP2 construct, containing the CLASP TOG2 domain. Is this weaker affinity due to the CLASP specific TOG domain, TOG2, or due to fewer TOG domains present? Future work, investigating whether CLASP or XMAP215 TOG domains can directly interact with F-actin will be necessary to better understand the role of CLASPs and XMAP215 in microtubule and actin crosstalk. Also, it has still not been demonstrated that XMAP215 can directly crosslink microtubules and actin filaments.

The minimal L-TOG2-S construct involved in actin filament interaction and crosslinking to microtubules contains a Ser-Arg rich region along with the TOG2 domain. The Ser-Arg rich region of CLASP not only provides electrostatic interactions with microtubules, but also includes the SxIP motif known to directly interact with EBs (Mimori-Kiyosue et al., 2005). EBs localize +TIPs to growing ends of microtubules and can then serve as a hot spot for actin interaction, crosslinking the two networks together (Dogterom and Koenderink, 2019; Pimm and Henty-Ridilla, 2021). One such example is with EB proteins binding to APC, where APC concentrates on microtubule ends and is transported to the leading edge of epithelial cells, where it can interact with the actin nucleator formin (Mimori-Kiyosue et al., 2000; Wen et al., 2004). Here, mDia1 was also shown to localize at microtubule ends (Wen et al., 2004). The APC has been linked to regulation of actin dynamics at focal adhesions as well. Migrating cells with a mutant of APC, that is defective in actin nucleation, was shown to have slower focal adhesion disassembly, with increased number and duration of microtubule capture events (Juanes et al., 2019). These studies emphasize the importance of EB interactions for the microtubule and actin crosstalk involved in cell migration, where CLASPs are strongly implicated (Lawrence et al., 2020).

It remains unknown how the CLASP-EB interaction regulates actin and microtubule crosstalk, *in vitro* or in cells. Whether EB interaction blocks the Ser-Arg rich region for binding with F-actin and whether the other domains of CLASP2α suffice for interactions with F-actin is an interesting question that can be answered in our assays. Our approach would involve creating smaller constructs of CLASP2α to interrogate the specific domains and their ability to crosslink F-actin to microtubules. For truncated constructs that do not localize to microtubules, we could also investigate actin filament interaction using colocalization or co-sedimentation experiments in case the CLASP affinity shifted to prefer F-actin over microtubules. Abelson (Abl) non-receptor tyrosine kinase -induced CLASP2 phosphorylation has been shown to shift CLASP localization to adhesive plaques in neuronal growth cones (Engel et al., 2014). Additionally, experiments with dynamic microtubules, actin filaments, CLASPs, and EBs are needed to better understand the interplay in

+TIP crosstalk mechanisms observed in cells.

6.2 Organization of actin filaments along the microtubule lattice

In our work, we observed multiple actin filaments landing along CLASP2-coated microtubules (Chapter 4). We were curious about the organization of the actin filaments on the microtubule. One type of organization could be actin bundle structures, where CLASP2 would mediate actin filaments binding to each other. Another type of structure could be actin filaments binding around the outside surface of the microtubule (Figure 6.2). To discern between the two potential structures, we investigated the ability of CLASP2 to bundle actin filaments alone. Ultimately, we found no evidence that CLASP2α can bundle F-actin (Chapter 4). Importantly, these experiments were done in identical buffer conditions as the F-actin landing experiments with CLASP2-coated microtubules. These findings suggest the latter structure, where actin filaments bind around the shaft of the microtubule (Figure 6.2).

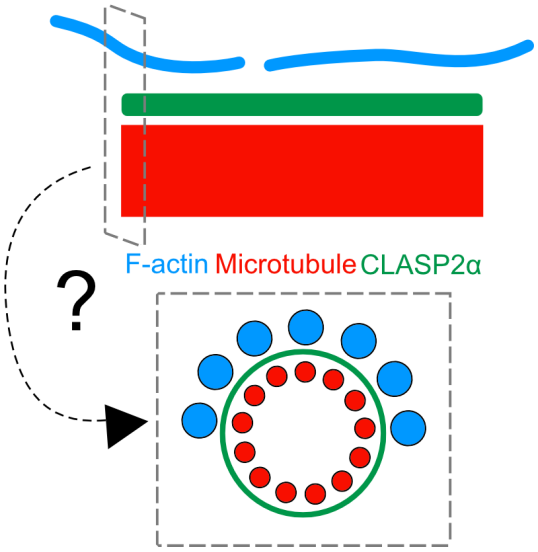

Figure 6.2: Cartoon of proposed organization of actin filaments on CLASP2α-coated microtubules
Gray dashed boxes represent cross-sectional view of a potential model for F-actin organization along microtubules coated with CLASP2α, where F-actin are binding around the microtubule shaft.

Another intriguing result that supports this prospective actin filament organization arises from the average number of actin filaments on microtubules. We measured an average of 6 actin filaments binding along microtubules and measured up to 11. Typically, microtubules are composed of 13 protofilaments, comparable to the maximum number of actin filaments we recorded. Due to the geometric constraints of our TIRF imaging experiments with microtubules tethered to the cover glass via a NeutrAvidin-biotin link (Chapter 2), the microtubule surface near the cover glass is likely inaccessible for F-actin binding. For the most part, we

found that actin filaments bound along the microtubules, regardless of the orientation of the microtubule to flow. This strong alignment speaks to the robust crosslinking interaction, as seen for hybrid bundle structures formed by tau, SB401, coronin, and doublecortin (Elie et al., 2015; Huang et al., 2007; Rothenberg et al., 2003; Tsukada et al., 2005). Surprisingly, a recent publication reported that actin filaments can reside inside the microtubule lumen in kinesore treated cells (Paul et al., 2020). We doubt that actin filaments are inside the microtubule in our experiments, since all polymers are stabilized with set lengths. High resolution structural approaches, such as cryo-electron tomography (cryo-ET), to determine the organization of actin filaments on CLASP2-coated microtubules would enlighten this study.

Cytoskeletal crosstalk has been observed in cells through instances of overlapping microtubules and bundled actin filaments. One protein implicated in such crosstalk is the well-studied neuronal MAP, tau, that is important in supporting microtubule navigation into the actin-rich area of growth cones (Biswas and Kalil, 2018). Tau binds, bundles, and crosslinks microtubules and actin filaments (Elie et al., 2015). Unlike tau, we have no evidence that CLASPs can bundle actin filaments. A question we wish to pursue in the future is, whether CLASP2-coated microtubules can support actin bundle formation by actin bundling proteins? Here, we would perform similar experiments as performed in Chapter 4, however we would include an actin bundling protein, such as α-actinin or fascin (Winkelman et al., 2016). These two proteins are of interest because they have implications in different structures in the cell (Castaneda et al., 2021). Actin stress fibers are formed by α-actinin, while filopodia are fascin-bundled actin filaments, two different networks that are involved in the crosstalk with microtubules. Interestingly, fascin bundles are tightly organized, with an 8 nm spacing, while α-actinin bundles have 35 nm spacing (Winkelman et al., 2016). Whether the different bundle architecture impacts actin filament organization along CLASP2-coated microtubules is a question of interest when considering interactions at the leading edge versus stress fibers in motile cells. However, there is no evidence to date that CLASPs interact directly with either fascin or α-actinin leading to enhanced bundle formation. This line of investigation is of particular interest considering our results in rat smooth muscle cells showing lack of robust ventral actin stress fibers when CLASPs are depleted. Whether and how CLASP2 is involved in the specific organization of actin filaments linked to microtubules to form actin stress fibers remains to be elucidated.

6.3 Dynamic co-organization of actin filaments and microtubules

In Chapter 5, we explored the ability of CLASP to organize dynamic actin filaments along microtubules. We demonstrated that CLASP2 can template dynamic actin, bridging between microtubules (Figure 6.3). Other crosslinking proteins of interest have been reported to facilitate similar crosslinking interactions, such

as septins. SEPT2/6/7 was very recently reported to be able to crosslink actin filaments to the microtubule lattice *in vitro* (Nakos et al., 2022). Strikingly, SEPT2/6/7 are also able to recruit polymerizing actin filaments, as described here for CLASP2 (Chapter 5). In contrast to our observations, they also reported partial attachments of dynamic actin filaments where the unbound segment branches off at an angle (Nakos et al., 2022). However similar, there may be subtle differences between the crosslinking interactions facilitated by CLASPs and septins that remain to be explained. Septins are filamentous proteins that interact with multiple components of the cytoskeleton. Septins form a heteromeric complex suggesting multivalent interactions with microtubules and actin filaments (Nakos et al., 2022), allowing for crosslinking interactions. Our results for CLASP and that reported for septins, demonstrate that the ability for actin filaments to polymerize on microtubules is indicative for low-affinity, transient interactions with actin, as thought for decades (Griffith and Pollard, 1982). We measured relatively low affinities for the F-actin: CLASP interaction (Chapter 3), supporting the mechanism by which CLASPs are also able to facilitate actin polymerization templated by microtubules.

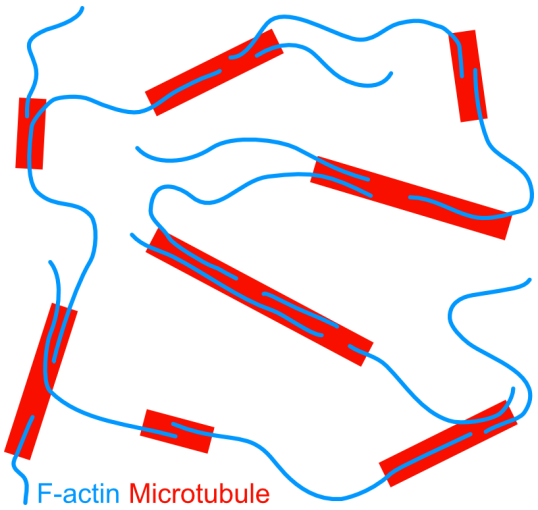

Figure 6.3: Cartoon representing dynamic organization of actin filaments as templated by microtubules Here, several instances of actin filament and microtubule co-organization are illustrated, i.e., actin filaments growing along microtubules, continued actin filament elongation from microtubule ends, and linking microtubules together by actin filaments bridges. These interactions were observed in this work and reported for other proteins involved in microtubule-actin crosstalk.

Another interesting potential role of CLASPs in these interactions include mechanisms from a recent report establishing how the +TIP complex, i.e. CLIP-170, EB, and mDia1, helps govern actin filament organization by microtubules (Henty-Ridilla et al., 2016). Here, the authors demonstrate how CLIP-170 localizes to growing microtubule ends by EB and bind mDia1 to initiate actin polymerization from microtubules. CLIP-170 was suggested to interact with mDia1 through the formin elongation effector domain (FEED)

sequence within the protein. These interactions are of particular interest due to the connections between CLASPs and CLIPs. CLASPs were first discovered by identifying the binding partners of CLIP-170 and CLIP-115, where CLASPs were shown to directly interact with CLIPs and microtubules (Akhmanova et al., 2001). Like CLASPs, CLIP-170 regulates the microtubule network by tip-tracking microtubules *in vitro* and in cells (Bieling et al., 2008; Dixit et al., 2009; Folker et al., 2005). Remarkably, CLIP-170 has also been reported to directly interact with actin, though appears to be unable to simultaneously bind microtubules and actin filaments as established with CLASPs in our study (Wu et al., 2021). This, however, does not rule out the possibility that in the cell, CLASPs and CLIPs work together to facilitate microtubule-actin crosstalk, such as described by Henty-Ridilla and colleagues. Potentially, CLASPs can help localize actin filaments to microtubules and interact with CLIPs at the end of the microtubule, where CLIPs attract formins through the FEED sequence to accelerate actin polymerization. In that context, CLASPs could further stabilize actin filament connections to microtubules through their crosslinking function. EBs provide additional anchoring of CLASPs and CLIPs to the microtubule end. The interplay between CLASPs, CLIPs, and EBs in these crosstalk interactions require further investigation.

Actin filaments connected to the microtubule ends have also been shown for APC, +TIPs, and branched actin networks as visualized using platinum replica electron microscopy (PREM) in hippocampal neurons (Efimova et al., 2020). Here, branched actin appeared to be connected to microtubule ends by immunogold labeled APC proteins in the growth cone. An additional density was identified to be a +TIP complex, which could include CLASPs. Furthermore, APC-mediated actin polymerization has been linked to focal adhesion dynamics. Here, human osteosarcoma cells with a separation of function APC mutant, abolishing actin nucleation, resulted in prolonged focal adhesion disassembly resulting from altered microtubule capture at focal adhesions and autophagosome transport (Juanes et al., 2017, 2019). CLASPs are also implicated in the disassembly of focal adhesions reported to facilitate interactions with the cell cortex (Efimova et al., 2014; Lawrence et al., 2020; Stehbens et al., 2014). The crosstalk between focal adhesions, actin stress fibers, and microtubules is very important in cell motility.

Overall, our results suggest a role of CLASP2 in organizing actin filaments along microtubules. We propose a model where CLASP2 can facilitate crosslinking between microtubules and actin filaments, when concentrated along the microtubule lattice due to the strong affinity of CLASPs for microtubules. Concentrated CLASP2 on microtubules provides a local abundance of weak F-actin binding sites, allowing for robust microtubule and actin coalignment. We determined that the minimal CLASP construct has a relatively low affinity for F-actin, which supports the ability of concentrated CLASP2 to crosslink actin filaments, as well

as support actin filament elongation along microtubules.

6.4 CLASP-mediated microtubule and actin crosstalk in cells

CLASPs in migrating cells, neuronal development, and plants have been well-studied and are considered essential for proper function of these processes (Lawrence et al., 2020). Microtubule-actin networks coordinate to remodel the cytoskeleton during cell migration, as observed through studies investigating both networks (Dogterom and Koenderink, 2019). One such example of microtubule and actin coordination in migrating cells are the interactions between microtubules and the cortical actin network. Cortical microtubule stabilizing complexes (CMSCs) are micron-size patches that capture microtubules once the plus end reaches the cortex (Bouchet et al., 2016). KANK1 is a protein known to recruit proteins to the CMSC and its interaction with talin mediates proper CLASP2 clustering at the cortex (Bouchet et al., 2016). It is thought that KANK1 is recruited by talin to the outer rims of focal adhesions for transport of CMSC proteins, such as CLASPs, to the actin cortex for focal adhesion regulation (Bouchet et al., 2016). Other +TIPs and partners of CLASP are implicated in this crosstalk (Kumar et al., 2009; Mimori-Kiyosue et al., 2005). These studies motivate the need to study the direct effect of CLASPs on the organization of the actin network near focal adhesion structures.

In our study, we examine the result of ventral stress fiber organization in CLASP-depleted rat vascular smooth muscle cells. Previous work demonstrated that microtubules and kinesin motor, KIF1C, are required for proper formation of actin-based protrusions called podosomes (Efimova et al., 2014). CLASP-rich microtubules are essential for KIF1C-mediated transport to the cortex, where lack of CLASPs also disrupts proper podosome formation (Efimova et al., 2014; Zhu et al., 2016). Further investigation has shown that CLASP depletion in these cells also disrupts ventral stress fiber organization. The disruption in the formation of ventral stress fibers due to a lack of CLASPs could be caused by the difficulty of microtubules to anchor to the cell cortex and template stress fiber formation. Also, CLASPs stabilize microtubule growth by promoting rescue, providing a stable highway for motor proteins to transport ABPs and other crosstalk factors needed. This result is consistent with podosome defects reported previously (Efimova et al., 2014; Zhu et al., 2016). Something else to consider, is that depletion of CLASPs leads to less dense microtubule networks and radially oriented microtubule network, rather than polarized (Efimov et al., 2007). Thus, there are fewer microtubules present near the edge of the cell to facilitate essential actin-microtubule crosstalk important for stress fiber organization.

Finally, our *in vitro* results indicate a strong crosslinking interaction while CLASPs are localized on the

microtubule lattice. In migrating epithelial cells, CLASPs are localized at microtubule ends in the cell body and shift to the lattice in the lamella (Wittmann and Waterman-Storer, 2005). This shift in CLASP localization occurs along the lattice when the microtubule is navigating the dense actin network, composed of branched filaments and bundles. A gradient of glycogen synthase kinase 3β (GSK3β) has been linked to inducing this shift in CLASP localization, where GSK3β phosphorylation inhibits plus end localization (Kumar et al., 2009). If CLASP localization is along the microtubule lattice in lamella, this could then function to guide, stabilize, and protect the microtubule as it navigates the actin-rich cortical network.

6.5 Implications for CLASP-mediated mechanical support of the cytoskeleton

Mechanical properties of cells are strongly influenced by the cytoskeleton (Fletcher and Mullins, 2010; Kasza et al., 2007). Notably, when the actin or microtubule networks are disrupted, using either cytochalasin D or nocodazole, respectively, the viscoelastic properties of the cell are affected (Wu et al., 2006). The mechanical stability of the cytoskeleton in a single-polymer context is a poorly studied concept, although known to change cytoskeletal architecture and dynamics in cellular physiology (Fletcher and Mullins, 2010; Hawkins et al., 2010; Stricker et al., 2010). Recent studies reported that the microtubule cytoskeleton can self-repair in response to mechanical damage to the lattice (Aumeier et al., 2016; Gazzola et al., 2023; Portran et al., 2017; Schaedel et al., 2015; Xu et al., 2017), and these sites of self-repair influence microtubule dynamics, promoting rescue, the transition from microtubule shrinkage to growth (Aumeier et al., 2016). With regards to actin filament networks, optical trapping was used to demonstrate that bundled actin filaments can adapt to buckling and stretching over time, indicating that mechanical stress can impact the underlying architecture of the actin bundle (Rückerl et al., 2017). Moreover, crosslinking proteins are known to change the mechanical properties of cytoskeletal polymers (Bathe et al., 2008; Claessens et al., 2006; Fletcher and Mullins, 2010; Hawkins et al., 2013). However, it is unclear how physical crosslinking of microtubules and actin filaments mechanically supports the cytoskeleton.

A new report investigating tubulin incorporation into the microtubule lattice in cells, compared the number of incorporations to the relative density of the actin network (Gazzola et al., 2023). The authors found that there were significantly more tubulin incorporation sites in microtubules located toward the rear of a micropatterned crossbow shaped cell, where the actin network is less dense. Here, the authors propose that more incorporation sites in this population of microtubules are due to microtubules experiencing more fluctuations and bending forces in the cytoplasm (Gazzola et al., 2023). Alternatively, could fewer tubulin incorporation sites in microtubules result from stable, protective interactions with proteins that mechanically support the lattice at the lamella of cells, such as CLASPs? Interestingly, CLASP2α has been reported to maintain mi-

crotubule integrity, specifically when microtubules are damaged with laser ablation or microfluidic-induced bending (Aher et al., 2020). By the same group, CLASP2α has also been shown to protect microtubule ends from force-induced catastrophe (Aher et al., 2018). CLASPs' stabilizing function on microtubules could aid in resisting lattice damage due to buckling and pushing forces imposed by contractile, dense actin networks. Elucidating the function of MAPs and repair of microtubules by tubulin incorporation in cells remains to be fully explored.

Larger scale mechanics, such as the mechanical response of bundles, are of great interest as well in our understanding of the mechanical stability of the cell. Bending forces are experienced by microtubules linked to filopodial bundle structures in cell migration and growth cone guidance. How does the crosslinking of microtubules to multiple actin filaments change the mechanical integrity of the structure when exposed to bending or pushing forces? Very few researchers have explored the mechanics of microtubule-actin hybrid structures. Using optical tweezers microrheology, one group has characterized the mechanical behavior of co-entangled microtubule and actin filament composites either randomly mixed (Ricketts et al., 2018) or crosslinked artificially and/or with MAP65 (Farhadi et al., 2020; Ricketts et al., 2019). Artificially crosslinked composites of microtubule and actin filaments, using biotin-NeutrAvidin links, exhibit an elastic response to mechanical perturbation, while networks not connected respond viscoelastically and soften (Ricketts et al., 2019). This group recently reported that MAP65 bundling of microtubules can reorganize the microtubule-actin network, where actin colocalizes with MAP65-bundled microtubules. However, they found little impact on the mechanical properties of these composites, suggesting mechanics are influenced by the actin network more so than the microtubule network (Farhadi et al., 2020). It would be interesting to investigate CLASP-mediated organization of microtubule-actin networks and mechanics, since like MAP65, CLASPs can bundle microtubules and unlike MAP65, CLASPs can weakly interact with F-actin. To date, MAP65 has not been reported to interact with actin. Thus potentially, CLASP-bundled microtubules would form larger hybrid structures of microtubules-actin and change the mechanical properties of the network.

Microfluidics and micropatterning can also be used to cross-examine mechanical properties of microtubule-actin structures. I propose future experiments where microfluidics is used to bend CLASP2-coated microtubule-actin structures over time to measure any changes in the integrity of the structure, mechanically or dynamically. Furthermore, using micropatterning, we can investigate microtubule buckling forces when guided and linked along actin bundles that then encounter a barrier. More modifications could be made in the experimental design to create barriers that mimic the cortical actin network and membrane to reconstitute capture of microtubules. I look forward to future investigations connecting mechanical function to microtubule-actin

crosstalk and more specifically, the role of CLASP-mediated crosslinking in the mechanics of the cytoskeleton.

6.6 Conclusions

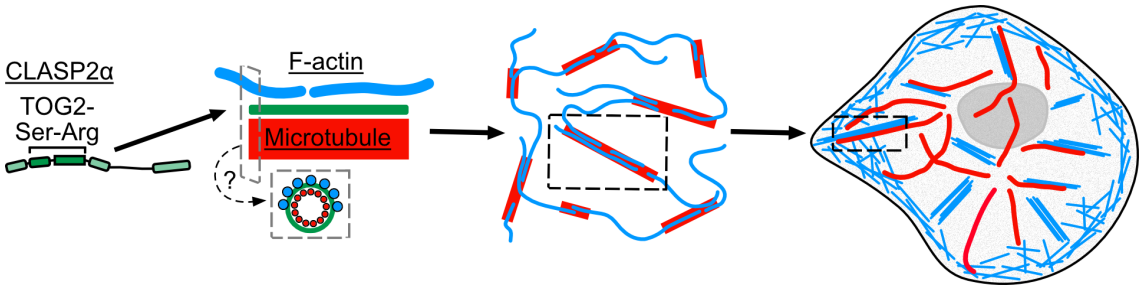

Figure 6.4: CLASP2 facilitates dynamic actin filament organization along the microtubule lattice Microtubules are in red, actin is in blue, and CLASP2 is green throughout figure. Gray dashed boxes represent cross-sectional view of a potential model for F-actin organization along microtubules coated with CLASP2α, where F-actin are binding around the microtubule shaft. Black dashed boxes are highlighted zoom ins representing instances of co-organization of actin filaments and microtubules observed *in vitro* and in cells.

Altogether, this work confirms the role of CLASPs in microtubule and actin filament crosstalk, notably demonstrating that CLASP2α can directly crosslink microtubules and actin filaments, a novel mechanism for CLASPs (Figure 6.4). Using newly developed *in vitro* reconstitution assays and rigorous image analysis techniques, we determined that CLASP weakly interacts with actin filaments and its interaction is stronger when concentrated on the microtubule lattice. In addition, CLASP2α can mediate dynamic filament organization as templated by the other cytoskeletal polymer. Finally, insights into the role of CLASPs in ventral actin stress fiber organization confirm the importance of the microtubule-CLASP-actin interaction in forming higher-order actin structures in cells. This work augments our understanding of the molecular players involved in the physical coordination of the cytoskeleton; nevertheless many questions and new directions are still left to explore.

Appendix A

Microtubule minus-end stability is dictated by the tubulin off-rate

Adapted from: Strothman, C., V. Farmer, G. Arpag, N. Rodgers, M. Podolski, S. Norris, R. Ohi, and M. Zanic. 2019. Microtubule minus-end stability is dictated by the tubulin off-rate. J. Cell Biol. 218:2841-2853. doi: 10.1083/jcb.201905019

I contributed to the experimental design, performance, and analysis of tubulin dilution experiments by microfluidics. I also performed tubulin dilution experiments with HSET. Included in this chapter are adaptations of figures from the above cited manuscript for which I contributed.

A.1 Introduction

Microtubules are dynamic polymers that undergo a unique behavior called 'dynamic instability.' Dynamic instability describes the stochastic switching between phases of microtubule growth and shrinkage. Microtubules are structurally polar, where the plus and minus end exhibit different rates of dynamic instability (Horio and Hotani, 1986; Mitchison and Kirschner, 1984; Walker et al., 1988). Distinctly, the minus ends have slower growth rates and less frequent catastrophe events, or the transition from growth to shrinkage. Tubulin is a GTPase, where microtubule polymerization occurs with the addition of GTP-tubulin subunits and incorporation into the microtubule lattice initiating GTP hydrolysis in the β-tubulin, after a short delay. This delay results in a 'cap' of GTP-tubulin at the ends of microtubules, where the rest of the lattice is composed of Guanosine diphosphate (GDP)-tubulin. Dynamic instability results from structural changes that occur within the lattice due to GTP hydrolysis, resulting in catastrophe when the GDP-tubulin is exposed (Duellberg et al., 2016; Nogales et al., 1998; Voter et al., 1991; Zhang et al., 2015). Minus ends are understudied due to their common anchoring or capping in cells, while the plus ends tend to be more dynamic (Akhmanova and Steinmetz, 2015). However, several cell types rely on microtubule networks with free minus ends.

Our current model for dynamic instability is based mostly on plus-end specific dynamics, where we know the minus-end dynamics are very different. It is thought in the field that a larger GTP-cap, leads to faster growth rates and less frequent catastrophes. In contrast, the minus end has slower growth rates and less frequent catastrophes (Horio and Hotani, 1986; Mitchison and Kirschner, 1984; Walker et al., 1988). It remains unclear how this contradiction exists for the minus end, hence we use a combination of microfluidics,

in vitro reconstitution, and TIRF microscopy to approximate the size of the GTP-cap of minus ends using tubulin dilution (Duellberg et al., 2016; Walker et al., 1991).

A.2 Results

A.2.1 Microtubule minus ends have small GTP-cap sizes, set by slower growth rates

To characterize the minus end, we performed tubulin dilution experiments to approximate the GTP-cap size. Here, we grew dynamic microtubules in the presence of 6, 12, or 18 μM tubulin in a microfluidic device and, while imaging, rapidly exchanged solutions to remove soluble tubulin from solution with sub-second resolution. Consistent with previous reports (Duellberg et al., 2016; Ti et al., 2016; Voter et al., 1991), we observed a characteristic delay between tubulin washout and the onset of microtubule catastrophe. This we interpreted as the time during which the stabilizing GTP-cap is lost. We found that, in all investigated conditions, minus ends displayed lower average delay times than plus ends (average across conditions: minus end: 4.7 ± 0.3 s, SE, N = 160; plus end: 8.6 ± 0.3 s, SE, N = 271) (Appendix Figure A.1A,B). Delay times increased with instantaneous growth rate determined prior to dilution (Appendix Figure A.1C), consistent with the idea that faster growth rates result in larger stabilizing caps. Like a recent finding for microtubule plus ends (Duellberg et al., 2016), we observed slight depolymerization of both microtubule ends during the delay period, distinct from the fast microtubule depolymerization that follows catastrophe. Based on these results, we conclude that growing minus ends have smaller stabilizing GTP-caps than plus ends, corresponding to their slower growth rates. Therefore, the increased stability of minus ends cannot be explained by the relative size of their stabilizing caps.

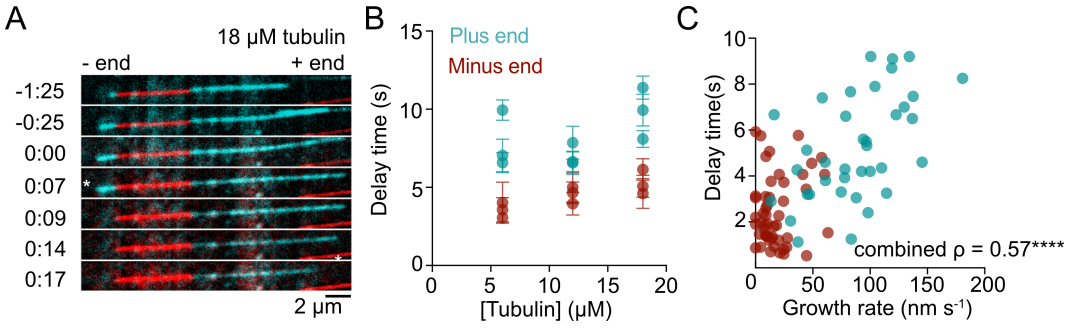

Figure A.1: Microtubule minus ends have small GTP-cap sizes, set by slower growth rates
A) Representative time lapse images of a microtubule pre-grown with 18 μM tubulin undergoing tubulin washout. 0:00 timepoint indicates time of washout; asterisks indicate time of catastrophe for each end. B) Mean delay times for each microtubule end are shown from three independent experiments of each tubulin concentration. C) Delay time as a function of instantaneous growth rate at plus and minus ends grown in 20 μM tubulin. Corresponding delay times after dilution per microtubule are shown. All points shown from three independent repeats. Spearman's rho test = 0.57; ****, $P < 0.0001$.

A.2.2 Kinesin-14, HSET, regulates GTP-tubulin off-rate at the microtubule minus end

We were next curious to probe the GTP-tubulin off rate using a minus end motor protein, kinesin-14 HSET/KIFC1. Little is known about how HSET regulates the microtubule minus end and it is of great interest due to its minus-end motor activity (Norris et al., 2018; Reinemann et al., 2018). To investigate whether HSET directly suppresses tubulin off-rate, we repeated tubulin dilution experiments using microtubules grown with 12 μM tubulin in the presence or absence of 100 nM GFP-HSET during both the growth and washout phases (Appendix Figure A.2A). We found that HSET had no significant effect on plus-end delay times; however, we observed a significant increase in minus-end delay times in the presence of HSET (Appendix Figure A.2B). Individual delay times correlated with the average GFP-HSET fluorescence intensity at the microtubule tip following tubulin washout (Appendix Figure A.2C), indicating that HSET directly stabilized minus ends after washout, consistent with suppressing the GTP-cap removal. We thus conclude that HSET directly suppresses the GTP-tubulin off-rate at microtubule minus ends.

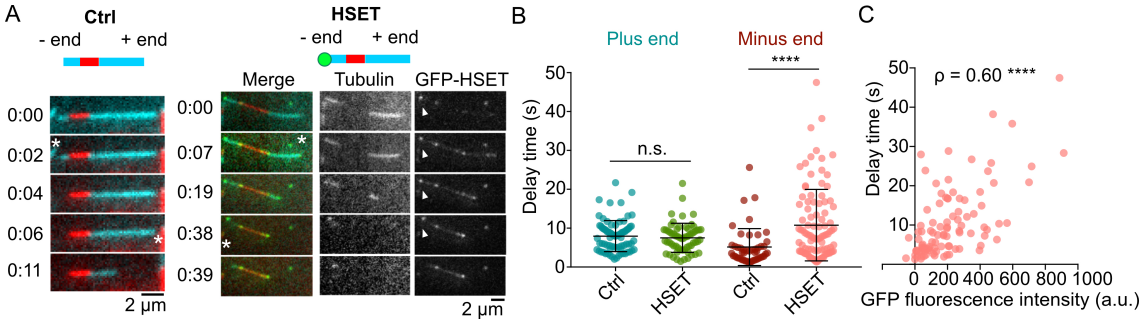

Figure A.2: Kinesin-14, HSET, regulates GTP-tubulin off-rate at the microtubule minus end
A) Representative timelapse images of dilution experiments in the absence or presence of 100 nM HSET. Asterisks mark time of catastrophe at either microtubule end. Arrow in HSET condition indicates GFP-HSET tip localization. Timestamp indicates time after washout (min:s). B) Delay times per end in the absence or presence of 100 nM HSET. N = 3 independent experiments for the control, and N = 4 independent repeats for +HSET condition. C) Minus end + HSET delay times as a function of GFP fluorescence intensity (background subtracted, see methods). N = 97 delay times from 4 independent experiments. Spearman rho's test r = 0.060, **** $p < 0.0001$.

A.3 Discussion

Microtubule catastrophe occurs via the loss of a protective cap of GTP-tubulin, the size of which is widely considered to be the determinant of microtubule plus-end stability. When microtubule growth rate is increased *in vitro* by increasing tubulin concentrations, the plus-end EB-comet size also increases (Bieling et al., 2007), while microtubule catastrophe is suppressed (Drechsel et al., 1992; Gardner et al., 2011; Walker et al., 1988). Furthermore, larger EB comets have been directly correlated with prolonged stability against dilution-induced catastrophe at microtubule plus ends (Duellberg et al., 2016). Correlating growth rate before washout to the delay time, we report that the minus end delay time scales with its lower growth rate. Despite less catastrophe

at the minus end, the GTP-cap size is not inherently bigger than the plus end. However, we also found that HSET can modulate the tubulin off-rate at the minus end. HSET can stabilize the GTP-tubulin at the minus end, prolonging the delay time or loss of the GTP-cap. This result added to our understanding of microtubule minus-end stability and the broader model of dynamic instability.

A.4 Methods

A.4.1 Protein Purification

Tubulin was purified and labeled as previously described in Chapter 2. His6-HSET tagged with enhanced GFP was expressed in *Spodoptera frugiperda* (Sf9 cells) and purified as previously described Norris et al. (2018) and stored in 10 mM K-HEPES, pH 7.7, 300 mM KCl, 1 mM dithiothreitol, 100 μM MgCl2, 100 μM ATP, and 20% sucrose. Human MCAK-His6 was expressed in Sf9 cells and purified as previously described (Helenius et al., 2006) and stored in BRB20 (20 mM Pipes/KOH, pH 6.8, 1 mM MgCl2, and 1 mM EGTA). Protein concentration was determined using absorbance at λ = 280 nm or a Bradford assay.

A.4.2 Microfluidic device preparation

Y-shaped microfluidic devices were prepared similarly to those previously described by Duellberg and colleagues, but with two branched inlets instead of three (Duellberg et al., 2016). Silicon molds with negative channel patterns were produced using deep reactive ion etching. A mixture of polydimethylsiloxane (PDMS) and curing agent (10:1 wt/wt) was poured over a mold, degassed for 20 min at room temperature, and polymerized for 4 h at 60°C. Holes for the inlet and outlet channels were created in the peeled-off PDMS block using biopsy punchers. The structured side of the PDMS and a 22 × 22-mm glass coverslip were treated with air plasma for 20 seconds. A small area of 4 × 10 mm, where imaging was to occur, was protected from plasma radiation by a small PDMS block to ensure the integrity of the surface functionalization. Immediately after plasma treatment, the exposed sides were bonded to form the channels, and tubing (Tygon; inner diameter of 0.5 mm) was connected to the PDMS inlets/outlet and Hamilton gas tight syringes (1,000 ml total volume; used for channel preparation only). The microfluidic devices were used for TIRF microscopy experiments immediately after assembly.

A.4.3 Tubulin dilution experiments

Fast solution exchange in the micro-channel was achieved by switching the flow from two different inlets that were controlled by independent and flow sensors between pumps and inlets. To assemble a sample, short GMPCPP-stabilized, TMR-labeled microtubule seeds were introduced through one inlet and allowed to attach to the functionalized glass surface. To initiate microtubule growth, 6, 12, or 18 μM 20% Alexa Fluor

647–labeled tubulin was introduced through the first inlet at a constantly maintained flow rate of 7 μl/min for 90 s, and then flow was stopped for the remaining growth period. Imaging buffer was supplemented with 0.05% methylcellulose. After a short period of growth (5–10 min), sub-second tubulin washout was induced using a 50 μl/min flow of a washout reaction containing BRB80 and imaging buffer, unchanged from the initial growth reaction besides tubulin. Plus and minus ends were differentiated by average growth rates before washout. Imaging during the growth phase was performed at 0.2 FPS and imaging of the 640-nm channel just before, during, and after washout was performed at 10 FPS for tubulin-only conditions using the CMOS camera (70-nm pixel). Reactions containing HSET were additionally supplemented with 1 mM ATP. GFP-HSET was diluted in BRB80, and control conditions contained an equivalent volume of HSET storage buffer (10 mM K-HEPES, pH 7.7, 300 mM KCl, 1 mM dithiothreitol, 100 μM MgCl2, 100 μM ATP, and 20% sucrose).

Appendix B

Chlamydomonas reinhardtii, axonemes and crowding agents can be used to induce microtubule bundle formation to study bundle dynamics in vitro

Adapted from: Wright, CJ., Richardson, LB., and Rodgers, NC. 2022. Purifying Chlamydomonas Reinhardtii Axonemes to Study Microtubule Bundles. In review at Young Scientist (A High School Research Journal)

This work was done with a high school summer-intern from the School for Science and Math at Vanderbilt (SSMV). The goal of the program is to provide hands-on, real world educational experiences in STEM for students from the Metropolitan Nashville Public School system. This work is under review in the Young Scientist, a High School Research Journal a peer-reviewed journal at Vanderbilt University.

B.1 Introduction

Microtubules are found to form complex structures in the cell, such as in the mitotic spindle, axonal bundles, and axonemes (Conde and Cáceres, 2009; Ishikawa, 2017; Prosser and Pelletier, 2017). Specifically, malfunctioning axonemes in sperm can lead to infertility, while malfunctioning axonemes in cilia can lead to Primary Ciliary Dyskinesia (PCD), a respiratory disease (Davis and Katsanis, 2012). Microtubules have been studied thoroughly individually, however it not reflective of how they perform in complex structures, such as in axonemal bundles. Thus, understanding larger microtubule bundle structure dynamics is very important for providing implications in disease treatment.

Axonemes consist of nine microtubule doublets in a circle, surrounding a central microtubule doublet in the middle (Nicastro et al., 2006). Axonemes can be found in flagella and cilia and, via motor proteins, provide a beating motion for cell motility (Nicastro et al., 2006; Owa et al., 2019). We propose to use axonemes to nucleate microtubules, since axonemes are composed of 9 microtubule-doublets that can serve as templates to grow multiple microtubule extensions in a controlled manner. Typically, microtubules nucleated from axonemal templates grow splayed out and plan to use crowding agents to bundle microtubules near each other (Park et al., 2021). Alternatively, MAPs are known to bundle microtubules in close proximity (Lansky et al., 2015; Prezel et al., 2018; Stoppin-Mellet et al., 2013; Subramanian et al., 2010) , however can be time consuming and costly to produce. Hence, we use cheaply available methylcellulose to create a bundling assay with microtubules nucleated from axonemes.

B.2 Results

B.2.1 Purification of axonemes from *Chlamydomonas reinhardtii*

To investigate microtubule dynamics in ensembles, we grew *Chlamydomonas reinhardtii* cells to then purify axonemes from (Appendix Figure B.1A). Once culture growth reached 3 - 7 x 106 cells per mL (Appendix Figure B.1C), we collected the cells for axoneme purification. Axonemes were purified by performing the following steps, i) washing cells, ii) deflagellation, iii-iv) collecting flagella, v) demembranation of flagella and isolation of pure axonemes (Appendix Figure B.1D-H). During the collection of the flagella, the resulting pellet contained a white halo with some green in the center, indicating a level of contamination (Appendix Figure B.1G). Since the pellet had a concentrated white halo, we were able to continue with our purification with negligible risk from the minor contamination (Alper et al., 2013). The final purification yielded 95 µL of axonemes, which is near our 100 µL aim (Appendix Figure B.1H).

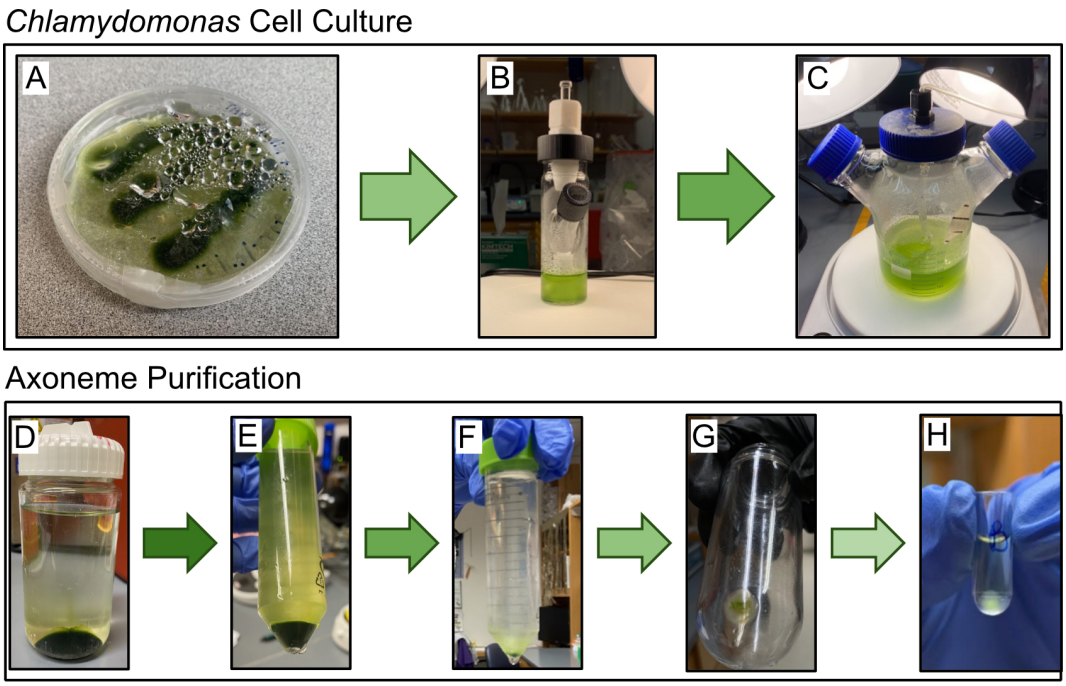

Figure B.1: Example flowchart of axoneme purification from *Chlamydomonas reinhardtii*
A) Chlamydomonas cell culture in TAP+agar plate. B) Small liquid culture of Chlamydomonas cells in spinner flask of TAP media, configured with a stir bar to hinder cell clumping and provide more aeration. Two desk lamps surround culture to allow for more cell growth. C) Large liquid culture of Chlamydomonas cells in spinner flask of TAP media. D) First wash spin of Chlamydomonas cells and pellet was kept. E) The first spin in deflagellation step, supernatant containing flagella is kept. F) Sucrose cushion spin to further remove cell bodies from flagella. Supernatant contains flagella G) Hard spin to concentrate flagella (pellet) to then be stored overnight at 4C. H) Demembranation spin resulting with axonemes in the pellet. Pellet was resuspended and sample was snap frozen and used for experiments. Green indicates Chlamydomonas cell (A-D) and cell debris (E-H). White/clear indicates flagella, which is the desired product for steps in panels E-H.

B.2.2 Dynamic microtubules, nucleated from axonemes, can be bundled by crowding agents

We next wanted to test axoneme functionality for nucleating microtubule extensions. Briefly, axonemes, with stable microtubule seeds used as a positive control, were added to non-specifically absorb to a coverslip surface for imaging. Using Internal reflection microscopy (IRM), widefield, and TIRF microscopy, we captured movies of the axoneme over time, and found axonemes growing multiple, dynamic microtubule extensions (Appendix Figure B.2A). As expected, microtubule extensions from stabilized microtubule seeds and axonemes underwent dynamic instability, indicating our conditions and axonemes are functioning correctly in our assays (Appendix Figure B.2B,C). In these low methylcellulose conditions (0.1%) multiple microtubules grew from one end of the axoneme, however mostly were splayed away from each other (Appendix Figure B.2A). There were a few instances of overlapped growth, suggesting an interaction between microtubules in a bundled organization. In low crowding conditions and with no additional microtubule associated proteins, microtubule extensions nucleated from axonemes behave like single microtubules, where there are very few overlapping interactions.

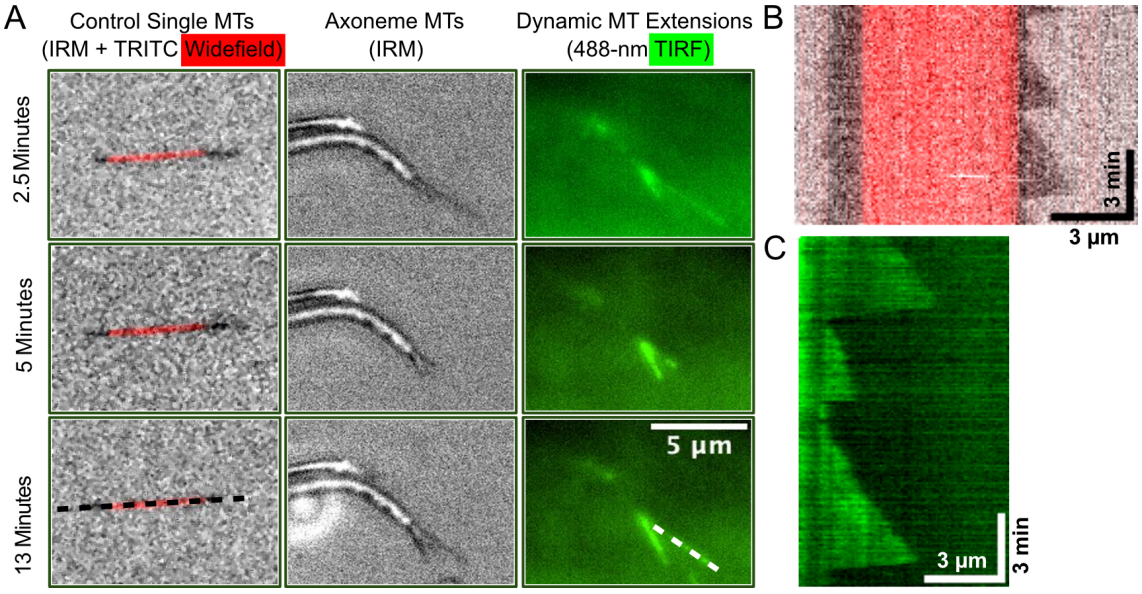

Figure B.2: Individual axonemes growing multiple microtubule extensions over time
A) Widefield (red) indicates microtubule seeds, TIRF (green) indicates tubulin localization which highlights microtubule extensions, IRM (gray) indicates axonemes and extensions. Images were taken from a 15-minute movie and demonstrate dynamic microtubule growth and decay over time with low, 0.1% methylcellulose concentration. Black and white dashed lines correspond to panels B and C, respectively. B) Kymograph of control, single microtubule growing from GMPCPP stabilized microtubule. C) Kymograph of 488-tubulin microtubule extension from axoneme undergoing dynamic instability. Experiments done in triplicate.

With the initial axoneme movie taken and repeated, we hypothesized that higher methylcellulose would

increase the number of overlapping microtubule events to measure microtubule bundle dynamics. High amounts of methylcellulose, ranging between 0.3-0.6%, have been reported to increase microtubule interactions and induce bundling in microtubule gliding assays (Farhadi et al., 2018). To test our hypothesis, we first grew microtubule extensions from axonemes in 0.1% methylcellulose conditions for 10 minutes (Appendix Figure B.3A). Then we added a new reaction mix with the same reagents, but with 0.3% methylcellulose, and imaged the microtubules for 15-30 minutes. Following the introduction of triple the crowding agent, we observed more microtubule extensions from axonemes, more bundled microtubules, and overall, the microtubule network was less dynamic (Appendix Figure B.3A). Drawing a kymograph along an extension with overlapping microtubules (Appendix Figure B.3B), we counted 4 microtubules to be growing stably together as a bundle (Appendix Figure B.3C). Overall, higher concentrations of methylcellulose can increase events of overlapping microtubules templated from axonemes to form networks of microtubule bundles.

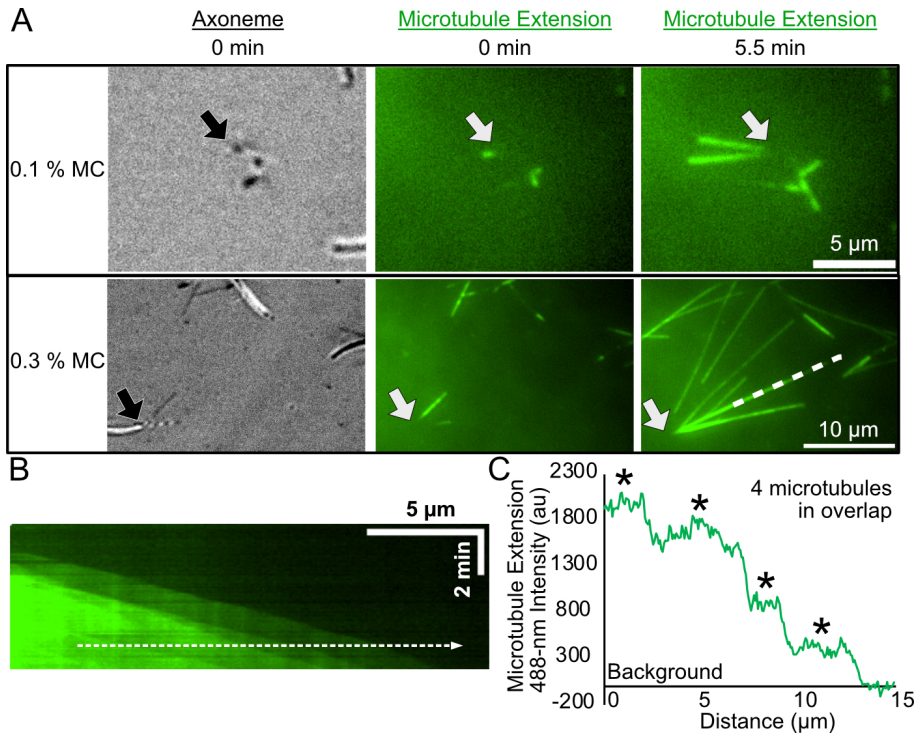

Figure B.3: Microtubule extensions from axonemes exposed to 0.1% and 0.3% methylcellulose (MC) induces overlapping of dynamic microtubules

A) First column is visualized with IRM, second and third columns are visualized using 488-nm TIRF. Row one depicts microtubule growth from an axoneme end over time (0 - 5.5 minutes) with 0.1% MC. Row two depicts microtubule growth from an axoneme end over time (0 - 5.5 minutes) with 0.3% MC. Arrows point to focal axonemes. White dashed line corresponds to kymograph in Panel B. B) Kymograph of overlapped microtubule extensions from axoneme structure in Panel A. Dotted line corresponds to intensity profile in Panel C. C) Microtubule extension intensity over the distance of the dotted white line in Panel B. Intensity is shifted to the average local background. Asterisks highlight intensity peaks analogous to a single microtubule.

B.3 Discussion

Microtubules are essential structures for cell function due to the many vital functions they perform. If microtubules, or the more complex structures they make up, malfunction: it could lead to disease. For this reason, it is extremely important to understand basic microtubule function. However, while microtubules are frequently studied, they are usually studied individually. This is not reflective of how microtubules exist in cells since microtubules here tend to work together in ensembles. Because of this, we attempted to determine a way to study microtubule ensembles *in vitro* for more reflective data of how they operate in cells. Our findings indicate that microtubule bundles can be grown *in vitro* from axonemes for a more reflective study to model microtubules within cells. Building off this experiment, future directions should aim to replicate growing microtubule extensions from axonemes. From there, our assay can be used for different methods of crowding, such as using different crowding reagents (Park et al., 2021) or bundling MAPs (Prezel et al., 2018; Stoppin-Mellet et al., 2013; Subramanian et al., 2010). Future work should also research the dynamics of bundled microtubules in larger bundle structures.

The process for growing *Chlamydomonas* cells was successful. There was a period of cell decay when they were growing in 25 ml spinner flask, but the decay stopped and reversed after we moved the cells to the larger culture and introduced aeration. The process of purifying axonemes was also successful. During the flagellar pellet stage of the purification, there was a slightly visible white halo with green in the center indicative of contamination. We used our protocols to judge that the green present in the pellet was not abundant enough to justify ending our purification. There were minimal consequences to the contamination; debris was occasionally visible when observing our final solution under the microscope. The step in the purification we believe to have caused some contamination was during the sucrose cushion step to separate flagella from remaining cell debris. We can optimize this step by adding another sucrose cushion spin (Alper et al., 2013; Orbach and Howard, 2020).

The procedure of visualizing our purified axonemes under a microscope was successful as well. Initially, we had issues seeing the axonemes, because they were not binding well to the microscope coverslip. This was solved by adding stable, microtubule seeds as a control, in addition to the axonemes, which had an unintended effect of crowding the axonemes near the surface to nonspecifically absorb to the coverslip. Upon imaging the axonemes, we observed multiple microtubule extensions growing from single axoneme ends. We can tell axonemes and microtubules apart by using IRM and TIRF imaging, confirming that our axonemes did grow microtubule extensions. The final process of bundling microtubule extensions together was successful. By

tripling the crowing agent (0.3%) and utilizing the same imaging techniques as before, we observed more bundling, indicated by brighter signal, and more stable extensions. This resulted in more stable extensions growing and encountering other microtubules, causing them to join and bundle together to create larger bundles with other axonemes.

Microtubule bundle dynamics have been studied previously, however as induced by MAPs (Prezel et al., 2018; Stoppin-Mellet et al., 2013). These experiments used stable microtubule seeds and grew single microtubule extensions, where microtubule extensions would eventually encounter each other at an angle and promote bundle formation by MAPs. However, bundle size was limited to 2-3 microtubules and computational simulations were needed to understand larger bundle sizes. Depending on the type of cell, there are instances of larger microtubule bundle networks, such as in the axon, where there can be 10-100 microtubules bundled in a crosssection (Fadić et al., 1985; Stoppin-Mellet et al., 2013). Our *in vitro*, axoneme assay for studying microtubule bundle dynamics allows for study of bundle sizes up to 9 microtubules from the same axoneme and can potentially go bigger with the microtubule extensions from nearby axoneme templates. Furthermore, methylcellulose is a relatively inexpensive reagent as compared to the cost of purifying MAPs to use as crosslinkers.

B.4 Methods

B.4.1 Chlamydomonas reinhardtii culture and axoneme purification

Methods for growing cells were derived from previously published work and adapted to scale (Alper et al., 2013; Orbach and Howard, 2020).

B.4.2 Microtubule dynamics from axonemes

Imaging channels and GMPCPP stabilized microtubules were prepared as described in Chapter 2 and Chapter 3, respectively. To prepare flow cells for experiments, 4 µl of microtubule seeds, 4 µl of axonemes, and 2 µl of BRB80 were flown into an imaging-channel and incubated for 15 minutes at room temperature to allow for non-specific absorption to the surface. Then the channel was washed with BRB80, and then blocked with 1% Pluronic F127 for 20 minutes at room temperature. Finally, the imaging channel was washed with BRB80, 5x the channel volume to ensure complete washout of reagents. To grow microtubule extensions, reaction mixes were prepared with the following reagents, 10 µM tubulin, 8-10% labeled with Alexa488 and imaging buffer (BRB80, 1 mM GTP, 40 mM Di-glucose, 40 µg/ml Glucose Oxidase, 16 µg/ml Catalase, 0.08 mg/ml casein, 10 mM DTT, and 1 mM MgCl2). For baseline conditions, 0.1% methylcellulose (MC) was added to the imaging buffer to help visualize growing microtubule extensions. In microtubule bundle conditions, 0.3%

methylcellulose was added to induce bundling. The axonemes were pushed to the surface of the coverslip due to the addition of the crowding agent.

Microtubule extensions and axonemes were visualized using IRM to visualize axoneme and microtubule extensions, TIRF microscopy to visualize microtubule extensions, and widefield microscopy to visualize the microtubule seeds on a Nikon Eclipse Ti2 microscope with 100x/1.49 n.a. TIRF objective, equipped with NEO sCMOS camera and 488-nm laser. Objective heater was used to maintain a sample temperature of 35 C. Images of microtubule extension growth in IRM and 488-nm TIRF were taken every 5 seconds for 15-30 minutes. Widefield images of microtubule seeds (TRITC filter) were imaged for the first frame.

References

Abraham, V. C., Krishnamurthi, V., Taylor, D. L., and Lanni, F. (1999). The Actin-Based Nanomachine at the Leading Edge of Migrating Cells. *Biophysical Journal*, 77(3):1721–1732.

Aher, A., Kok, M., Sharma, A., Rai, A., Olieric, N., Rodriguez-Garcia, R., Katrukha, E. A., Weinert, T., Kapitein, L. C., Steinmetz, M. O., Dogterom, M., and Akhmanova, A. (2018). CLASP Suppresses Microtubule Catastrophes through a Single TOG Domain. *Developmental Cell*, 46(1):1–19.

Aher, A., Rai, D., Schaedel, L., Gaillard, J., John, K., Liu, Q., Altelaar, M., Blanchoin, L., Thery, M., and Akhmanova, A. (2020). CLASP Mediates Microtubule Repair by Restricting Lattice Damage and Regulating Tubulin Incorporation. *Current Biology*, 30(11):2175–2183.e6.

Akhmanova, A., Hoogenraad, C. C., Drabek, K., Stepanova, T., Dortland, B., Verkerk, T., Vermeulen, W., Burgering, B. M., De Zeeuw, C. I., Grosveld, F., and Galjart, N. (2001). CLASPs Are CLIP-115 and -170 Associating Proteins Involved in the Regional Regulation of Microtubule Dynamics in Motile Fibroblasts. *Cell*, 104(6):923–935.

Akhmanova, A. and Steinmetz, M. O. (2015). Control of microtubule organization and dynamics: two ends in the limelight. *Nature Reviews Molecular Cell Biology*, 16(12):711–726.

Al-Bassam, J., Kim, H., Brouhard, G., van Oijen, A., Harrison, S. C., and Chang, F. (2010). CLASP promotes microtubule rescue by recruiting tubulin dimers to the microtubule. *Developmental Cell*, 19(2):245–258.

Alberico, E. O., Zhu, Z. C., Wu, Y. F. O., Gardner, M. K., Kovar, D. R., and Goodson, H. V. (2016). Interactions between the Microtubule Binding Protein EB1 and F-Actin. *Journal of Molecular Biology*, 428(6):1304–1314.

Alkemade, C., Wierenga, H., Volkov, V. A., López, M. P., Akhmanova, A., ten Wolde, P. R., Dogterom, M., and Koenderink, G. H. (2022). Cross-linkers at growing microtubule ends generate forces that drive actin transport. *Proceedings of the National Academy of Sciences of the United States of America*, 119(11):1–12.

Alper, J., Geyer, V., Mukundan, V., and Howard, J. (2013). *Reconstitution of flagellar sliding*, volume 524. Elsevier Inc., 1 edition.

Amos, L. A. and Klug, A. (1974). Arrangement of Subunits in Flagellar Microtubules. *Journal of Cell Science*, 14(3):523–549.

Applewhite, D. A., Grode, K. D., Keller, D., Zadeh, A. D., Slep, K. C., and Rogers, S. L. (2010). The Spectraplakin Short Stop Is an Actin–Microtubule Cross-Linker That Contributes to Organization of the Microtubule Network. *Molecular Biology of the Cell*, 21(10):1714–1724.

Arnal, I. and Wade, R. H. (1995). How does taxol stabilize microtubules? *Current Biology*, 5(8):900–908.

Aumeier, C., Schaedel, L., Gaillard, J., John, K., Blanchoin, L., and Théry, M. (2016). Self-repair promotes microtubule rescue. *Nature Cell Biology*, 18(10):1054–1064.

Ballatore, C., Lee, V. M. Y., and Trojanowski, J. Q. (2007). Tau-mediated neurodegeneration in Alzheimer's disease and related disorders. *Nature Reviews Neuroscience*, 8(9):663–672.

Bartolini, F., Moseley, J. B., Schmoranzer, J., Cassimeris, L., Goode, B. L., and Gundersen, G. G. (2008). The formin mDia2 stabilizes microtubules independently of its actin nucleation activity. *Journal of Cell Biology*, 181(3):523–536.

Bathe, M., Heussinger, C., Claessens, M. M. A. E., Bausch, A. R., and Frey, E. (2008). Cytoskeletal bundle mechanics. *Biophysical Journal*, 94(8):2955–2964.

Bazellières, E., Massey-Harroche, D., Barthélémy-Requin, M., Richard, F., Arsanto, J.-P., and Le Bivic, A. (2012). Apico-basal elongation requires a drebrin-E–EB3 complex in columnar human epithelial cells. *Journal of Cell Science*, 125(4):919–931.

Bieling, P., Kandels-Lewis, S., Telley, I. A., Van Dijk, J., Janke, C., and Surrey, T. (2008). CLIP-170 tracks growing microtubule ends by dynamically recognizing composite EB1/tubulinbinding sites. *Journal of Cell Biology*, 183(7):1223–1233.

Bieling, P., Laan, L., Schek, H., Munteanu, E. L., Sandblad, L., Dogterom, M., Brunner, D., and Surrey, T. (2007). Reconstitution of a microtubule plus-end tracking system in vitro. *Nature*, 450(7172):1100–1105.

Biosse Duplan, M., Zalli, D., Stephens, S., Zenger, S., Neff, L., Oelkers, J. M., Lai, F. P. L., Horne, W., Rottner, K., and Baron, R. (2014). Microtubule Dynamic Instability Controls Podosome Patterning in Osteoclasts through EB1, Cortactin, and Src. *Molecular and Cellular Biology*, 34(1):16–29.

Biswas, S. and Kalil, K. (2018). The microtubule associated protein tau mediates the organization of microtubules and their dynamic exploration of actin-rich lamellipodia and filopodia of cortical growth cones. *The Journal of Neuroscience*, 38(2):2217–2281.

Blanchoin, L., Boujemaa-Paterski, R., Sykes, C., and Plastino, J. (2014). Actin Dynamics, Archi-tecture, and Mechanics in Cell Motility. *Physiol Rev*, 94:235–263.

Bolte, S. and Cordelières, F. P. (2006). A guided tour into subcellular colocalization analysis in light microscopy. *Journal of Microscopy*, 224(3):213–232.

Bosveld, F., Markova, O., Guirao, B., Martin, C., Wang, Z., Pierre, A., Balakireva, M., Gaugue, I., Ainslie, A., Christophorou, N., Lubensky, D. K., Minc, N., and Bellaiche, Y. (2016). Epithelial tricellular junctions act as interphase cell shape sensors to orient mitosis. *Nature*, 530(7591):495–498.

Bouchet, B. P., Gough, R. E., Ammon, Y. C., van de Willige, D., Post, H., Jacquemet, G., Maarten Altelaar, A. F., Heck, A. J. R., Goult, B. T., and Akhmanova, A. (2016). Talin-KANK1 interaction controls the recruitment of cortical microtubule stabilizing complexes to focal adhesions. *eLife*, 5(JULY):1–23.

Bré, M. H., Kreis, T. E., and Karsenti, E. (1987). Control of microtubule nucleation and stability in Madin-Darby canine kidney cells: the occurrence of noncentrosomal, stable detyrosinated microtubules. *The Journal of Cell Biology*, 105(3):1283–1296.

Breitsprecher, D., Koestler, S. A., Chizhov, I., Nemethova, M., Mueller, J., Goode, B. L., Small, J. V., Rottner, K., and Faix, J. (2011). Cofilin cooperates with fascin to disassemble filopodial actin filaments. *Journal of Cell Science*, 124(19):3305–3318.

Bringmann, H. and Hyman, A. A. (2005). A cytokinesis furrow is positioned by two consecutive signals. *Nature*, 436(7051):731–734.

Bronson, J. E., Fei, J., Hofman, J. M., Gonzalez, R. L., and Wiggins, C. H. (2009). Learning rates and states from biophysical time series: A Bayesian approach to model selection and single-molecule FRET data. *Biophysical Journal*, 97(12):3196–3205.

Cabrales Fontela, Y., Kadavath, H., Biernat, J., Riedel, D., Mandelkow, E., and Zweckstetter, M. (2017). Multivalent cross-linking of actin filaments and microtubules through the microtubule-associated protein Tau. *Nature Communications*, 8(1):1–12.

Castaneda, N., Park, J., and Kang, E. H. (2021). Regulation of Actin Bundle Mechanics and Structure by Intracellular Environmental Factors. *Frontiers in Physics*, 9(May):1–7.

Castoldi, M. and Popov, A. V. (2003). Purification of brain tubulin through two cycles of polymerization–depolymerization in a high-molarity buffer. *Protein Expression and Purification*, 32(1):83–88.

Chesarone, M. A., DuPage, A. G., and Goode, B. L. (2010). Unleashing formins to remodel the actin and microtubule cytoskeletons. *Nature Reviews Molecular Cell Biology*, 11(1):62–74.

Claessens, M. M. A. E., Bathe, M., Frey, E., and Bausch, A. R. (2006). Actin-binding proteins sensitively mediate F-actin bundle stiffness. *Nature Materials*, 5(9):748–753.

Colin, A., Singaravelu, P., Théry, M., Blanchoin, L., and Gueroui, Z. (2018). Actin-Network Architecture Regulates Microtubule Dynamics. *Current Biology*, 28(0):1–10.

Conde, C. and Cáceres, A. (2009). Microtubule assembly, organization and dynamics in axons and dendrites. *Nature Reviews Neuroscience*, 10(5):319–332.

Davis, E. E. and Katsanis, N. (2012). The ciliopathies: A transitional model into systems biology of human genetic disease. *Current Opinion in Genetics and Development*, 22(3):290–303.

Dixit, R., Barnett, B., Lazarus, J. E., Tokito, M., Goldman, Y. E., and Holzbaur, E. L. F. (2009). Microtubule plus-end tracking by CLIP-170 requires EB1. *Proceedings of the National Academy of Sciences of the United States of America*, 106(2):492–497.

Dogterom, M. and Koenderink, G. H. (2019). Actin–microtubule crosstalk in cell biology. *Nature Reviews Molecular Cell Biology*, 20(1):38–54.

Doki, C., Nishida, K., Saito, S., Shiga, M., Ogara, H., Kuramoto, A., Kuragano, M., Nozumi, M., Igarashi, M., Nakagawa, H., Kotani, S., and Tokuraku, K. (2020). Microtubule elongation along actin filaments induced by microtubule-associated protein 4 contributes to the formation of cellular protrusions. *The Journal of Biochemistry*, 168(3):295–303.

Drechsel, D. N., Hyman, A. A., Cobb, M. H., and Kirschner, M. W. (1992). Modulation of the dynamic instability of tubulin assembly by the microtubule-associated protein tau. *Molecular Biology of the Cell*, 3(10):1141–1154.

Drees, F., Pokutta, S., Yamada, S., Nelson, W. J., and Weis, W. I. (2005). α-Catenin Is a Molecular Switch that Binds E-Cadherin-β-Catenin and Regulates Actin-Filament Assembly. *Cell*, 123(5):903–915.

Duellberg, C., Cade, N. I., Holmes, D., and Surrey, T. (2016). The size of the EB cap determines instantaneous microtubule stability. *eLife*, 5(APRIL2016):1–23.

Dunn, K. W., Kamocka, M. M., and McDonald, J. H. (2011). A practical guide to evaluating colocalization in biological microscopy. *American Journal of Physiology - Cell Physiology*, 300(4):723–742.

Efimov, A., Kharitonov, A., Efimova, N., Loncarek, J., Miller, P. M., Andreyeva, N., Gleeson, P., Galjart, N., Maia, A. R. R., McLeod, I. X., Yates, J. R., Maiato, H., Khodjakov, A., Akhmanova, A., and Kaverina, I. (2007). Asymmetric CLASP-Dependent Nucleation of Noncentrosomal Microtubules at the trans-Golgi Network. *Developmental Cell*, 12(6):917–930.

Efimova, N., Grimaldi, A., Bachmann, A., Frye, K., Zhu, X., Feoktistov, A., Straube, A., and Kaverina, I. (2014). Podosome-regulating kinesin KIF1C translocates to the cell periphery in a CLASP-dependent manner. *Journal of Cell Science*, 127(24):5179–5188.

Efimova, N., Yang, C., Chia, J. X., Li, N., Lengner, C. J., Neufeld, K. L., and Svitkina, T. M. (2020). Branched actin networks are assembled on microtubules by adenomatous polyposis coli for targeted membrane protrusion. *Journal of Cell Biology*, 219(9).

Elie, A., Prezel, E., Guérin, C., Denarier, E., Ramirez-Rios, S., Serre, L., Andrieux, A., Fourest-Lieuvin, A., Blanchoin, L., and Arnal, I. (2015). Tau co-organizes dynamic microtubule and actin networks. *Scientific Reports*, 5:1–10.

Engel, U., Zhan, Y., Long, J. B., Boyle, S. N., Ballif, B. A., Dorey, K., Gygi, S. P., Koleske, A. J., and VanVactor, D. (2014). Abelson phosphorylation of CLASP2 modulates its association with microtubules and actin. *Cytoskeleton*, 71(3):195–209.

Fadić, R., Vergara, J., and Alvarez, J. (1985). Microtubules and caliber of central and peripheral processes of sensory axons. *The Journal of Comparative Neurology*, 236(2):258–264.

Fan, J., Griffiths, A. D., Lockhart, A., Cross, R. A., and Amos, L. A. (1996). Microtubule Minus Ends can be Labelled with a Phage Display Antibody Specific to Alpha-Tubulin. *Journal of Molecular Biology*, 259(3):325–330.

Farhadi, L., Fermino Do Rosario, C., Debold, E. P., Baskaran, A., and Ross, J. L. (2018). Active Self-Organization of Actin-Microtubule Composite Self-Propelled Rods. *Frontiers in Physics*, 6(July):1–16.

Farhadi, L., Ricketts, S. N., Rust, M. J., Das, M., Robertson-Anderson, R. M., and Ross, J. L. (2020). Actin and microtubule crosslinkers tune mobility and control co-localization in a composite cytoskeletal network. *Soft Matter*, 16(31):7191–7201.

Fehon, R. G., McClatchey, A. I., and Bretscher, A. (2010). Organizing the cell cortex: The role of ERM proteins. *Nature Reviews Molecular Cell Biology*, 11(4):276–287.

Fish, K. N. (2022). Total Internal Reflection Fluorescence (TIRF) Microscopy. *Current Protocols*, 2(8):1–16.

Fletcher, D. A. and Mullins, R. D. (2010). Cell mechanics and the cytoskeleton.

Folker, E. S., Baker, B. M., and Goodson, H. V. (2005). Interactions between CLIP-170, Tubulin, and Microtubules: Implications for the Mechanism of CLIP-170 Plus-End Tracking Behavior. *Molecular Biology of the Cell*, 16(11):5373–5384.

Forscher, P. and Smith, S. J. (1988). Actions of Cytochalasins on the Organization of Actin Filaments and Microtubules in a Neuronal Growth Cone. *Journal of Cell Biology*, 107(October):1505–1516.

Fulga, T. A., Elson-Schwab, I., Khurana, V., Steinhilb, M. L., Spires, T. L., Hyman, B. T., and Feany, M. B. (2007). Abnormal bundling and accumulation of F-actin mediates tau-induced neuronal degeneration in vivo. *Nature Cell Biology*, 9(2):139–148.

Gaillard, J., Ramabhadran, V., Neumanne, E., Gurel, P., Blanchoin, L., Vantard, M., and Higgs, H. N. (2011). Differential interactions of the formins INF2, mDia1, and mDia2 with microtubules. *Molecular Biology of the Cell*, 22(23):4575–4587.

Gardner, M. K., Zanic, M., Gell, C., Bormuth, V., and Howard, J. (2011). Depolymerizing kinesins Kip3 and MCAK shape cellular microtubule architecture by differential control of catastrophe. *Cell*, 147(5):1092–1103.

Gazzola, M., Schaeffer, A., Butler-Hallissey, C., Friedl, K., Vianay, B., Gaillard, J., Leterrier, C., Blanchoin, L., and Théry, M. (2023). Microtubules self-repair in living cells. *Current Biology*, 33(1):122–133.e4.

Gell, C., Bormuth, V., Brouhard, G. J., Cohen, D. N., Diez, S., Friel, C. T., Helenius, J., Nitzsche, B., Petzold, H., Ribbe, J., Schäffer, E., Stear, J. H., Trushko, A., Varga, V., Widlund, P. O., Zanic, M., and Howard, J. (2010). Microtubule Dynamics Reconstituted In Vitro and Imaged by Single-Molecule Fluorescence Microscopy. In *Methods in Cell Biology*, volume 95, pages 221–245.

Geraldo, S., Khanzada, U. K., Parsons, M., Chilton, J. K., and Gordon-Weeks, P. R. (2008). Targeting of the F-actin-binding protein drebrin by the microtubule plus-tip protein EB3 is required for neuritogenesis. *Nature Cell Biology*, 10(10):1181–1189.

Gil-Henn, H., Destaing, O., Sims, N. A., Aoki, K., Alles, N., Neff, L., Sanjay, A., Bruzzaniti, A., De Camilli, P., Baron, R., and Schlessinger, J. (2007). Defective microtubule-dependent podosome organization in osteoclasts leads to increased bone density in Pyk2-/- mice. *Journal of Cell Biology*, 178(6):1053–1064.

Gilbert, T., Le Bivic, A., Quaroni, A., and Rodriguez-Boulan, E. (1991). Microtubular organization and its involvement in the biogenetic pathways of plasma membrane proteins in Caco-2 intestinal epithelial cells. *Journal of Cell Biology*, 113(2):275–288.

Girdler, G. C., Applewhite, D. A., Perry, W. M. G., Rogers, S. L., and Röper, K. (2016). The Gas2 family protein Pigs is a microtubule +TIP that affects cytoskeleton organisation. *Journal of Cell Science*, 129(1):121–134.

Gomez, J. M., Chumakova, L., Bulgakova, N. A., and Brown, N. H. (2016). Microtubule organization is determined by the shape of epithelial cells. *Nature Communications*, 7(1):13172.

Goode, B. L., Wong, J. J., Butty, A.-C., Peter, M., McCormack, A. L., Yates, J. R., Drubin, D. G., and Barnes, G. (1999). Coronin Promotes the Rapid Assembly and Cross-linking of Actin Filaments and May Link the Actin and Microtubule Cytoskeletons in Yeast. *Journal of Cell Biology*, 144(1):83–98.

Griffith, L. M. and Pollard, T. D. (1978). Evidence for actin filament-microtubule interaction mediated by microtubule-associated proteins. *Journal of Cell Biology*, (18).

Griffith, L. M. and Pollard, T. D. (1982). The interaction of actin filaments with microtubules and microtubule-associated proteins. *Journal of Biological Chemistry*, 257(15):9143–9151.

Gupton, S. L., Salmon, W. C., and Waterman-Storer, C. M. (2002). Converging Populations of F-Actin Promote Breakage of Associated Microtubules to Spatially Regulate Microtubule Turnover in Migrating Cells. *Current Biology*, 12(22):1891–1899.

Hagiwara, A., Tanaka, Y., Hikawa, R., Morone, N., Kusumi, A., Kimura, H., and Kinoshita, M. (2011). Submembranous septins as relatively stable components of actin-based membrane skeleton. *Cytoskeleton*, 68(9):512–525.

Hawkins, T., Mirigian, M., Selcuk Yasar, M., and Ross, J. L. (2010). Mechanics of microtubules. *Journal of Biomechanics*, 43(1):23–30.

Hawkins, T. L., Sept, D., Mogessie, B., Straube, A., and Ross, J. L. (2013). Mechanical properties of doubly stabilized microtubule filaments. *Biophysical Journal*, 104(7):1517–1528.

Helenius, J., Brouhard, G., Kalaidzidis, Y., Diez, S., and Howard, J. (2006). The depolymerizing kinesin MCAK uses lattice diffusion to rapidly target microtubule ends. *Nature*, 441(7089):115–119.

Henty-Ridilla, J. L., Juanes, M. A., and Goode, B. L. (2017). Profilin Directly Promotes Microtubule Growth through Residues Mutated in Amyotrophic Lateral Sclerosis. *Current Biology*, 27(22):3535–3543.e4.

Henty-Ridilla, J. L., Rankova, A., Eskin, J. A., Kenny, K., and Goode, B. L. (2016). Accelerated actin filament polymerization from microtubule plus ends. *Science*, 352(6288):1004–1009.

Horio, T. and Hotani, H. (1986). Visualization of the dynamic instability of individual microtubules by dark-field microscopy. *Nature*, 321(6070):605–607.

Hotta, A., Kawakatsu, T., Nakatani, T., Sato, T., Matsui, C., Sukezane, T., Akagi, T., Hamaji, T., Grigoriev, I., Akhmanova, A., Takai, Y., and Mimori-Kiyosue, Y. (2010). Laminin-based cell adhesion anchors microtubule plus ends to the epithelial cell basal cortex through LL5α/β. *Journal of Cell Biology*, 189(5):901–907.

Huang, S., Jin, L., Du, J., Li, H., Zhao, Q., Ou, G., Ao, G., and Yuan, M. (2007). SB401, a pollen-specific protein from Solanum berthaultii, binds to and bundles microtubules and F-actin. *The Plant Journal*, 51(3):406–418.

Hyman, A., Drechsel, D., Kellogg, D., Salser, S., Sawin, K., Steffen, P., Wordeman, L., and Mitchison, T. (1991). Preparation of modified tubulins. *Methods in Enzymology*, 196:478–485.

Inoue, D., Obino, D., Pineau, J., Farina, F., Gaillard, J., Guerin, C., Blanchoin, L., Lennon-Duménil, A., and Théry, M. (2019). Actin filaments regulate microtubule growth at the centrosome. *The EMBO Journal*, 38(11):e99630.

Ishikawa, T. (2017). Axoneme structure from motile cilia. *Cold Spring Harbor Perspectives in Biology*, 9(1).

Jaulin, F. and Kreitzer, G. (2010). KIF17 stabilizes microtubules and contributes to epithelial morphogenesis by acting at MT plus ends with EB1 and APC. *Journal of Cell Biology*, 190(3):443–460.

Juanes, M. A., Bouguenina, H., Eskin, J. A., Jaiswal, R., Badache, A., and Goode, B. L. (2017). Adenomatous polyposis coli nucleates actin assembly to drive cell migration and microtubuleinduced focal adhesion turnover. *Journal of Cell Biology*, 216(9):2859–2875.

Juanes, M. A., Fees, C. P., Hoeprich, G. J., Jaiswal, R., and Goode, B. L. (2020). Report EB1 Directly Regulates APC-Mediated Actin Nucleation EB1 Directly Regulates APC-Mediated Actin Nucleation. *Current Biology*, 30:1–10.

Juanes, M. A., Isnardon, D., Badache, A., Brasselet, S., Mavrakis, M., and Goode, B. L. (2019). The role of APC-mediated actin assembly in microtubule capture and focal adhesion turnover. *The Journal of cell biology*, pages 1–21.

Kasai, M., Asakura, S., and Oosawa, F. (1962). The cooperative nature of G-F transformation of actin. *BBA - Biochimica et Biophysica Acta*, 57(1):22–31.

Kasza, K. E., Rowat, A. C., Liu, J., Angelini, T. E., Brangwynne, C. P., Koenderink, G. H., and Weitz, D. A. (2007). The cell as a material. *Current Opinion in Cell Biology*, 19(1):101–107.

Khanal, I., Elbediwy, A., Diaz de la Loza, M. d. C., Fletcher, G. C., and Thompson, B. J. (2016). Shot and Patronin polarise microtubules to direct membrane traffic and biogenesis of microvilli in epithelia. *Journal of Cell Science*, 129:2651 – 2659.

Koestler, S. A., Rottner, K., Lai, F., Block, J., Vinzenz, M., and Small, J. V. (2009). F- and G-Actin Concentrations in Lamellipodia of Moving Cells. *PLoS ONE*, 4(3):e4810.

Kopp, P., Lammers, R., Aepfelbacher, M., Woehlke, G., Rudel, T., Machuy, N., Steffen, W., and Linder, S. (2006). The Kinesin KIF1C and Microtubule Plus Ends Regulate Podosome Dynamics in Macrophages. *Molecular Biology of the Cell*, 17(6):2811–2823.

Kučera, O., Gaillard, J., Guérin, C., Théry, M., and Blanchoin, L. (2022a). Actin architecture steers microtubules in active cytoskeletal composite. *Nano Letters*.

Kučera, O., Gaillard, J., Guérin, C., Théry, M., and Blanchoin, L. (2022b). Actin–microtubule dynamic composite forms responsive active matter with memory. *Proceedings of the National Academy of Sciences*, 119(31):1–7.

Kumar, P., Lyle, K. S., Gierke, S., Matov, A., Danuser, G., and Wittmann, T. (2009). GSK33 phosphorylation modulates CLASP-microtubule association and lamella microtubule attachment. *Journal of Cell Biology*, 184(6):895–908.

Kwon, M., Bagonis, M., Danuser, G., and Pellman, D. (2015). Direct Microtubule-Binding by Myosin-10 Orients Centrosomes toward Retraction Fibers and Subcortical Actin Clouds. *Developmental Cell*, 34(3):323–337.

Lancaster, O. M., Le Berre, M., Dimitracopoulos, A., Bonazzi, D., Zlotek-Zlotkiewicz, E., Picone, R., Duke, T., Piel, M., and Baum, B. (2013). Mitotic Rounding Alters Cell Geometry to Ensure Efficient Bipolar Spindle Formation. *Developmental Cell*, 25(3):270–283.

Lansbergen, G., Grigoriev, I., Mimori-Kiyosue, Y., Ohtsuka, T., Higa, S., Kitajima, I., Demmers, J., Galjart, N., Houtsmuller, A. B., Grosveld, F., and Akhmanova, A. (2006). CLASPs Attach Microtubule Plus Ends to the Cell Cortex through a Complex with LL5β. *Developmental Cell*, 11(1):21–32.

Lansky, Z., Braun, M., Lüdecke, A., Schlierf, M., Ten Wolde, P. R., Janson, M. E., and Diez, S. (2015). Diffusible crosslinkers generate directed forces in microtubule networks. *Cell*, 160(6):1159–1168.

Lawrence, C. J., Morris, N. R., Meagher, R. B., and Dawe, R. K. (2001). Dyneins have run their course in plant lineage. *Traffic*, 2(5):362–363.

Lawrence, E. J., Arpag, G., Norris, S. R., and Zanic, M. (2018). Human CLASP2 specifically regulates microtubule catastrophe and rescue. *Molecular biology of the cell*, 29(10):1168–1177.

Lawrence, E. J., Zanic, M., and Rice, L. M. (2020). CLASPs at a glance. *Journal of Cell Science*, 133(8):1–7.

Leano, J. B., Rogers, S. L., and Slep, K. C. (2013). A cryptic TOG domain with a distinct architecture underlies CLASP-dependent bipolar spindle formation. *Structure*, 21(6):939–950.

López, M. P., Huber, F., Grigoriev, I., Steinmetz, M. O., Akhmanova, A., Koenderink, G. H., and Dogterom, M. (2014). Actin–microtubule coordination at growing microtubule ends. *Nature Communications*, 5(1):4778.

Lowery, L. A., Stout, A., Faris, A. E., Ding, L., Baird, M. A., Davidson, M. W., Danuser, G., and Van Vactor, D. (2013). Growth cone-specific functions of XMAP215 in restricting microtubule dynamics and promoting axonal outgrowth. *Neural Development*, 8(1).

Maier, B., Kirsch, M., Anderhub, S., Zentgraf, H., and Krämer, A. (2013). The novel actin/focal adhesion-associated protein MISP is involved in mitotic spindle positioning in human cells. *Cell Cycle*, 12(9):1457–1471.

Maki, T., Grimaldi, A. D., Fuchigami, S., Kaverina, I., and Hayashi, I. (2015). CLASP2 has two distinct TOG domains that contribute differently to microtubule dynamics. *Journal of Molecular Biology*, 427(14):2379–2395.

Marx, A., Godinez, W. J., Tsimashchuk, V., Bankhead, P., Rohr, K., and Engel, U. (2013). Xenopus cytoplasmic linker-associated protein 1 (XCLASP1) promotes axon elongation and advance of pioneer microtubules. *Molecular Biology of the Cell*, 24(10):1544–1558.

Merriam, E. B., Millette, M., Lumbard, D. C., Saengsawang, W., Fothergill, T., Hu, X., Ferhat, L., and Dent, E. W. (2013). Synaptic regulation of microtubule dynamics in dendritic spines by calcium, F-actin, and Drebrin. *Journal of Neuroscience*, 33(42):16471–16482.

Mimori-Kiyosue, Y., Grigoriev, I., Lansbergen, G., Sasaki, H., Matsui, C., Severin, F., Galjart, N., Grosveld, F., Vorobjev, I., Tsukita, S., and Akhmanova, A. (2005). CLASP1 and CLASP2 bind to EB1 and regulate microtubule plus-end dynamics at the cell cortex. *Journal of Cell Biology*, 168(1):141–153.

Mimori-Kiyosue, Y., Shiina, N., and Tsukita, S. (2000). Adenomatous polyposis coli (APC) protein moves along microtubules and concentrates at their growing ends in epithelial cells. *Journal of Cell Biology*, 148(3):505–517.

Mitchison, T. and Kirschner, M. (1984). Dynamic instability of microtubule growth. *Nature*, 312(5991):237–242.

Moon, H. M. and Wynshaw-Boris, A. (2013). Cytoskeleton in action: lissencephaly, a neuronal migration disorder. *Wiley Interdisciplinary Reviews: Developmental Biology*, 2(2):229–245.

Morales, E. A., Arnaiz, C., Krystofiak, E. S., Zanic, M., and Tyska, M. J. (2022). Mitotic Spindle Positioning (MISP) is an actin bundler that selectively stabilizes the rootlets of epithelial microvilli. *Cell Reports*, 39(3):110692.

Mostowy, S. and Cossart, P. (2012). Septins: The fourth component of the cytoskeleton.

Nakos, K., Alam, M. N. A., Radler, M. R., Kesisova, I. A., Yang, C., Okletey, J., Tomasso, M. R., Padrick, S. B., Svitkina, T. M., and Spiliotis, E. T. (2022). Septins mediate a microtubule–actin crosstalk that enables actin growth on microtubules. *Proceedings of the National Academy of Sciences*, 119(50):2017.

Nakos, K., Radler, M. R., and Spiliotis, E. T. (2019). Septin 2/6/7 complexes tune microtubule plus-end growth and EB1 binding in a concentration- and filament-dependent manner. *Molecular Biology of the Cell*, 30(23):2913–2928.

Nejedla, M., Sadi, S., Sulimenko, V., de Almeida, F. N., Blom, H., Draber, P., Aspenström, P., and Karlsson, R. (2016). Profilin connects actin assembly with microtubule dynamics. *Molecular Biology of the Cell*, 27(15):2381–2393.

Nicastro, D., Schwartz, C., Pierson, J., Gaudette, R., Porter, M. E., and McIntosh, J. R. (2006). The Molecular Architecture of Axonemes Revealed by Cryoelectron Tomography. *Science*, 313(5789):944–948.

Noble, M., Lewis, S. A., and Cowan, N. J. (1989). The microtubule binding domain of microtubule-associated protein MAP1B contains a repeated sequence motif unrelated to that of MAP2 and tau. *Journal of Cell Biology*, 109(6):3367–3376.

Nogales, E., Whittaker, M., Milligan, R. A., Downing, K. H., and Berkeley, L. (1999). High-Resolution Model of the Microtubule University of California at Berkeley. *Cell*, 96:79–88.

Nogales, E., Wolf, S. G., and Downing, K. H. (1998). Structure of the aB tubulin dimer by electron crystallography. *Nature*, 391(January):199–204.

Noordstra, I., Liu, Q., Nijenhuis, W., Hua, S., Jiang, K., Baars, M., Remmelzwaal, S., Martin, M., Kapitein, L. C., and Akhmanova, A. (2016). Control of apico-basal epithelial polarity by the microtubule minus-end binding protein CAMSAP3 and spectraplakin ACF7. *Journal of Cell Science*, pages 4278–4288.

Norris, S. R., Jung, S., Singh, P., Strothman, C. E., Erwin, A. L., Ohi, M. D., Zanic, M., and Ohi, R. (2018). Microtubule minus-end aster organization is driven by processive HSET-tubulin clusters. *Nature Communications*, 9(1):2659.

Oberhofer, A., Reithmann, E., Spieler, P., Stepp, W. L., Zimmermann, D., Schmid, B., Frey, E., and Ökten, Z. (2020). Molecular underpinnings of cytoskeletal cross-talk. *Proceedings of the National Academy of Sciences*, 117(8):3944–3952.

Oberhofer, A., Spieler, P., Rosenfeld, Y., Stepp, W. L., Cleetus, A., Hume, A. N., Mueller-Planitz, F., and Ökten, Z. (2017). Myosin Va's adaptor protein melanophilin enforces track selection on the microtubule and actin networks in vitro. *Proceedings of the National Academy of Sciences of the United States of America*, 114(24):E4714–E4723.

Orbach, R. and Howard, J. (2020). Purification of Ciliary Tubulin from Chlamydomonas reinhardtii. *Current Protocols in Protein Science*, 100(1):1–16.

Owa, M., Uchihashi, T., aki Yanagisawa, H., Yamano, T., Iguchi, H., Fukuzawa, H., ichi Wakabayashi, K., Ando, T., and Kikkawa, M. (2019). Inner lumen proteins stabilize doublet microtubules in cilia and flagella. *Nature Communications*, 10(1):1–10.

Pardee, J. D. and Spudich, J. A. (1982). Purification of Muscle Actin. In *Methods in Cell Biology*, volume 24, pages 271–289.

Park, J., Lee, M., Lee, B., Castaneda, N., Tetard, L., and Kang, E. H. (2021). Crowding tunes the organization and mechanics of actin bundles formed by crosslinking proteins. *FEBS Letters*, 595(1):26–40.

Patel, K., Nogales, E., and Heald, R. (2012). Multiple domains of human CLASP contribute to microtubule dynamics and organization in vitro and in Xenopus egg extracts. *Cytoskeleton*, 69(3):155–165.

Paul, D. M., Mantell, J., Borucu, U., Coombs, J., Surridge, K. J., Squire, J., Verkade, P., and Dodding, M. P. (2020). In situ cryo-electron tomography reveals filamentous actin within the microtubule lumen. *Journal of Cell Biology*, 219(9).

Pimm, M. L. and Henty-Ridilla, J. L. (2021). New twists in actin–microtubule interactions. *Molecular Biology of the Cell*, 32(3):211–217.

Pollard, T. D. and Borisy, G. G. (2003). Cellular motility driven by assembly and disassembly of actin filaments. *Cell*, 112(4):453–465.

Portran, D., Schaedel, L., Xu, Z., Théry, M., and Nachury, M. V. (2017). Tubulin acetylation protects long-lived microtubules against mechanical ageing. *Nature cell biology*, 19(May 2016):391–398.

Preciado López, M., Huber, F., Grigoriev, I., Steinmetz, M. O., Akhmanova, A., Dogterom, M., and Koenderink, G. H. (2014). In Vitro Reconstitution of Dynamic Microtubules Interacting with Actin Filament Networks. In *Methods in Enzymology*, volume 540, pages 301–320.

Prezel, E., Elie, A., Delaroche, J., Stoppin-Mellet, V., Bosc, C., Serre, L., Fourest-Lieuvin, A., Andrieux, A., Vantard, M., and Arnal, I. (2018). Tau can switch microtubule network organizations: from random networks to dynamic and stable bundles. *Molecular Biology of the Cell*, 29(2):154–165.

Prezel, E., Stoppin-Mellet, V., Elie, A., Zala, N., Denarier, E., Serre, L., and Arnal, I. (2017). TIRF assays for real-time observation of microtubules and actin coassembly: Deciphering tau effects on microtubule/actin interplay. In *Methods in Cell Biology*, volume 141, pages 199–214.

Prosser, S. L. and Pelletier, L. (2017). Mitotic spindle assembly in animal cells: a fine balancing act. *Nature Reviews Molecular Cell Biology*, 18(3):187–201.

Reilein, A. and Nelson, W. J. (2005). APC is a component of an organizing template for cortical microtubule networks. *Nature Cell Biology*, 7(5):463–473.

Reinemann, D. N., Norris, S. R., Ohi, R., and Lang, M. J. (2018). Processive Kinesin-14 HSET Exhibits Directional Flexibility Depending on Motor Traffic. *Current Biology*, 28(14):2356–2362.

Ricketts, S. N., Francis, M. L., Farhadi, L., Rust, M. J., Das, M., Ross, J. L., and Robertson-Anderson, R. M. (2019). Varying crosslinking motifs drive the mesoscale mechanics of actin-microtubule composites. *Scientific Reports*, 9.

Ricketts, S. N., Ross, J. L., and Robertson-Anderson, R. M. (2018). Co-entangled actin-microtubule composites exhibit tunable nonlinear stiffness and power-law stress relaxation. *Biophysical Journal*, 115(6):1055–1067.

Rochlin, M. W., Dailey, M. E., and Bridgman, P. C. (1999). Polymerizing microtubules activate site-directed F-actin assembly in nerve growth cones. *Molecular biology of the cell*, 10(7):2309–2327.

Rodriguez, O. C., Schaefer, A. W., Mandato, C. A., Forscher, P., Bement, W. M., and Waterman-Storer, C. M. (2003). Conserved microtubule-actin interactions in cell movement and morphogenesis. *Nature Cell Biology*, 5(7):599–609.

Rodriguez-Boulan, E. and Macara, I. G. (2014). Organization and execution of the epithelial polarity programme. *Nature Reviews Molecular Cell Biology*, 15(4):225–242.

Roger, B., Al-Bassam, J., Dehmelt, L., Milligan, R. A., and Halpain, S. (2004). MAP2c, but not tau, binds and bundles F-actin via its microtubule binding domain. *Current Biology*, 14(5):363–371.

Roth-Johnson, E. A., Vizcarra, C. L., Bois, J. S., and Quinlan, M. E. (2014). Interaction between microtubules and the drosophila formin cappuccino and its effect on actin assembly. *Journal of Biological Chemistry*, 289(7):4395–4404.

Rothenberg, M. E., Rogers, S. L., Vale, R. D., Jan, L. Y., and Jan, Y. N. (2003). Drosophila pod-1 crosslinks both actin and microtubules and controls the targeting of axons. *Neuron*, 39(5):779–791.

Rowinsky, E. K., Cazenave, L. A., and Donehower, R. C. (1990). Taxol: A novel investigational antimicrotubule agent. *Journal of the National Cancer Institute*, 82(15):1247–1259.

Rückerl, F., Lenz, M., Betz, T., Manzi, J., Martiel, J.-L., Safouane, M., Paterski-Boujemaa, R., Blanchoin, L., and Sykes, C. (2017). Adaptive Response of Actin Bundles under Mechanical Stress. *Biophysical Journal*, 113(5):1072–1079.

Salmon, W. C., Adams, M. C., and Waterman-Storer, C. M. (2002). Dual-wavelength fluorescent speckle microscopy reveals coupling of microtubule and actin movements in migrating cells. *Journal of Cell Biology*, 158(1):31–37.

Schaedel, L., John, K., Gaillard, J., Nachury, M. V., Blanchoin, L., and Théry, M. (2015). Microtubules self-repair in response to mechanical stress. *Nature Materials*, 14(11):1156–1163.

Schindelin, J., Arganda-Carreras, I., Frise, E., Kaynig, V., Longair, M., Pietzsch, T., Preibisch, S., Rueden, C., Saalfeld, S., Schmid, B., Tinevez, J. Y., White, D. J., Hartenstein, V., Eliceiri, K., Tomancak, P., and Cardona, A. (2012). Fiji: An open-source platform for biological-image analysis. *Nature Methods*, 9(7):676–682.

Seetharaman, S. and Etienne-Manneville, S. (2020). Cytoskeletal Crosstalk in Cell Migration. *Trends in Cell Biology*, 30(9):720–735.

Shekhar, S. (2017). Microfluidics-Assisted TIRF Imaging to Study Single Actin Filament Dynamics. *Current Protocols in Cell Biology*, 77(1):12.13.1–12.13.24.

Sider, J. R., Mandato, C. a., Weber, K. L., Zandy, a. J., Beach, D., Finst, R. J., Skoble, J., and Bement, W. M. (1999). Direct observation of microtubule-f-actin interaction in cell free lysates. *Journal of cell science*, 112:1947–1956.

Slater, P. G., Cammarata, G. M., Samuelson, A. G., Magee, A., Hu, Y., and Lowery, L. A. (2019). XMAP215 promotes microtubule-F–actin interactions to regulate growth cone microtubules during axon guidance in Xenopus laevis. *Journal of Cell Science*, 132(9):jcs224311.

Small, J. V., Iseberg, G., and Celis, J. E. (1978). Polarity of actin at the leading edge of cultured cells. *Nature*, 272(5654):638–639.

Solinet, S., Mahmud, K., Stewman, S. F., El Kadhi, K. B., Decelle, B., Talje, L., Ma, A., Kwok, B. H., and Carreno, S. (2013). The actin-binding ERM protein Moesin binds to and stabilizes microtubules at the cell cortex. *Journal of Cell Biology*, 202(2):251–260.

Spiliotis, E. T. and Nakos, K. (2021). Cellular functions of actin- and microtubule-associated septins. *Current Biology*, 31(10):R651–R666.

Stehbens, S. J., Paszek, M., Pemble, H., Ettinger, A., Gierke, S., and Wittmann, T. (2014). CLASPs link focal-adhesion-associated microtubule capture to localized exocytosis and adhesion site turnover. *Nature Cell Biology*, 16(6):558–570.

Stoppin-Mellet, V., Fache, V., Portran, D., Martiel, J. L., and Vantard, M. (2013). MAP65 Coordinate Microtubule Growth during Bundle Formation. *PLoS ONE*, 8(2).

Stricker, J., Falzone, T., and Gardel, M. L. (2010). Mechanics of the F-actin cytoskeleton. *Journal of Biomechanics*, 43(1):9–14.

Stroud, M. J., Nazgiewicz, A., McKenzie, E. A., Wang, Y., Kammerer, R. A., and Ballestrem, C. (2014). GAS2-like proteins mediate communication between microtubules and actin through interactions with end-binding proteins. *Journal of Cell Science*, 127(12):2672–2682.

Subramanian, R., Wilson-Kubalek, E. M., Arthur, C. P., Bick, M. J., Campbell, E. A., Darst, S. A., Milligan, R. A., and Kapoor, T. M. (2010). Insights into antiparallel microtubule crosslinking by PRC1, a conserved nonmotor microtubule binding protein. *Cell*, 142(3):433–443.

Suozzi, K. C., Wu, X., and Fuchs, E. (2012). Spectraplakins: Master orchestrators of cytoskeletal dynamics. *Journal of Cell Biology*, 197(4):465–475.

Suter, D. M. and Forscher, P. (2000). Substrate – Cytoskeletal Coupling as a Mechanism for the Regulation of Growth Cone Motility and Guidance. *Journal of Neurobiology*, 44:97–113.

Szent-Gyorgyi, A. (1942). Myosin and muscular contraction. *Protoplasma*, 37(1):319.

Ti, S. C., Pamula, M. C., Howes, S. C., Duellberg, C., Cade, N. I., Kleiner, R. E., Forth, S., Surrey, T., Nogales, E., and Kapoor, T. M. (2016). Mutations in Human Tubulin Proximal to the Kinesin-Binding Site Alter Dynamic Instability at Microtubule Plus- and Minus-Ends. *Developmental Cell*, 37(1):72–84.

Tilney, L. G., Bryan, J., Bush, D. J., Fujiwara, K., Mooseker, M. S., Murphy, D. B., and Snyder, D. H. (1973). MICROTUBULES: EVIDENCE FOR 13 PROTOFILAMENTS. *Journal of Cell Biology*, 59(2):267–275.

Toya, M., Kobayashi, S., Kawasaki, M., Shioi, G., Kaneko, M., Ishiuchi, T., Misaki, K., Meng, W., and Takeichi, M. (2016). CAMSAP3 orients the apical-to-basal polarity of microtubule arrays in epithelial cells. *Proceedings of the National Academy of Sciences*, 113(2):332–337.

Toyoshima, F. and Nishida, E. (2007). Integrin-mediated adhesion orients the spindle parallel to the substratum in an EB1- and myosin X-dependent manner. *EMBO Journal*, 26(6):1487–1498.

Tseng, K.-F., Wang, P., Lee, Y.-R. J., Bowen, J., Gicking, A. M., Guo, L., Liu, B., and Qiu, W. (2018). The preprophase band-associated kinesin-14 OsKCH2 is a processive minus-end-directed microtubule motor. *Nature Communications*, 9(1):1067.

Tsukada, M., Prokscha, A., Oldekamp, J., and Eichele, G. (2003). Identification of neurabin II as a novel doublecortin interacting protein. *Mechanisms of Development*, 120(9):1033–1043.

Tsukada, M., Prokscha, A., Ungewickell, E., and Eichele, G. (2005). Doublecortin association with actin filaments is regulated by neurabin II. *Journal of Biological Chemistry*, 280(12):11361–11368.

Tsvetkov, A. S., Samsonov, A., Akhmanova, A., Galjart, N., and Popov, S. V. (2007). Microtubule-binding proteins CLASP1 and CLASP2 interact with actin filaments. *Cell Motility and the Cytoskeleton*, 64(7):519–530.

Umezu, N., Umeki, N., Mitsui, T., Kondo, K., and Maruta, S. (2011). Characterization of a novel rice kinesin O12 with a calponin homology domain. *Journal of Biochemistry*, 149(1):91–101.

Vale, R. D. (2014). Preface: The role of reconstitution in cytoskeleton research. *Methods in Enzymology*, 540.

van de Willige, D., Hummel, J. J. A., Alkemade, C., Kahn, O. I., Au, F. K. C., Qi, R. Z., Dogterom, M., Koenderink, G. H., Hoogenraad, C. C., and Akhmanova, A. (2019). Cytolinker Gas2L1 regulates axon morphology through microtubule-modulated actin stabilization. *EMBO reports*, 20(11):1–20.

van Oostende Triplet, C., Jaramillo Garcia, M., Haji Bik, H., Beaudet, D., and Piekny, A. (2014). Anillin interacts with microtubules and is part of the astral pathway that defines cortical domains. *Journal of Cell Science*, 127(17):3699–3710.

Voter, W. A., O'Brien, E. T., and Erickson, H. P. (1991). Dilution-induced disassembly of microtubules: Relation to dynamic instability and the GTP cap. *Cell Motility and the Cytoskeleton*, 18(1):55–62.

Walker, R. A., Brien, O., Pryer, K., Soboeiro, M. E., Voter, W. A., Erickson, H. P., and Salmon, E. D. (1988). Dynamic Instability of Individual Microtubules. *The Journal of cell biology*, 107(October):1437–1448.

Walker, R. A., Pryer, N. K., and Salmon, E. D. (1991). Dilution of individual microtubules observed in real time in vitro: Evidence that cap size is small and independent of elongation rate. *Journal of Cell Biology*, 114(1):73–81.

Walter, W. J., MacHens, I., Rafieian, F., and Diez, S. (2015). The non-processive rice kinesin-14 OsKCH1 transports actin filaments along microtubules with two distinct velocities. *Nature Plants*, 1(August):1–5.

Waterman-Storer, C. M. and Salmon, E. D. (1997). Actomyosin-based retrograde flow of microtubules in the lamella of migrating epithelial cells influences microtubule dynamic instability and turnover and is associated with microtubule breakage and treadmilling. *Journal of Cell Biology*, 139(2):417–434.

Weber, K. L., Sokac, A. M., Berg, J. S., Cheney, R. E., and Bement, W. M. (2004). A microtubule-binding myosin required for nuclear anchoring and spindle assembly. *Nature*, 431(7006):325–329.

Weisenberg, R. C. (1972). Microtubule Formation in vitro in Solutions Containing Low Calcium Concentrations. *Science*, 177(4054):1104–1105.

Wen, Y., Eng, C. H., Schmoranzer, J., Cabrera-Poch, N., Morris, E. J. S., Chen, M., Wallar, B. J., Alberts, A. S., and Gundersen, G. G. (2004). EB1 and APC bind to mDia to stabilize microtubules downstream of Rho and promote cell migration. *Nature Cell Biology*, 6(9):820–830.

Widlund, P. O., Stear, J. H., Pozniakovsky, A., Zanic, M., Reber, S., Brouhard, G. J., Hyman, A. A., and Howard, J. (2011). XMAP215 polymerase activity is built by combining multiple tubulin-binding TOG domains and a basic lattice-binding region. *Proceedings of the National Academy of Sciences*, 108(7):2741–2746.

Winkelman, J. D., Suarez, C., Hocky, G. M., Harker, A. J., Morganthaler, A. N., Christensen, J. R., Voth, G. A., Bartles, J. R., and Kovar, D. R. (2016). Fascin- and α-Actinin-Bundled Networks Contain Intrinsic Structural Features that Drive Protein Sorting. *Current Biology*, 26(20):2697–2706.

Wittmann, T., Bokoch, G. M., and Waterman-Storer, C. M. (2003). Regulation of leading edge microtubule and actin dynamics downstream of Rac1. *Journal of Cell Biology*, 161(5):845–851.

Wittmann, T. and Waterman-Storer, C. M. (2005). Spatial regulation of CLASP affinity for microtubules by Rac1 and GSK3β in migrating epithelial cells. *Journal of Cell Biology*, 169(6):929–939.

Woodrum, D. T., Rich, S. A., and Pollard, T. D. (1975). Evidence for Biased Bidirectional Polymerization of Actin Filaments Using Heavy Meromyosin Prepared by an Improved Method. *Journal of Cell Biology*, 67:231–237.

Wu, H. W., Kuhn, T., and Moy, V. T. (2006). Mechanical properties of L929 cells measured by atomic force microscopy: Effects of anticytoskeletal drugs and membrane crosslinking. *Scanning*, 20(5):389–397.

Wu, S.-Z. and Bezanilla, M. (2014). Myosin VIII associates with microtubule ends and together with actin plays a role in guiding plant cell division. *eLife*, 3:1–20.

Wu, S.-Z. and Bezanilla, M. (2018). Actin and microtubule cross talk mediates persistent polarized growth. *Journal of Cell Biology*, 217(10):3531–3544.

Wu, X., Bowers, B., Rao, K., Wei, Q., and Hammer, J. A. (1998). Visualization of Melanosome Dynamics within Wild-Type and Dilute Melanocytes Suggests a Paradigm for Myosin V Function In Vivo. *Journal of Cell Biology*, 143(7):1899–1918.

Wu, X., Kodama, A., and Fuchs, E. (2008). ACF7 Regulates Cytoskeletal-Focal Adhesion Dynamics and Migration and Has ATPase Activity. *Cell*, 135(1):137–148.

Wu, Y.-F. O., Miller, R. A., Alberico, E. O., Nelson, N. T., Jonasson, E. M., and Goodson, H. V. (2021). Characterizing interactions between the microtubule-binding protein CLIP-170 and F-actin. *bioRxiv*.

Xu, K., Zhong, G., and Zhuang, X. (2013). Actin, Spectrin, and Associated Proteins Form a Periodic Cytoskeletal Structure in Axons. *Science*, 339(6118):452–456.

Xu, Z., Schaedel, L., Portran, D., Aguilar, A., and Gaillard, J. (2017). Microtubules acquire resistance from mechanical breakage through intralumenal acetylation. *Science*, 356(0000):1–5.

Yamamoto, S., Gaillard, J., Vianay, B., Guerin, C., Orhant-Prioux, M., Blanchoin, L., and Thery, M. (2022). The architecture of the actin network can balance the pushing forces produced by growing microtubules. *bioRxiv*, page 2022.01.21.476947.

Yue, J., Zhang, Y., Liang, W. G., Gou, X., Lee, P., Liu, H., Lyu, W., Tang, W.-J., Chen, S.-Y., Yang, F., Liang, H., and Wu, X. (2016). In vivo epidermal migration requires focal adhesion targeting of ACF7. *Nature Communications*, 7(1):11692.

Zhang, R., Alushin, G. M., Brown, A., and Nogales, E. (2015). Mechanistic origin of microtubule dynamic instability and its modulation by EB proteins. *Cell*, 162(4):849–859.

Zhu, M., Settele, F., Kotak, S., Sanchez-Pulido, L., Ehret, L., Ponting, C. P., Gönczy, P., and Hoffmann, I. (2013). MISP is a novel Plk1 substrate required for proper spindle orientation and mitotic progression. *Journal of Cell Biology*, 200(6):773–787.

Zhu, X., Efimova, N., Arnette, C., Hanks, S. K., and Kaverina, I. (2016). Podosome dynamics and location in vascular smooth muscle cells require CLASP-dependent microtubule bending. *Cytoskeleton*, 73(6):300–315.